Physical and chemical interaction in the interior of the Caledonian mountains of Norway

J.C.Vrijmoed

February 2009

Series of dissertations submitted to the
Faculty of Mathematics and Natural Sciences, University of Oslo
Nr. 862

ISSN 1501-7710

Cover: Inger Sandved Anfinsen.
Printed in Norway: AiT e-dit AS, Oslo, 2009.

Produced in co-operation with Unipub AS.
The thesis is produced by Unipub AS merely in connection with the
thesis defence. Kindly direct all inquiries regarding the thesis to the copyright
holder or the unit which grants the doctorate.

Unipub AS is owned by
The University Foundation for Student Life (SiO)

Principal supervisor:

Professor Yuri Y. Podladchikov

Subsidiary supervisors:

Professor Håkon Austrheim
Professor Torgeir B. Andersen

"Start by doing what's necessary;
then do what's possible;
and suddenly you are doing the impossible."
- *Francis of Assisi*

Contents

Preface

Although we might not notice it during our every day life, the ground we are standing on is moving, very slowly, and it has been doing so for billions of years. Today's common view of the Earth is that it has a hot and heavy solid inner and a liquid outer core, with a thick mantle around it, which is simply called the Earth's mantle. Roughly speaking, driven by temperature differences rocks of the mantle flow continuously, a process known as convection, similar to air that flows up when it is heated, but much slower. The outermost skin of our globe, also known as the Earth's lithosphere is wrapped around the Earth's mantle, not as a whole piece but as pieces of a puzzle, fitting together. These pieces or plates, all together called lithosphere, consist of two components: thin oceanic lithosphere and thick continental lithosphere (on which we live). Lithosphere floats on the underlying mantle but oceanic lithosphere float deeper than continental lithosphere because they are heavy. It is therefore a natural place for all the water to collect in oceans, because those are the lowest places on the Earth's surface. Lithosphere has travelled around the globe quite a lot through Earth's history. It had already been recognised centuries ago that the coastline of Africa and South America fit nicely together. Most of the important work that proved these continents were once positioned next to each other done by Alfred Wegener was of course based on how the continents fitted together because they were not covered by oceans and we could see and map them. It therefore became known as continental drift, although the oceanic lithosphere had to move as well. This phenomenon, continental drift, though unnoticable for many of us on a daily basis, never proceeds quietly. Because the upper part of the moving lithosphere, the Earth's crust, is strong (we build our houses on it) forces resulting from plates moving in opposite directions build up until at some point some parts of the plate break which causes earthquakes. Earthquakes happen continuously every day spread over the whole world as a result of this movement in the Earth's crust. In particular (most spectacular) cases when two plates collide with each other mountains develop at the surface. Of course this is accompanied by earthquakes, but also volcanism is a common phenomenon associated with it. These often catastrophic events are the surface expressions of processes associated with the collision of plates. Therefore an understanding of these processes is fundamental to our understanding of catastrophic events and this knowledge may possibly help to avoid human catastrophies. On the other hand, curiosity of human kind is a driving force to understand how things work in general. The way to study processes below the surface is by measuring shockwaves from earthquakes (seismology), or study the volcanic rocks that erupted at the surface. But we cannot go there. Fortunately, there are places on Earth where we can find rocks or whole areas that once have

been in the interior of collision of plates. There we can actually walk through a part of an old collisional zone and study the result of processes frozen in time. Along the westcoast of Norway rocks from the deep interior of the former Caledonian mountains that resulted from the collision of two plates Baltica in the east and Laurentia in the west crop out at the surface (in the field). The work presented in this thesis is done on rocks from that area.

The question how we know that the rocks found along the westcoast of Norway were part of the deep interior of the Caledonian mountains is closely related to the scientific questions addressed in this thesis. In fact, most of this work consists of finding out where the rocks come from. They obviously come from deeper in the Earth, but how deep is a question that can be debated. To find this out there are two different approaches in use, corresponding to two different groups of specialisation. One group consists of petrologists and the other of structural geologists. Structural geologists make reconstructions by measuring structures in the field. Once this is established it is possible to see which rocks have been at the deepest structural level.

What petrologists look at in the rocks that crop out at the surface are the minerals that make up the rock. By studying these minerals we can try to work out the origin of formation of the rock. A lot of valuable knowledge of minerals comes from laboratory experiments.

Rocks usually have a long history during which the original minerals can have reacted to form different minerals following a change in temperature (T) and pressure (P) and this process of metamorphosis is called metamorphism. In addition, very important for this thesis is that we can also have a change in chemical rock composition (C) that causes minerals to transform into other minerals. This process is called metasomatism. Metamorphic and metasomatic processes are not necessarily complete when the rocks finally arrive at the surface and rocks often show several stages of metamorphism or metasomatism. Therefore we need to study textures and chemistry of rocks using a microcope or electron microprobe to analyse the chemistry of individual minerals. This can help to determine the different stages of reactions between minerals. In addition we can date rocks by measuring the isotopic composition of certain elements that can decay radioactivally to other elements like uranium can decay to lead. Once we are certain about P-T-C and time of the rocks and minerals we can start thinking about the processes and mechanisms behind the formation of the studied rocks.

This thesis is a collection of papers, either published (Chapter 1 and 2), submitted (Chapter 5) or in the final stages before submitting it to a journal (Chapter 3 and 4). Along the coast between the villages Bud and Tornes, north of Molde in West Norway below a hill named Svartberget, an Fe-Ti type garnet-peridotite crosscut by garnet-phlogopite-websterite veins is exposed. These rocks are studied in this thesis. The order of the chapters follows the course of research questions described in a popular scientific way in the previous paragraphs. Chapter 1 to 4 deal with the identification of the rocks, the estimates of P-T and all complications of multiple overprinting phases of incomplete metamorphism and metasomatism. With Chapter 5 the thesis ends by presenting a model that includes a mechanism behind all the observed features of the Svartberget body. The title of the thesis becomes most clear in this chapter because it couples ultra-high pressures (UHP) and fracturing with the effect of melting and chemical reactions along the fractures.

In other words, physical and chemical processes interact and provide a mechanism for the processes that took place in the interior of the Caledonian mountains.

The first chapter can be seen as a pioneer study in which we found rocks that were part of the deep interior of the Caledonian mountains. It describes the discovery of the high pressure Svartberget peridotitic rocks along the westcoast of Norway that form an enclave (or body) in a part of the old continent Baltica that became involved in a continental collision with Laurentia to form the Caledonian mountains. A first detailed map presents the regional geology surrounding the Svartberget peridotite and a second small scale detailed geological map shows the peridotite body itself. It shows how the body is crosscut by fractures filled with veins. P-T estimates and Sm-Nd dating of the Svartberget body serve as first evidence that the original mineralogy of these rocks became metamorphosed to UHP during the Caledonian Orogeny. In addition Sr isotopes indicate that fluids were involved during the formation of the crosscutting veins.

The second chapter is still in the fase of identifying where the rocks come from and what pressures they have experienced. It presents the discovery of diamond in veins that cut the peridotite, discusses some of the history of the UHP in Norway and shortly describes a classical controversy. It provides an introductionary background to the problems to be explored in the other chapters.

The third chapter explores the Svartberget peridotite and the crosscutting fracture system in more detail. Now that the problems were defined in the previous chapters a new and more detailed look at the rock was needed and the chapter comes with a more detailed geological map of the Svartberget peridotite. Detailed whole rock and mineral chemistry, Sr isotopes and U-Pb dating is used to investigate the reactions along the fracture system. A conceptual model for the formation of the veins is presented. The chapter shows how metasomatism can change rocks completely so that the origin of the original rock is obscured.

The fourth chapter discusses a major problem that rises when trying to estimate the P-T conditions of the Svartberget peridotite. It proposes several possible solutions to the problem.

Finally in the fifth chapter the mechanisms behind the formation of all the rocks are discussed. A complete conceptual model ties up all data into an alternative model for UHP in the Svartberget peridotite. It test the feasibility of this conceptual model using finite element method (FEM) to calculate forces and pressures resulting from melting of rocks deep in the Earth's crust.

The work in this thesis was performed at 'Physics of Geological Processes (PGP)' during the period November 2005-February 2009. PGP is an incredibly inspiring, independent, multi-disciplinary research group paid by the Norwegian Research Council, hosted by the Department of Physics at the University of Oslo and lead by Professor Bjørn Jamtveit. It consists of physicists and geologists that work together to bridge the gap between physics and geology, a very challenging goal, but not impossible as shown in this thesis.

Many people have contributed to this thesis one way or another.

My first gratitude goes to my principal scientific supervisor Yuri Podladchikov. Besides being a very pleasant and intriguing person at the same time, Yuri spends an extraordinary amount of time on education, scientific discussions and social activity with his students including me. During these three years we have covered

an enormous range of concepts, theories, methods in thermodynamics, physics and mathematics by having long-lasting lectures and discussions in the seminar room at PGP; too much to be possibly digested by the brain, fully understood and presented in a single thesis in such a short period of time. However, to have learned about all of it is the best start to continue the attempt to bridge the gap between physics and geology in my future career.

I am also grateful to the infinite amount of time, patience and devotion my second scientific supervisor Håkon Austrheim has had for me. Håkon was always there when I had questions and I had the priviledge to learn from his enormous talent and experience in petrography. He pointed out important problems and possible clues from looking at the textures and mineral-chemistry in the rocks, which inspired me and puzzled me at the same time.

Torgeir Andersen, as third scientific supervisor, has acted as a diplomatic advisor, supporting ideas and helping me to maintain the balance between the often very opposing views of Yuri and Håkon on the subject.

Many thanks also for my coauthors, Herman van Roermund, Gareth Davies, David Smith, Timm John, Fernando Corfu and Remco Hin and my students in the field that contributed to some of the data in this thesis, Ineke Wijbrans en Marinus den Hartogh.

Timm John who has been working in the office next to me, has contributed to a lot of discussion on the subject of this thesis and I could count on his advice and support any time I needed it.

I want to thank Nina Simon for many discussions and for updating me regularly with the relevant and most recent scientific articles.

I thank my group leader Karen Mair for her advice on the practical aspects of doing a PhD.

Of course, I thank all my friends and collegues at PGP for their scientific and social contributions.

Although they did not contribute scientifically, I thank my family and friends that contributed indirectly by supporting me during the PhD through sometimes difficult times, especially in the beginning of the PhD after leaving home and starting a whole new life. During this time my Norwegian cousin Ann-Kristin and her husband Stein have invited me numerous times and I had good fun with the kids and enjoyed nice Norwegian dinners and parties at their place, which certainly made life beyond the PhD more enjoyable.

Finally, I thank my wife Arianne for all her support, patience, happiness and care for me during the whole period of my PhD.

Introduction

This thesis deals with some of the classical problems that rise from the discoveries of ultra-high pressure (UHP) mineralogy in rocks of the Western Gneiss Region (WGR) in Norway (Smith, 1984). The WGR is well known for its occurrences of HP to UHP rocks, mainly found as eclogite and peridotite boudins and lenses and more rarely within felsic gneisses. The HP-UHP metamorphism (HPM-UHPM) was associated with the continental collision between Baltica and Laurentia around 400 Ma ago (Torsvik et al., 1996). Present observations document a regional metamorphic gradient increasing towards the northwest (Labrousse et al., 2004), and structures in the field can account for the exhumation of the (U)HP rocks from 2.5 to 3 GPa. Three distinct 'UHPM domains' have been identified, predominantly along the NW margin of the WGR (Root et al., 2005).

A new UHP microdiamond locality in the northernmost UHPM domain, called Svartberget, is presented in the first part of the thesis. At the Svartberget locality an Fe-Ti type grt[1]-peridotite that is crosscut by Caledonian phl-grt-websterite and garnetite veins is exposed. Peak P-T estimates for the crosscutting veins reach about 5.5 GPa at a temperature of 800 °C, supported by the presence of microdiamond. Initial $^{87}Sr/^{86}Sr$ ratios in bulk rock and mineral samples from the veins and peridotite have values of 0.735-0.743 and 0.723, respectively, and indicate that crustally derived fluids interacted with the Svartberget peridotite.

The study of interaction of fluids with rocks at UHP conditions is fundamental for the understanding of P-T estimates derived with equilibrium thermodynamic calculations. Fluids are also critical for the behaviour of major and trace elements and isotopes that are used to infer the origin and age of observed UHP rocks. It is therefore necessary to investigate this in detail before dealing with large scale geodynamic implications. This detailed investigation forms the middle part of the thesis.

Assuming lithostatic pressures diamond-bearing rocks in the northernmost UHP domain of the WGR must have come from a burial depth of more than 150 km. However there is a lack of observable structures in the field to explain exhumation from extreme UHP conditions (5.5 GPa or more) to normal HP-UHP conditions (2.5-3GPa), which are common pressures calculated from eclogites in western parts of the WGR. Because of the regional and mostly coherent metamorphic gradient across the WGR terrain it is difficult to account for local extreme pressure excursions such as documented from within the Svartberget peridotite. The last part of the thesis is devoted to this problem and a conceptual model is presented that explains the pressure variations and extreme pressures and fits available structural

[1]Mineral abbreviations according to Kretz (1983)

field observations.

After introducing the Svartberget Fe-Ti type grt-peridotite in Chapter 1 and providing evidence for the existence of microdiamond at this locality in Chapter 2, the Svartberget peridotite is investigated in detail. In Chapter 3 evidence to obtain understanding of mineral reactions and interaction of the peridotite with its hosting felsic gneiss is presented. It shows how the body is metasomatised along crosscutting fractures resulting in formation of websterite and garnetite zones. In Chapter 4 the problem of incomplete reactions and variable pressure estimates is discussed and possible solutions are evaluated. Chapter 5 ends the thesis by describing a conceptual model for the UHP and variable pressure variations observed in the Svartberget rocks supported by a test of the feasibility of such a model using finite element method (FEM). The suggestions that extreme UHP conditions may be achieved by a different mechanism than burial have profound influence on the concepts of UHP-metamorphism and in turn on the geodynamics of continental collision. It introduces a concept that allows a different view on UHP-metamorphism and will be developed in future research.

Chapter 1 introduces the Svartberget Fe-Ti type garnet-peridotite locality in the WGR of Norway. It describes the regional geology surrounding the body and presents a detailed geological map of the peridotite, which shows that the body is crosscut by a network of phl-grt-websterite and garnetite veins. P-T estimates are presented for a sample from peridotite and from a websterite vein that yield pressure (P) and temperature (T) estimates around 3.4 GPa, and 800 °C for the peridotite body and 5.5 GPa, and 800 °C for the websterite veins consistent with UHP conditions. Garnet-cpx mineral pairs yield a Sm-Nd cooling age of 393 ± 3 Ma for the peridotite and 381 ± 6 Ma for the vein assemblage. High $^{87}Sr/^{86}Sr$ ratios in these grt-cpx mineral pairs are presented and combined with polyphase solid inclusions in garnet, consisting of silicates, carbonates, sulphates and elemental carbon (including microdiamond), that are typical for supercritical COH fluids, it concludes with the possibility that the peridotite body was infiltrated by crustal-derived COH melts/fluids at UHPM conditions during the Caledonian Orogeny to form the phl-grt-websterite veins at diamond-grade P-T conditions.

Chapter 2 presents Raman spectroscopic data that proof the existence of microdiamond in the polyphase solid inclusion assemblages in garnet from the websterite veins that crosscut the Svartberget peridotite. It starts with a short overview of the problems and existing explanations related to UHP metamorphic terrains followed by a short history of UHP discoveries in the WGR. After characterising the microdiamond and associated mineral assemblage the chapter concludes that the microdiamond is formed during the Caledonian Orogeny.

Chapter 3 investigates in detail the metasomatism in the Svartberget peridotite and its crosscutting veins. An updated and more detailed map of the body and surrounding gneiss is presented along with a detailed description of the mineralogy of different lithological zones that can be found in the veins. Field observations show different stages in the alteration of the peridotite rocks, which is most intense in the

core of the veins. The most pristine samples of the body are already affected by a crustally derived metasomatic agent suggested by elevated $^{87}Sr/^{86}Sr$ initial ratios. This is supported by textural evidence in these samples. Then there are blocks of the body that consist of grt-ol-websterite followed by more altered blocks that lack olivine and some patches of opx-rich coarse-grained phl-grt-websterite that look like former blocks of the main body. Between all those blocks are ultra-coarse phl-grt-websterite, followed by coarse phl-grt-websterite, grt-websterite and garnetite. Locally these garnetites become eclogitic towards a core of retrograde-omphacitite which occassionally have an amph-pegmatite core. Changes in mineral modes are accompanied by changes in mineral-chemistry from most pristine peridotite to most altered samples. All minerals become less Mg-rich with increasing alteration. Garnet, cpx, and amph display decreasing Cr contents towards the most altered rocks, with a positive excursion within the various websterites. The Na concentrations in amphibole and most significant in cpx increase with degree of alteration. FeO and CaO generally follow a positive linear trend from most pristine towards the most altered samples. In contrast, they generally follow a negative trend for SiO_2 and Al_2O_3. Concentrations of the fluid mobile elements increase from the most pristine samples towards the garnetites. Initial $^{87}Sr/^{86}Sr$ values start from elevated values about 0.723 in most pristine samples and show an increasing trend up to ~ 0.743 in most altered samples. Single zircon U-Pb dating suggest metamorphic growth of zircon in the garnetite at 397.2 ± 1.2 Ma, either coinciding or predating an initial phase of leucosomes formation, crystallization of amph-pegmatite cores, rutile and monazite at 393-388 Ma. Sharp compositional contrasts of Cr within individual grains display rather complex vein-like or patchy zoning of Cr in grt and cpx and Al in opx in grt-peridotite, grt-phl-websterite and garnetite samples. The detailed geological digitised map was used together with bulk rock chemistry to perform mass balance calculations that quantify the metasomatism. Finally a conceptual model is presented based on the provided data. In the early stages of fracturing garnetite-websterite formation is limited. When fractures opened by forceful injection of felsic material element exchange between these pegmatites and the wall rock resulted (a) in the transformation of pegmatite to garnetite and (b) wall rock peridotite to several distinct websterite zones.

Chapter 4 documents the survival of low pressure primary spinel assemblages in the wall rock of the peridotite, in constrast to the diamond-bearing crosscutting phl-grt-websterite veins. It describes microtextures that reveal various stages of incomplete reactions and equilibration. The earliest preserved assemblage consists of mt-ilm-sp aggregates that occur randomly throughout the rock. Olivine most likely belongs to this early stage and occurs in texturally equilibrated domains. These domains are partly resorbed by opx and cpx that have a strong crustal signature, leaving no doubt that the cpx and opx are secondary. The pyroxenes are texturally equilibrated. Garnet formed latest, has irregular grain boundaries and resorb the olivine and pyroxene domains. Garnet is often interstitial, poikilitic and contains rounded inclusions of cpx-opx-ol. Occassionaly garnet shows equilibrium textures with the pyroxenes. In the veins oxides and olivine disappear, phlogopite appears, grainsize increases and all minerals developed more towards an equilibrated texture, the pyroxenes being euhedral and garnet less poikilitic and resorptive than in the pe-

ridotite. Sharp compositional contrasts occur within a few micron in garnet and are 'frozen' in time. They indicate that diffusion stopped before smoothening compositional gradients. The chapter discusses unusually slow diffusion, rapid exhumation, metasomatically controlled mineral reactions at low-temperature conditions or any combination of the three as possible explanations to the contrasting pressure estimates and preserved sharp compositional contrasts in minerals and veins. Finally, it is suggested that the pressure vessel effect that results in large pressure variations during the preservation of coesite in garnet may be applied up to the outcrop scale during UHP metamorphism.

Chapter 5 concludes the thesis with a conceptual model that combines all data from previous chapters into a coherent explanation. An alternative mechanism to burial for the origin of UHP in the Svartberget peridotite is proposed. The model starts from the point that the Svartberget body is enclosed in basement gneiss of the WGR somewhere in the lower crust. During burial and heating rocks surrounding the peridotite start to melt, but surrounding non-molten rocks confine the space and pressure builds up. The small amount of interstitial melt that accumulates between grains adjacent to the peridotite lower the yield strength of the peridotite which causes the rock to reach the brittle fracture criterion and conjugate brittle shear fractures develop. Melt (or supercritical fluid) that has the same pressure (5.5 GPa) as the surrounding gneiss can flow in as soon as fractures propagate into the peridotite. This supercritical fluid is now highly reactive and metasomatism takes place at UHP conditions along the fractures capturing microinclusions of diamond while growing. Finally the lithosphere holding the overpressured gneiss constrained breaks due to formation of large scale fractures in the crust and decompression melting starts. Now that the gneiss is not constrained to a certain volume it can flow ductily and it is highly unlikely that any UHP mineral survived in such a deforming fluid rich environment. The chapter further presents a first feasibility study using finite element method (FEM). Using a set up with three materials, geometrically arranged as two rings around a small enclave, the largest volume and outer ring similates the lithospheric non-molten rocks, included in this in the inner ring are migmatitic gneisses with an enclave in the middle representing the peridotite. Melting of the gneiss results in pressure variations when gneiss is ten times weaker than surroundings and peridotite enclave. These pressure variations are qualitatively similar to observations in the field. With a viscosity of 10^{22} Pa·s and thermal expansion coefficient derived from the solidus and liquidus for a comparable chemical system a pressure of several GPa is maintained for a period of 10 000 Ma. This is enough for UHP mineralogy to develop.

Appendices of the thesis consist of supplementary material that includes the detailed geological map of the Svartberget body (Appendix A.1) and a table that belongs to Chapter 3 (Appendix A.2). Appendix B is an essay about metasomatic zoning including application to the Svartberget metasomatic zoning. This essay contains preliminary results which illustrate how metasomatic zoning such as observed in Svartberget can be produced by infiltration of a fluid and subsequent reaction with the wall rock. The main zoning of garnetite and websterite observed in the fractures of the peridotite body is reproduced with numerical modelling. Finally, ap-

pendix C presents all codes (except for standard geothermobarometric calculations) used for the calculations in this thesis.

References

Kretz, R. (1983). Symbols for Rock-Forming Minerals. *American Mineralogist*, 68(1-2):277–279.

Labrousse, L., Jolivet, L., Andersen, T., Agard, P., Maluski, H., and Schärer, U. (2004). Pressure-temperature-time-deformation history of the exhumation of ultra-high-pressure rocks in the Western Gneiss Region, Norway. *Geol. Soc. Am., Special Paper*, 380:155–183.

Root, D. B., Hacker, B. R., Gans, P. B., Ducea, M. N., Eide, E. A., and Mosenfelder, J. L. (2005). Discrete ultrahigh-pressure domains in the Western Gneiss Region, Norway: implications for formation and exhumation. *Journal of Metamorphic Geology*, 23(1):45–61.

Smith, D. C. (1984). Coesite in clinopyroxene in the Caledonides and its implications for geodynamics. *Nature*, 310(5979):641–644.

Torsvik, T. H., Smethurst, M. A., Meert, J. G., VanderVoo, R., McKerrow, W. S., Brasier, M. D., Sturt, B. A., and Walderhaug, H. J. (1996). Continental break-up and collision in the Neoproterozoic and Palaeozoic - A tale of Baltica and Laurentia. *Earth-Science Reviews*, 40(3-4):229–258.

Chapter 1

Evidence for diamond-grade ultra-high pressure metamorphism and fluid interaction in the Svartberget Fe-Ti garnet peridotite-websterite body, Western Gneiss Region, Norway [1]

1.1 Abstract

Based on mineral-chemical evidence we propose that the northernmost Scandian ultra-high pressure (UHP) metamorphic domain within the Western Gneiss Region of Norway can be extended 25 km northeastwards. A newly discovered, well preserved, fine-grained, Fe-Ti type garnet peridotite body at Svartberget, located in the Ulla Gneiss of the Møre og Romsdal area north of Molde, is cut by a network of systematically orientated coarse-grained garnet-websterite and garnetite veins. Standard thermobarometric techniques based on electron microprobe analyses yield pressure (P) and temperature (T) estimates around 3.4 GPa, and 800°C for the peridotite body and 5.5 GPa, and 800°C for the websterite veins consistent with UHP conditions. In addition, polyphase solid inclusions, consisting of silicates, carbonates, sulphates and elemental carbon (including microdiamond), are randomly located in garnet and clinopyroxene of the websterite vein assemblage. Garnet-clinopyroxene mineral pairs yield a Sm-Nd cooling age of 393 ± 3 Ma for the peridotite and 381 ± 6 Ma for the vein assemblage suggesting that the Svartberget body was overprinted during the UHPM of the Scandian Orogeny. The initial ratio of the mineral isochron and Nd model ages suggest a mid-Proterozoic origin for the peridotite body. The polyphase inclusions, coupled with high $^{87}Sr/^{86}Sr$ ratios may indicate that the peridotite body was infiltrated by crustal-derived C-O-H melts/fluids at UHPM conditions to form the websterite veins in the diamond field. We

[1]Vrijmoed, J. C., H. L. M. van Roermund, G. R. Davies, 2006, *Mineralogy and Petrology*, 88, 381-405

propose that fracturing and vein emplacement were the result of local high fluid pressure during subduction of the Baltic plate.

1.2 Introduction

The Western Gneiss Region (WGR) (Fig. 1.1) of SW-Norway consists of Proterozoic basement gneisses, remobilised in the Caledonian, that are interpreted to represent the outermost western part of the Baltic plate and overlying allochthonous units that have been correlated with the Caledonian nappes in northern and central Scandinavia (Krill, 1980; Bryhni, 1989; Robinson, 1995). The coastal part of the WGR (Fig. 1.1) is characterized by the occurrence of ultra-high pressure metamorphic (UHPM) rocks. Evidence for UHPM comes from the discovery of coesite and micro-diamond in peridotite, eclogite and kyanite-garnet gneiss (Smith, 1984; Dobrzhinetskaya et al., 1995; Van Roermund et al., 2002) and/or from the application of standard geothermobarometric techniques (Terry et al., 2000). Three distinct UHPM domains have previously been recognised (Root et al., 2005) (Fig. 1.1). In this paper we will focus on the size and magnitude of the northernmost UHPM terrane, initially discovered by Dobrzhinetskaya et al. (1995) and following vigorous debate, subsequently confirmed by Terry et al. (2000) and Van Roermund et al. (2002). Lateral eastwards and southwards expansions of the northernmost UHPM terrane towards, and across the islands of Otrøy and Fjørtoft were recently reported (Van Straaten et al., 2003; Van Roermund et al., 2005; Carswell et al., 2006). During the summers of 2003 and 2004, we performed a detailed field study/mapping project along the continuously exposed western coastline between Bud and Tornes (north of Molde; Figs. 1.1 and 1.2). This study reports the discovery of a well preserved Fe-Ti type garnet peridotite body, named Svartberget, exposed within felsic gneisses of the WGR (Carswell and Harvey, 1982). The felsic gneisses are often migmatitic and have tonalitic to dioritic compositions. This gneiss unit is recognised in neighbouring areas (e.g. Fjørtoft, Otrøy) as the Ulla Gneiss (Terry and Robinson, 2003). We present electron microprobe (EMP) mineral analyses and use standard geothermobarometric techniques and mineralogy to demonstrate that the Svartberget body has been metamorphosed within the UHPM field indicating that the northernmost UHP domain extends more than 25 km further northeastwards than previously recognised (Fig. 1). In addition, we report isotope geochemical data that give strong indications for fluid infiltration of the Svartberget peridotite, and we investigate the original intrusion and subsequent metamorphic age of the Svartberget Fe-Ti peridotite body.

1.3 Regional geology

The large-scale structure and geology of the WGR and surrounding areas are presented in Fig. 1.1. The WGR is a reworked large Caledonian basement window, presumably connected to the Baltic plate in the east (Cuthbert et al., 2000). During the Caledonian Orogeny the Iapetus Ocean closed (Torsvik et al., 1996) and oceanic fragments, island arcs, microcontinents, imbricated basement slivers and overlying late Proterozoic-early Paleozoic sediments were thrust, from west to east, over the

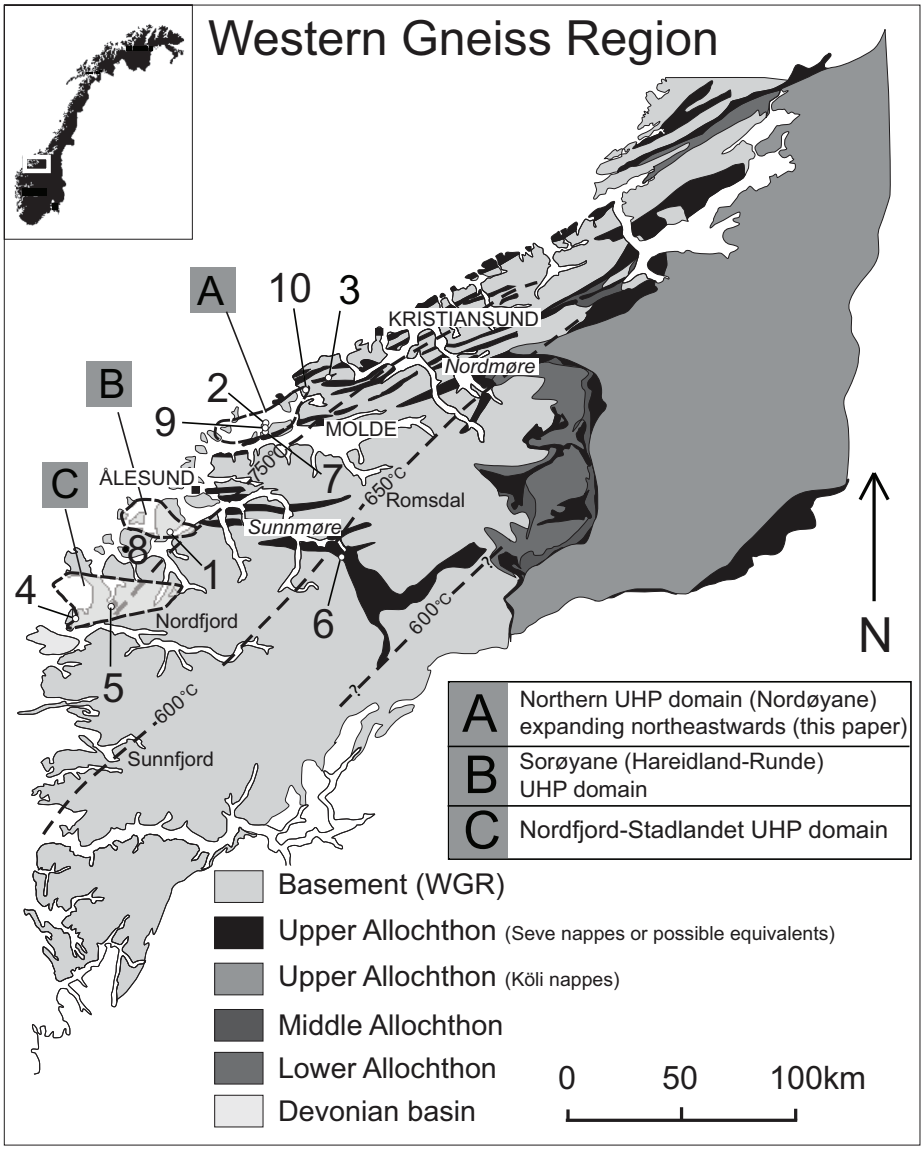

Figure 1.1: Overview of the Western Gneiss Region (WGR) and overlying Caledonian thrust nappes in the surrounding area. The three distinct UHP domains within the WGR are shaded. Numbers indicate the following garnet peridotite localities: Fe-Ti type: *1* Eiksunddalen; *2* Raknestangen; *3* Kolmannskog; *4* Lyngenes; *10* Svartberget. Mg-Cr type: *5* Almklovsdalen; *6* Kalskaret; *7* Ugelvik; *8* Sandvik; *9* Raudhaugene (from Carswell et al., 1983). The temperature gradients are shown (after Krogh, 1977). The Figure is compiled after data from Krogh (1977); Bryhni and Sturt (1985); Griffin et al. (1985); Robinson (1995); Root et al. (2005).

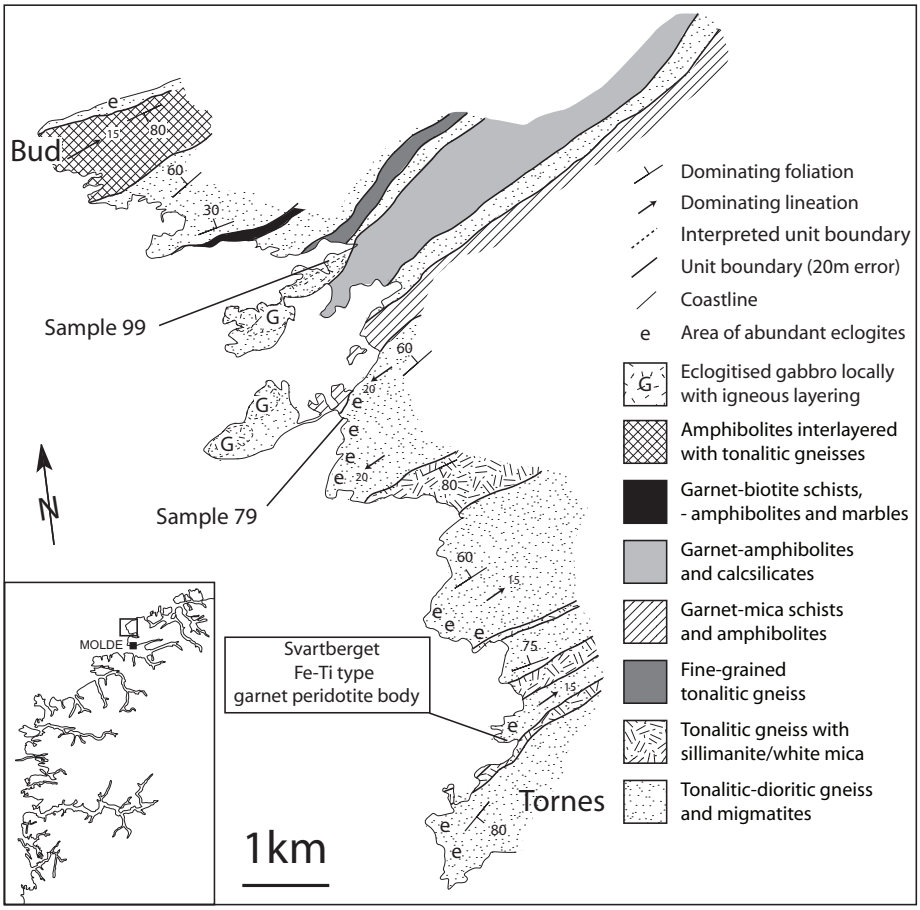

Figure 1.2: Geological map of the Tornes-Bud area

basement/Baltic plate as nappes (Roberts, 2003; Brueckner and Van Roermund, 2004). Post-dating regional nappe transport, Baltica subducted to UHP conditions during the latest part of the Scandian Orogeny (Hacker et al., 2001; Carswell et al., 2003b). The overlying supracrustal nappes can now be found to the north, east and south of the WGR, underneath the Devonian basins in the west and at isolated, scattered, areas throughout the WGR.

1.3.1 The Bud-Tornes area

Post-dating the Scandian UHPM, the rocks of the WGR were strongly folded at the macro-scale (km) resulting in a NE-SW trending structural pattern in which the Caledonian nappes can be traced in dominantly syn- but also anti-formal structures with subvertical axial planes (Krill, 1985; Robinson, 1995; Krabbendam and Dewey, 1998). These folds are interpreted to be related to the exhumation of the UHPM terrane (Seranne, 1992; Andersen, 1998; Krabbendam and Dewey, 1998). Whether

the folds are synchronous or actually post-date exhumation is still debated, but they were formed in rocks that were at amphibolite facies conditions. Two of these, apparent synclinal, folds are exposed in the studied area and involve possible Caledonian nappes and Proterozoic basement elements (Robinson, 1995; Tveten et al., 1998). Our structural and lithological analysis of these NE-SW trending supracrustal 'synforms' revealed that the investigated structures are much more complicated than previously mapped (Tveten et al., 1998). We found no evidence that was consistent with a synformal character. The detailed geological map, illustrated in Fig. 1.2, is a simplified version of our field-map, which displayed too many individual lithological units to be reproduced here. Individual units were grouped into major units on the basis of field characteristics and rock type to form Fig. 1.2. All units are strongly deformed and often mylonitic. The major lithological units in Fig. 1.2 are:

1. *Tonalitic-dioritic gneiss and migmatites.* This unit is referred to as Ulla Gneiss in neighbouring areas, shows transpositional folds in many places and variable degrees of migmatisation and strain=mylonitisation. The unit contains abundant eclogites, amphibolites and some gabbros.

2. *Tonalitic gneiss with sillimanite and/or white mica.* This unit occurs within unit (1) described above. Garnet is present locally and in some places the dominant rock type is schist, especially where white mica is more abundant.

3. *Fine-grained tonalitic gneiss.* This unit displays strong deformation in localised shear zones. Abundant feldspar (often <0.5 cm in size), and subordinate garnet porphyroclasts are present.

4. *Garnet-biotite schist, amphibolite and marble.* Different rock units alternate on a scale of several decimeters to meters. The schist contains 1-2 cm sized garnet porphyroclasts, abundant biotite, plagioclase and amphibole. The amphibolite consists of amphibole, plagioclase and in some layers abundant garnet porphyroclasts. Marble was found as single layers with a maximum thickness of 20-30 cm.

5. *Garnet-amphibolite and calcsilicate.* Dominantly layered amphibolites with plagioclase, biotite and abundant garnet porphyroclasts. Minor amounts of foliated biotite-rich amphibolites and single calcsilicate layers (10-20 cm thick).

6. *Amphibolite interlayered with tonalitic gneiss and garnet-biotite schist.* Amphibolitic bands alternating with quartzo-feldspathic gneiss bands and rusty weathered garnet-biotite schists. Some amphibolite layers contain abundant garnet porphyroclasts.

7. *Garnet-mica schists and amphibolites.* Layered unit consisting dominantly of mylonitic garnet mica-schist, and garnet amphibolite, and subordinate fine grained biotite-plagioclase-quartz gneiss up to several meters thick.

Previous workers have mapped this and neighbouring regions (Carswell and Harvey, 1982; Mørk, 1985b; Bryhni et al., 1989; Robinson, 1995; Terry et al., 2000) and a 1:250.000 geological map was recently published (Tveten et al., 1998). In general the divisions made to form our field units (see Fig. 1.2) are in agreement with

those of Bryhni et al. (1989). In this area no correlation can be made with the mid-Proterozoic augen gneiss units found northwest of Molde and on Otrøy (Carswell and Harvey, 1982). Our tonalitic-dioritic gneiss and migmatite (unit 1), Ulla Gneiss, correlates with the undifferentiated paragneiss unit of Carswell and Harvey (1982); Harvey (1983) and the Baltica basement described by Robinson (1995). Bryhni et al. (1989) describe this unit as undifferentiated, usually migmatitic gneiss of Precambrian age, named the Valsøyfjorden Complex. The tonalitic gneiss with sillimanite/white mica (unit 2) also correlates to the Valsøyfjorden Complex of Bryhni et al. (1989). All other units are equivalent to the metamorphosed supracrustal rocks from the Ertvagøy Group (Bryhni et al., 1989). Our garnet-biotite schist, amphibolite and marble unit (unit 7) may be correlated to the Blahø-Surna Nappe of Robinson (1995). Our experience, however, is that regional correlation between individual units remains difficult. Possible thrust contacts between individual units are unrecognisable because the area is dominantly a high-strain/ mylonite zone.

1.4 The Svartberget Fe-Ti type garnet peridotite-websterite body

Garnet peridotites in the WGR have been divided into Mg-Cr and Fe-Ti type (Carswell et al., 1983; Krogh and Carswell, 1995). The Mg-Cr type garnet peridotites have upper mantle affinities; whereas the Fe-Ti type garnet peridotites form most likely in the mid-Proterozoic as lower crustal cumulates of layered mafic igneous intrusions (Schmidt, 1963; Mørk, 1985a,b; Jamtveit, 1987b,a). They are called Fe-Ti type because: 1) the bulk chemistry is high in iron (Fo 70-80) and 2) the rocks contain 1-5 modal% Fe-Ti oxides and green spinels (Carswell et al., 1983). In Fig. 1.1 it can be seen that the Svartberget garnet peridotite body lies along strike with other known occurrences of Fe-Ti type peridotite (Raknestangen, nr. 2 on the island Otrøy and Kollmanskog, nr. 3 north of Molde). The Svartberget Fe-Ti type garnet peridotite body (1600 m^2) has been mapped in detail (Fig. 1.3). Figure 3 shows that the peridotite body has undergone extensive fracturing prior to, or associated with the emplacement of garnet-bearing websterites, that are variable in their modal abundance and distribution of garnet and pyroxene, and that are strongly associated with garnetites (garnetite-websterite veins, Fig.1.3). The websterite veins associated with garnetite and the garnetite form a unit that define a network with pronounced preferred orientations (poles to the planes: ∼260/10 and ∼200/10, Fig. 1.3b) that cut the peridotite into individual blocks that range in area from 1 to 10 m^2. In regions where websterite is strongly associated with garnetite (e.g. garnetite-websterite veins in Fig. 1.3), the garnet-bearing websterite veins are themselves cut by garnetite. The garnetite can form layers up to 10 cm thick, and is usually found in the cores of the websterites, but it can also form pods or complex networks of smaller veins that cross-cut the websterites. Thick garnetite veins may have a core of phlogopite (<0.5 cm thick). In the south-western part of the body cross-cutting relationships indicate that coarse-grained to ultra-coarse grained garnet websterite occurs in a zone that is relatively older than the websterites cored by garnetites (Fig. 1.3). Post eclogite facies pegmatites occur in the northern part of the body. Locally some of the peridotite blocks are heavily altered or retrogressed. The peri-

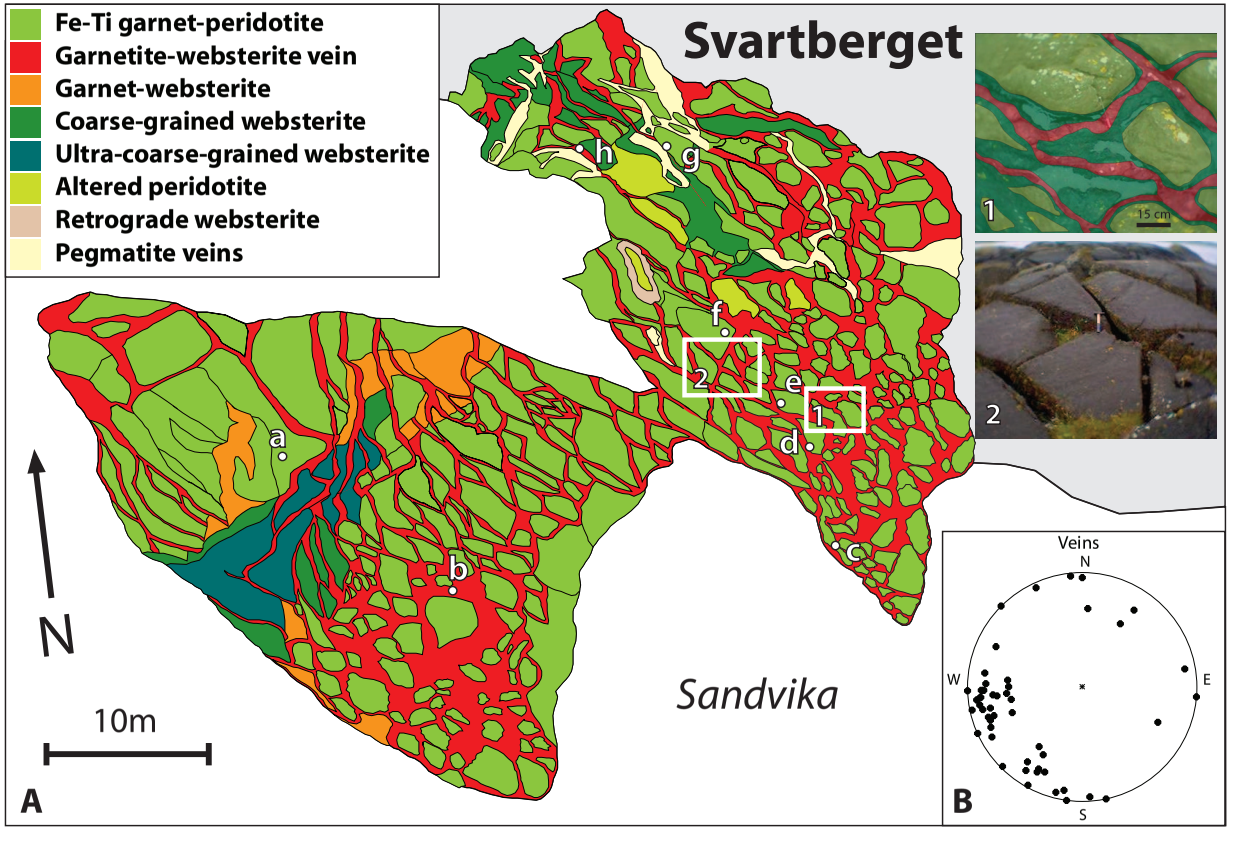

Figure 1.3: **(a)** Detailed map of the Svartberget Fe-Ti type garnet peridotite body (see text for further explanation). Samples taken for Sm-Nd isotope analysis are: a = 04-31; b = 04-33; c = 04-38; d = 04-37; e = 8; f = 04-2; g = 7; h = 6. Rectangles show location of inset Figs. 1 and 2. Inset 1 is an annotated field picture showing how the red coloured unit in the map, indicated in the legend by 'garnet-websterite veins', looks in more detail. Colours in inset 1: green = garnet-peridotite, dark-green = garnet websterite, red = garnetite. Inset 2 shows the preferred orientation of the veins. **(b)** Stereographic projection (lower hemisphere) of poles to the planes from measured veins (n = 50) establishing the preferred orientation of the veins seen in Fig. a.

dotite body consists of (<1 mm) garnet, clinopyroxene, orthopyroxene, olivine and 1-5 modal% Fe-Ti oxides. The modal olivine (Fo = 83) content varies between 20 and 30%, where approximately 5-10% is serpentinised. Cross-cutting garnet-bearing websterite consists of (1-5 mm) clinopyroxene, orthopyroxene, garnet and phlogopite (and very minor secondary amphibole). The garnetite veins generally consist of garnet and phlogopite. (Ultra) coarse grained websterite consists of orthopyroxene, clinopyroxene, garnet and phlogopite with grain sizes ranging between 2 and 5 cm (coarse grained) up to 20 cm (ultra coarse grained). Figure 1.3 (insets 1 and 2) illustrates some of the general structural relationships between the main body and garnet websterite and garnetite veins.

1.5 Methods and techniques

Electron microscopy was performed at the Electron Microscopy and Structure Analyses Centre, Utrecht University. EMP analyses were performed with the JEOL JXA-8600 Superprobe at Utrecht University. Operating conditions were 15 KV accelerating voltage and a beam current of 20 nA. Line-scans were made across all single grains to check for chemical-heterogeneity. Peak pressures (P) and temperatures (T) were estimated using the aluminium in orthopyroxene (in the presence of garnet) barometers $P_{H\&G82}$ (Harley and Green, 1982), PH_{84}, (Harley, 1984b), $P_{N\&G85}$, (Nickel and Green, 1985) and $P_{B\&K1990}$ (Brey and Köhler, 1990)in combination with the garnet-orthopyroxene Fe-Mg exchange thermometers T_{H84} (Harley, 1984a), $T_{L\&G88}$, (Lee and Ganguly, 1988), $T_{L\&G88}$ using $W_{Ca} = 1500$ (Carswell and Harley, 1990), $T_{B\&K90}$ (Brey and Köhler, 1990), and garnet-clinopyroxene Fe-Mg exchange thermometers $T_{R\&G74}$,(Råheim and Green, 1974), $T_{E\&G79}$ (Ellis and Green, 1979), T_{P85} (Powell, 1985), T_{K88} (Krogh, 1988), T_{R2000} (Ravna, 2000), two pyroxene thermometers T_{W77} (Wells, 1977) and $T_{B\&K90}$ (Brey and Köhler, 1990), the calcium in orthopyroxene and sodium in orthopyroxene thermometers $T_{B\&K90Ca}$ and $T_{B\&K90Na}$ (Brey and Köhler, 1990), respectively, and the garnet-olivine Fe-Mg thermometer $T_{O\&W79}$ (O'Neill and Wood, 1979) including the correction term of O'Neill (1980). Where used, ferric iron in clinopyroxene is estimated using the method of Droop (1987). Representative EMP analyses and P-T estimates of selected minerals are presented in Tables 1.1 and 1.2, respectively. Isotopic analyses were performed on a Finnigan Mat 262 RPQ plus thermal ionisation mass spectrometer (TIMS) at the Vrije Universiteit, Amsterdam, Sm-Nd isotope systematics are reported for 8 whole-rock samples (Table 1.3). The results of 2 garnet and 2 clinopyroxene separates from samples of the Svartberget body are given in Table 1.3. In addition minerals from surrounding 'country-rock' eclogites (sample locations, see Fig. 1.2) were analysed (Table 1.3). Sample locations for the Svartberget body are given in Fig. 1.3a. Rb-Sr isotope systematics were determined on garnet and clinopyroxene mineral separates. The minerals were leached for 15 minutes in 1.0 N ultra-clean HCl in an ultrasonic bath. The same procedure was repeated using 1.4 N ultra-clean HNO_3. The time of peak Scandian metamorphism in the region is estimated around 400 Ma (Hacker et al., 2001; Carswell et al., 2003a; Krogh et al., 2003), therefore all initial isotope ratios are reported for 400 Ma unless otherwise stated (Table 1.3), to allow assessment of the possible involvement of the continental crust

in the formation of the peridotite-websterite body.

1.6 Results and discussion

1.6.1 Mineral chemistry

We obtained mineral-chemical data from well-preserved parts of thin sections from a garnet-websterite vein (sample 6) and the peridotite body (sample 8). Sample 6 consists of 1-5 mm sized crystals of diopsidic clinopyroxene ($Wo_{46}En_{46}Fs_8$, Jd_4), orthopyroxene (En_{81-82}), garnet ($Pyr_{50-52}Alm_{35}Gross_{11-13}$) and phlogopitic biotite (Phl_{85}) (Fig. 1.4a). In contrast, the sample 8 is composed of smaller (<1 mm) diopsidic clinopyroxene ($Wo_{47}En_{48}Fs_5$, Jd_{1-2}), orthopyroxene (En_{84-86}, Al_2O_3), garnet ($Pyr_{56}Alm_{29}Gross_{13}$) and olivine ($Fo_{83}$) (Fig. 1.4b). Profiles of the Al_2O_3 abundances across selected orthopyroxene grains from samples 6 and 8 are illustrated in Fig. 1.4. The bowl-shaped Al_2O_3 profiles suggest that diffusion processes were operating along grain margins, due to partial re-equilibration during retrogression (Dodson, 1973; Ganguly and Tirone, 1999). In contrast, garnet, clinopyroxene and olivine show constant composition profiles across the grains.

1.6.2 Polyphase solid inclusions

Polyphase solid inclusions were found inside garnet and clinopyroxene from garnet websterite and garnetite vein samples. The inclusions are not found in the garnet peridotite body itself. The assemblages comprise carbon, magnesite, dolomite, monazite, apatite, xenotime, titanite, pyrite, chalcopyrite, pentlandite, galena, Fe-oxides, orthite, gypsum, Ba-sulphates (+Sr), Ca-sulphate (+Sr), (unknown) W-, Al- and Al-Cl-silicates, Al-Fe-Mg-oxides, opx, cpx and grt (Fig. 1.6a and b). Similar inclusions were described by Carswell and Van Roermund (2005) from the Bardane peridotite on Fjørtoft. A micro-Raman spectroscopic study of some carbon grains, performed by D. C. Smith in Paris, verified the presence of micro-diamond (Vrijmoed et al., prep). The inclusions are irregularly shaped and randomly distributed within garnet but some also occur in clinopyroxene. Many of the minerals that define the polyphase solid inclusion assemblage are not included in the mineralogy of the main peridotite body or the websterite veins (e.g. monazite, magnesite, dolomite etc.) implying that (some and/or all) elements must have been introduced from outside the garnet peridotite body. From the major element chemistry of these silicate, carbonate, phosphate and sulphate inclusions, in combination with elemental carbon it can be concluded that immiscible silicate-carbonate-sulphate fluids (or melts) were involved in the formation of these polyphase inclusions. Carbon precipitated under reducing conditions and some carbon formed as micro-diamonds, indicating that crystallisation took place within the diamond UHPM field. At UHPM conditions these immiscible fluids/melts are probably well above the so called second critical point where there is no distinction between melt and fluid (Stalder et al., 2000; Hermann, 2003). Such fluids/melts were referred to by (Carswell and Van Roermund, 2005) as C-O-H rich fluids.

1.6.3 Geothermobarometry

Peak P-T values were obtained using the lowest Al_2O_3 contents in cores of orthopyroxene grains in combination with core values of adjacent, chemically unzoned minerals (Table 1.1). The pressure-temperature conditions listed in Table 1.2 were obtained by combining the various thermometers reported in the method section with the Brey and Köhler (1990) barometer. The thermometers have also been

Table 1.1: Representative electron microprobe analyses of selected minerals from a specimen of the garnet peridotite body (sample 8) and a cross-cutting garnet websterite vein (sample 6)

Locality:	Svartberget						
Sample :	Main body				Garnet websterite vein		
Mineral:	Grt	Cpx	Opx	Ol	Grt	Cpx	Opx
Line no.:	8-4a	8-4b	8-4c	8-4d	6-20f	6-20d	6-20d
Spot:	Grt	Cpx	Opx	Ol	Grt	Cpx	Opx
SiO_2:	41.46	55.18	57.40	39.93	40.88	54.70	57.17
TiO_2:	0.01	0.00	0.02	-	0.03	0.01	0.00
Al_2O_3:	21.97	0.51	0.51	-	21.84	1.14	0.16
Cr_2O_3:	0.50	0.09	0.01	0.00	0.39	0.19	0.03
FeO:	14.66	2.98	10.23	15.82	18.12	4.67	11.78
Fe_2O_3:	-	-	-	-	-	-	-
MnO:	0.87	0.19	0.09	0.26	0.86	0.10	0.18
MgO:	15.73	32.39	32.39	44.60	14.53	15.88	31.16
CaO:	5.25	0.17	0.17	0.00	4.11	22.00	0.18
Na_2O:	0.01	0.01	0.01	-	0.01	1.07	0.00
NiO:	-	-	-	0.25	-	-	-
Total:	100.47	100.54	100.94	100.87	100.77	99.76	100.65
Py:	55.73	-	-	-	51.63	-	-
Alm:	29.14	-	-	-	36.13	-	-
Gr:	13.37	-	-	-	10.51	-	-
Sps:	1.76	-	-	-	1.73	-	-
Wo:	-	47.37	0.31	-	-	46.08	0.35
En:	-	48.02	84.68	-	-	46.30	82.20
Fs:	-	4.61	15.01	-	-	7.62	17.45
Jd:	-	0.92	-	-	-	2.58	-
Ac:	-	1.01	-	-	-	1.21	-
Di+Hed:	-	97.54	-	-	-	93.63	-
Fo:	-	-	-	83.40	-	-	-
Fa:	-	-	-	16.60	-	-	-
Cations:							
Si:	3.03	2.00	1.99	1.00	3.01	2.00	2.00
Ti:	0.00	0.00	0.00	-	0.00	0.00	0.00
Al:	1.89	0.02	0.02	-	1.90	0.05	0.01
Cr:	0.03	0.00	0.00	0.00	0.02	0.01	0.00
Fe(II):	0.89	0.07	0.30	0.33	1.12	0.12	0.35
Fe(III):		0.02	0.00	-	-	0.02	0.00
Mn:	0.05	0.00	0.01	0.01	0.05	0.00	0.01
Mg:	1.71	0.94	1.68	1.66	1.60	0.87	1.63
Ca:	0.41	0.92	0.01	0.00	0.32	0.86	0.01
Na:	0.00	0.03	0.00	-	0.00	0.08	0.00
Ni:	-	-	-	0.01	-	-	-
Total:	8.02	4.01	4.00	4.00	8.03	4.01	3.99

Table 1.2: Representative P-T estimates for the garnet websterite vein (sample 6) and the garnet peridotite (sample 8). See text for further explanation and abbreviations.

Geothermobarometer		Fe^{3+} estimated		Fe_{total}=Fe^{2+}	
		T(° C)	*P(GPa)*	*T(° C)*	*P(GPa)*
Garnet websterite vein (sample 6)					
T_{H84}	$P_{B\&K1990}$	1000	7.1		
$T_{L\&G88}$	$P_{B\&K1990}$	1317	10.6		
$T_{L\&G88^*}$	$P_{B\&K1990}$	1192	9.2		
$T_{B\&K90}$	$P_{B\&K1990}$	919	6.3		
$T_{R\&G74}$	$P_{B\&K1990}$	1585	11.8	1555	12.6
$T_{E\&G79}$	$P_{B\&K1990}$	939	6.5	849	5.6
T_{P85}	$P_{B\&K1990}$	899	6.1	810	5.3
T_{K88}	$P_{B\&K1990}$	794	5.1	701	4.3
T_{R2000}	$P_{B\&K1990}$	1019	7.3	821	5.4
T_{W77}	$P_{B\&K1990}$	829	5.5	838	5.5
$T_{B\&K90}$	$P_{B\&K1990}$	881	5.9	873	5.9
$T_{B\&K90Ca}$	$P_{B\&K1990}$	907	6.2		
$T_{B\&K90Na}$	$P_{B\&K1990}$	error	error		
Peridotite main body (sample 8)					
T_{H84}	$P_{B\&K1990}$	926	4.3		
$T_{L\&G88}$	$P_{B\&K1990}$	1178	6.4		
$T_{L\&G88^*}$	$P_{B\&K1990}$	1068	5.5		
$T_{B\&K90}$	$P_{B\&K1990}$	847	3.7		
$T_{R\&G74}$	$P_{B\&K1990}$	976	4.7	854	3.8
$T_{E\&G79}$	$P_{B\&K1990}$	784	3.3	714	2.8
T_{P85}	$P_{B\&K1990}$	753	3.1	682	2.6
T_{K88}	$P_{B\&K1990}$	674	2.5	601	2.0
T_{R2000}	$P_{B\&K1990}$	632	2.3	539	1.7
T_{W77}	$P_{B\&K1990}$	808	3.5	814	3.5
$T_{B\&K90-2px}$	$P_{B\&K1990}$	732	2.9	729	2.9
$T_{B\&K90Ca}$	$P_{B\&K1990}$	779	3.3		
$T_{B\&K90Na}$	$P_{B\&K1990}$	895	4.1		
$T_{O\&W79}$	$P_{B\&K1990}$	794	3.4		

*W_{Ca}=1500 (Carswell and Harley, 1990)

combined with other barometers (e.g. $P_{H\&G82}$, P_{H84} and $P_{N\&G85}$), however, the obtained geothermobarometric results were not significantly different. A wide range of P-T estimates can thus be obtained using various combinations of different geothermobarometers. It is, however, beyond the scope of this paper to evaluate which thermometers and barometers represent the most reliable results. For this we refer the reader to Carswell and Harley (1990), Krogh and Carswell (1995) and Ravna-Krogh and Paquin (2003). Our results, shown in Fig. 1.5 and listed in Table 1.2, demonstrate that for the garnet- websterite vein (sample 6) most calculated P-T conditions are well above the graphite-diamond phase boundary line (see Fig. 1.5a and b), in agreement with the presence of micro-diamond (Vrijmoed et al., prep). These observations provide unambiguous evidence that the cross-cutting garnet websterite vein records UHPM conditions within the diamond stability field. We conclude that 5.5 GPa and 800° C is representative of the formation conditions of the UHP mineralogy in the veins. In contrast, most geothermobarometric results from the peridotite

body (sample 8) record UHPM conditions restricted to the coesite field. The data in Table 1.2 imply that the last recorded equilibration of the main body occurred at 3.4 GPa and 800° C. Although most of the latter results still define UHPM conditions, we interpret the lower P-T estimates in the peridotite body compared to the veins, to be due to post-peak metamorphic aluminium diffusion effects in orthopyroxene related to exhumation. These pressure estimates for the peridotite body are therefore regarded to represent minimum pressure conditions. Our geothermobarometric results thus support an expansion of the northernmost UHP terrain in the WGR in Norway at least 25 km northeastwards. The garnet websterite preserves higher equilibrium conditions than the peridotite. Our explanation for this apparent difference in metamorphic grade is that the garnet websterite veins have a 2-10 times larger grain size than the surrounding Fe-Ti type peridotite body resulting in a higher

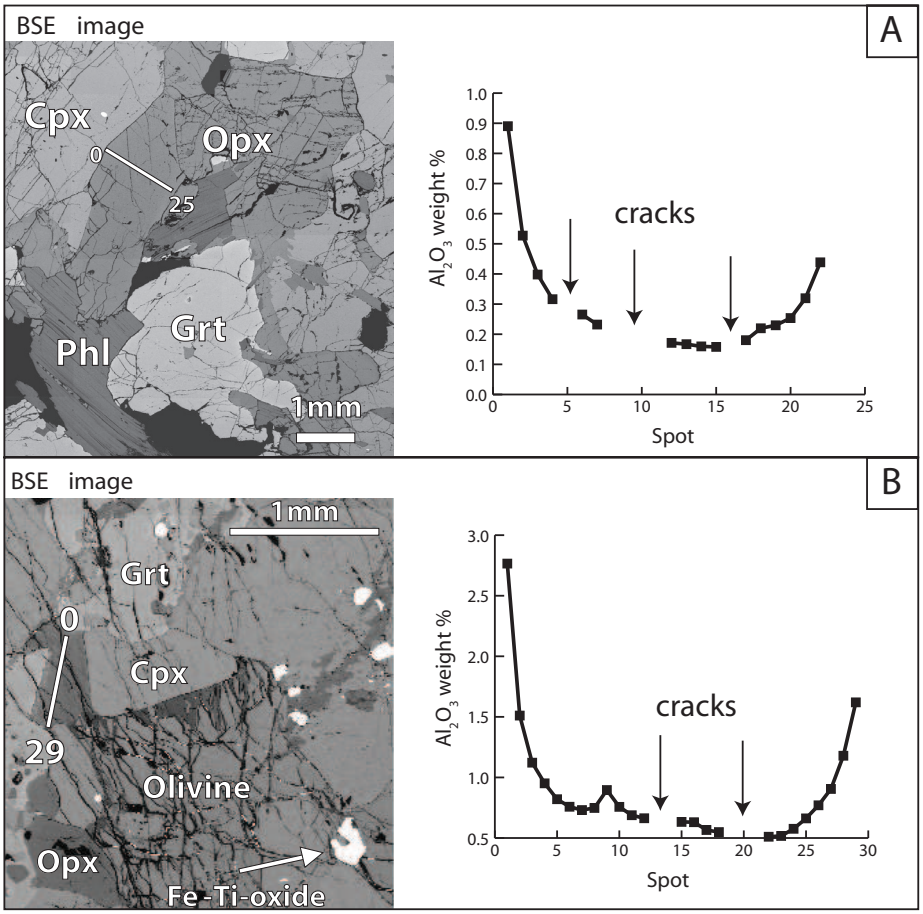

Figure 1.4: **(a)** Back-scatter electron image from a selected part in a thin section of the garnet websterite vein (a) sample 6 and **(b)** sample 8. The lines show location of the Al_2O_3 abundance profile (diagram to the right) along the orthopyroxene grain. Also visible are the Fe-Ti oxides characteristic of the Fe-Ti type garnet peridotites

effective closure temperature for the Sm-Nd isotope system. More work is required to fully explain the apparent pressure difference between UHP mineralogy of the websterite veins and peridotite body.

1.7 Isotope geochemistry

1.7.1 Sm-Nd

Isotopic results are reported in Table 1.3. Sm-Nd garnet-clinopyroxene isochrons of samples 6 (garnet websterite vein) and 8 (garnet peridotite body) are presented

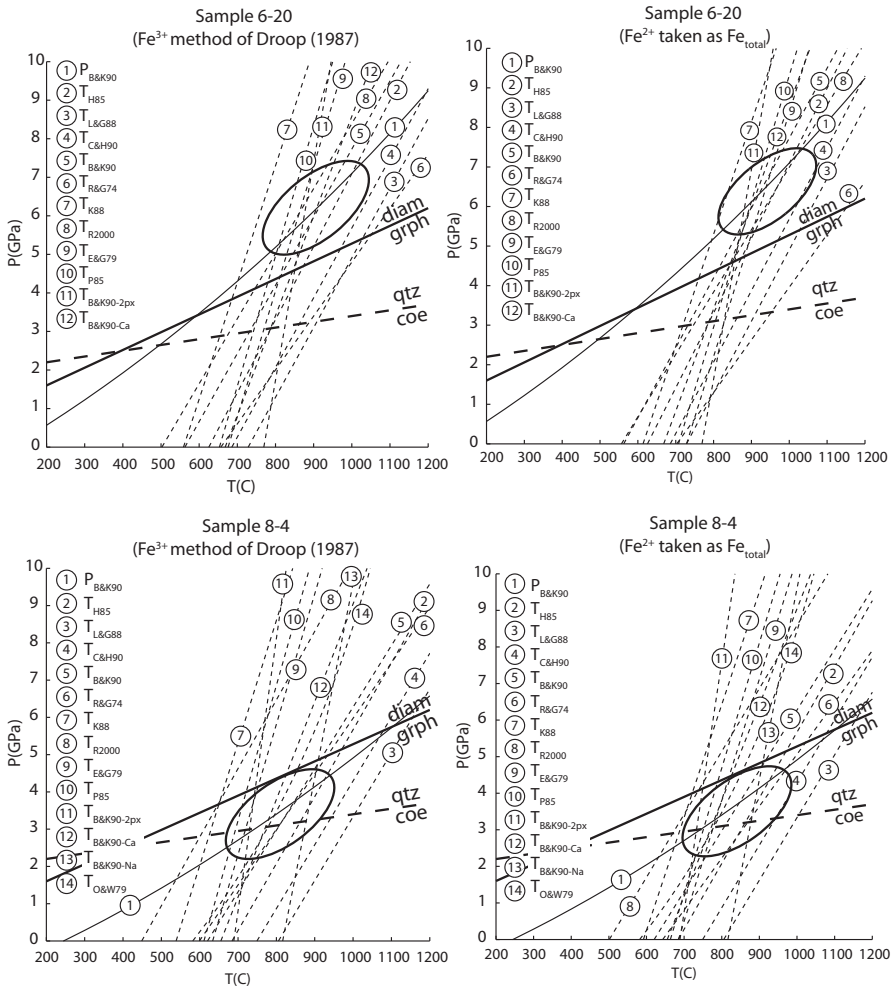

Figure 1.5: Geothermobarometry results for selected samples 6 (garnet websterite vein) and 8 (garnet peridotite body). Diamond-graphite equilibrium line from Bundy (1980), coesite-quartz equilibrium line from Hemingway et al. (1998)

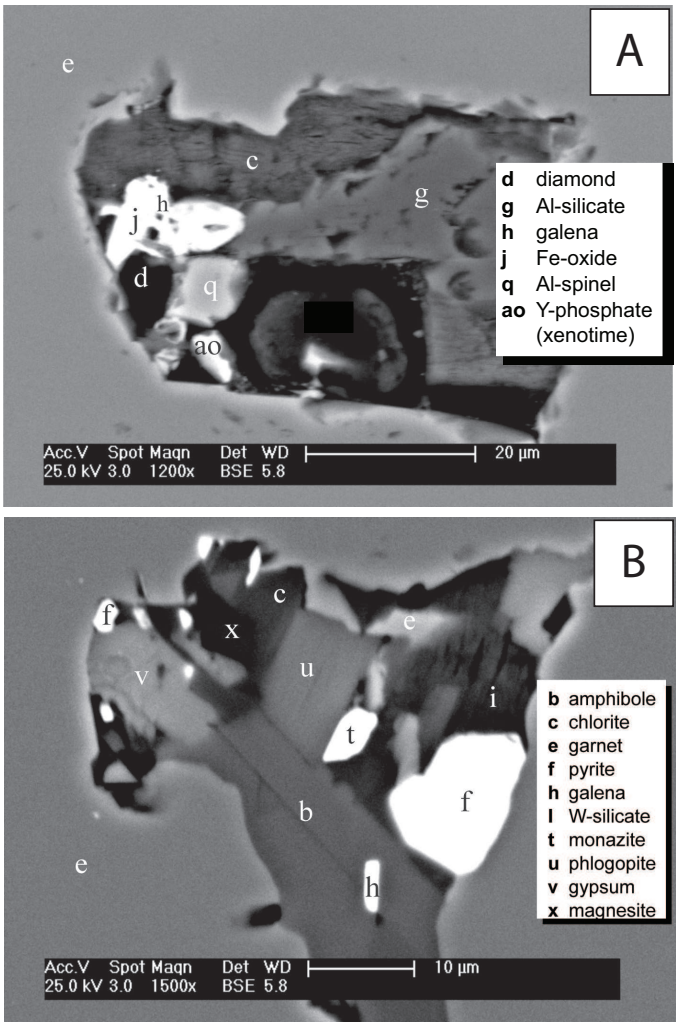

Figure 1.6: Polyphase solid inclusions in garnets of the websterite (sample 6) showing a variety of minerals in a single inclusion assemblage, with microdiamond in Fig. (a)

in Fig. 1.7. The two Sm-Nd isochron ages of 381 ± 6 Ma and 393 ± 3 Ma are significantly different but define roughly similar initial $^{143}Nd/^{144}Nd$ isotope ratios of 0.51171 ± 0.00002 and 0.51195 ± 0.00001 respectively. These ratios equate to ϵNd values of 8.5 and 3.6 respectively. These ages are significantly younger than the time proposed for peak metamorphism in the Caledonian Orogeny (Hacker et al., 2001; Carswell et al., 2003b). Nd model ages of the whole rocks are summarised in Fig. 1.8 and Table 1.3. Initial $^{143}Nd/^{144}Nd$ ratios at 400 Ma are between 0.51167 and 0.51191, comparable to the $^{143}Nd/^{144}Nd$ values of the two mineral isochrons (Fig. 1.7a and b). There is, however, no distinction between the initial ratios of the whole rock samples of the websterite vein and peridotite body. Below we will use the isotope geochemistry of the peridotites to examine the petrogenesis of these rocks to assess the geological significance of the mineral and model ages and discuss the petrogenesis of the Svartberget peridotite body.

Table 1.3: Rb-Sr and Sm-Nd isotope data. All errors are 2σ. Errors of $^{147}Sm/^{144}Nd$ are 0.15%, based on repeated standard measurements by previous users at the Vrije Universiteit, Amsterdam. N.D. not determined. Initial Sr and Nd isotope ratios are calculated for minerals and whole rock samples at 400Ma BP. Model age errors were propagated according to Sambridge and Lambert (1997)

Sample	Min.	Sr (ppm)	Rb (ppm)	Rb/Sr	$^{87}Sr/^{86}Sr$	$^{87}Rb/^{86}Sr$	$^{87}Sr/^{86}Sr_i$	Nd (ppm)	Sm (ppm)	Sm/Nd	$^{147}Sm/^{144}Nd$	$^{143}Nd/^{144}Nd$	$^{143}Nd/^{144}Nd_i$	$\epsilon CHUR^0$	$\epsilon CHUR^t$	$T_{grt-cpx}$ (Ma)	T_{CHUR} (Ga)	T_{DM} (Ga)
Svartberget Fe-Ti peridotite/websterite body																		
Pyroxenite veins																		
6	grt	1.937	0.064	0.033	0.73865±2	0.097	0.73811	0.506	1.075	2.127	1.287	0.51492±4	0.51171±2	44.5	-8.5±0.5	380.7	-	-
6	cpx	166.310	0.666	0.004	0.74257±1	0.012	0.74251	10.478	2.634	0.251	0.152	0.51209±2	0.51171±2	-10.7	-8.5±0.5	±5.7	-	-
6	w.r.	-	-	-	-	-	-	3.837	1.174	0.306	0.185	0.51215±1	0.51169±2	-9.6	-	-	6.30±0.29	5.22±0.11
04-37	w.r.	-	-	-	-	-	-	8.100	2.257	0.279	0.168	0.51211±1	0.51169±1	-10.4	-	-	2.85±0.08	3.44±0.06
Garnetite vein																		
04-38	w.r.	-	-	-	-	-	-	3.416	1.781	0.521	0.315	0.51269±1	0.51190±1	0.9	-	-	0.06±0.01	-0.70±0.01
Peridotite/websterite blocks																		
8	grt	1.977	0.012	0.006	0.72309±3	0.017	0.72299	0.760	1.100	1.448	0.876	0.51420±1	0.51195±1	30.5	-3.6±0.2	393.4	-	-
8	cpx	99.758	n.d	n.d	0.72702±1	n.d	n.d	6.256	1.514	0.242	0.146	0.51233±1	0.51195±1	-6.1	-3.6±0.2	±3.4	-	-
8	w.r.	-	-	-	-	-	-	2.777	0.927	0.334	0.202	0.51238±1	0.51186±1	-5.0	-	-	-7.74±0.85	9.55±0.43
7	w.r.	-	-	-	-	-	-	2.869	0.883	0.308	0.186	0.51236±1	0.51188±1	-5.4	-	-	3.94±0.23	4.27±0.10
04-2	w.r.	-	-	-	-	-	-	2.111	0.605	0.287	0.173	0.51230±1	0.51185±1	-6.6	-	-	2.21±0.08	3.15±0.05
04-31	w.r.	-	-	-	-	-	-	4.605	1.144	0.248	0.150	0.51207±1	0.51168±1	-11.1	-	-	1.86±0.03	2.56±0.03
04-33	w.r.	-	-	-	-	-	-	4.241	1.205	0.284	0.172	0.51217±1	0.51173±1	-9.1	-	-	2.84±0.08	3.53±0.06
Country-rock eclogites																		
79	grt	2.131	0.080	0.038	0.71003±3	0.109	0.70942	0.694	1.105	1.592	0.963	0.51425±2	0.51176±3	31.3	-7.2±0.6	394.1	-	-
79	cpx	176.536	0.090	0.001	0.70960±1	0.001	0.70959	10.472	2.816	0.269	0.163	0.51218±3	0.51176±3	-9.0	-7.2±0.6	±6.2	-	-
99	grt	26.256	0.111	0.004	0.70296±4	0.012	0.70289	1.745	2.856	1.637	0.990	0.51444±1	0.51198±3	35.2	-3.3± 0.5	380.1	-	-
99	cpx	123.652	0.033	0.000	0.70523±1	0.001	0.70522	17.272	5.553	0.321	0.194	0.51246±2	0.51198±3	-3.4	-3.3±0.5	±4.5	-	-

1.7.2 Sr-Nd isotopes

Rb-Sr isotope analyses of leached minerals from the peridotite body, a crosscutting garnet websterite vein and two 'country-rock' eclogite lenses were conducted to constrain the potential origin of the fluids that produced the polyphase solid inclusions. Sr-Nd isotope ratios are plotted at 400 Ma in Fig. 1.7d and show that $^{87}Sr/^{86}Sr$ ratios are extremely high for the garnet peridotite and even higher for the garnet websterite vein minerals compared to the eclogite boudins occurring in the area (sample 79 and 99) and expected mantle compositions at that time. Rb concentrations are very low so that the radiogenic Sr cannot be a consequence of Rb decay or an incorrect calculation of the initial Sr isotope ratios. The high Sr ratios for the garnet websterites implies that they contain a component originating from the crust. High $^{87}Sr/^{86}Sr$ ratios unsupported by Rb have previously been reported in the WGR and were explained by Rb loss associated with high temperature metamorphism (Griffin and Brueckner, 1985; Austrheim et al., 2003). However, the presence of the polyphase solid inclusions strongly suggests that infiltrating C-O-H rich melts from external (felsic) sources transported radiogenic Sr into the peridotites to form the websterites and garnetites. The mineral isochron ages (380-395 Ma) are significantly younger than the generally accepted 400 Ma age for UHPM in the WGR (Hacker et al., 2001; Carswell et al., 2003b). Sm-Nd isotope dating using 2-points isochrons will provide geologically unrealistic ages if garnet or clinopyroxene contain phases of different paragenesis that contain a significant proportion of the Sm and or Nd. Although mineral separates were extremely carefully hand-picked and subjected to leaching, it is well known that minor phases can remain undetected (Thöni, 2002). In the case of the Svartberget body, there are polyphase solid inclusions of among other minerals monazite (Fig. 1.6b), which have high REE concentrations. The presence of such phases may have led to mineral ages that are too young. The mineral isochrons record the end of diffusion of Sm and Nd between the constituent minerals in the rock. The closure temperature for the Sm-Nd system depends on many factors such as composition, grain-size, cooling rate, diffusion parameters (Ganguly et al., 1998; Van Orman et al., 2002). Current values for some of these parameters are experimentally determined on gem quality phases and are therefore subject to geological uncertainty. Our best estimate of the closure temperature, derived using the diffusion program of Ganguly and Tirone (1999), yielded temperatures around 750-800° C. Considering the fact that the temperature of the amphibolite facies metamorphism was around 750-800° C (Cuthbert et al., 2000), and assuming that the closure temperatures are about 750-800 ° C, it is probable that we have dated closure of the Sm-Nd system during amphibolite facies conditions. Krogh et al. (2003) reported 415 Ma zircon age from eclogites from the Averøya area northeast of the area investigated in this study and 385 Ma for zircons from pegmatites in amphibolite facies boudin necks in the same area. The Sm-Nd mineral cooling ages from the garnet peridotite body may therefore also be recording a thermal event associated with pegmatite activity. The garnet websterite (sample 6) was sampled within 1 m of low pressure pegmatite veins post-dating the main body and the garnet websterite veins. Nevertheless, this Sm-Nd isochron age of 380 Ma gives an indication that the (UHP) metamorphic event that formed the garnet-websterite mineralogy was Scandian in age and not Proterozoic. We conclude that there are

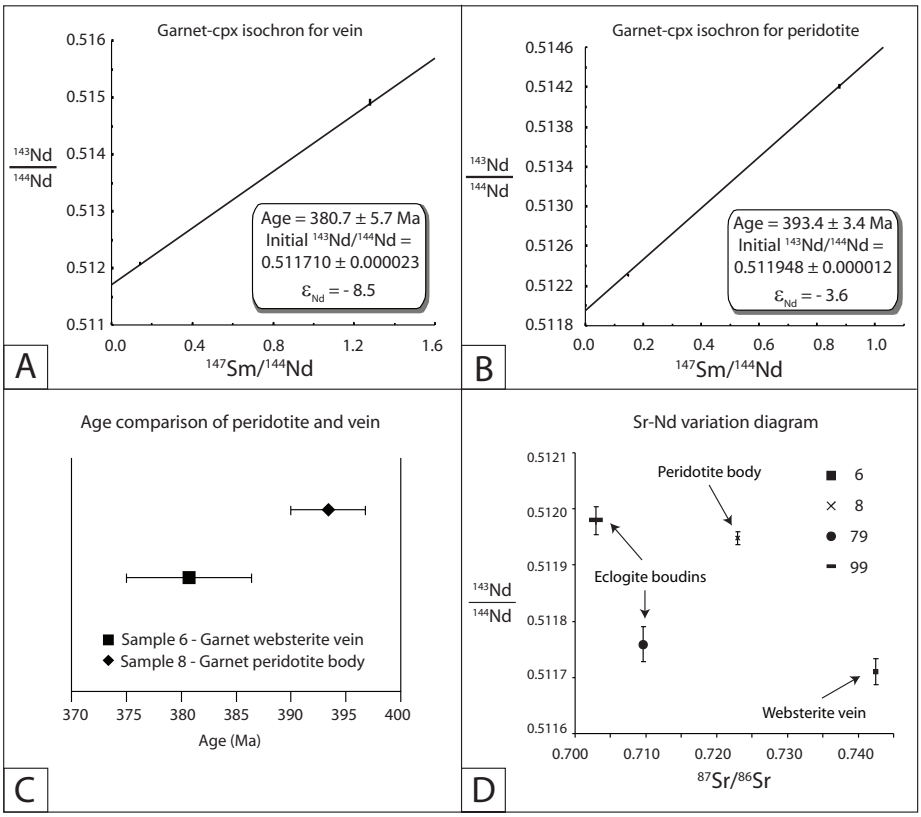

Figure 1.7: **(a)** Sm-Nd grt-cpx isochron of garnet websterite vein (sample 6) and **(b)** Sm-Nd grt-cpx isochron of garnet peridotite (sample 8). **(c)** Comparison diagram of the two ages (a) and (b) with their error bars. **(d)** Sr-Nd isotope ratios diagram of the garnet websterite (sample 6) the garnet peridotite (sample 8) and two 'country-rock' eclogites from our area (sample 79 and 99, see Fig. 1.2)

several potential explanations for the fact that the Sm-Nd mineral ages are younger than the timing of Caledonian peak metamorphic conditions; (1) The obtained ages may record cooling following amphibolite facies metamorphism; (2) The minerals may have been affected thermally by late pegmatite veins; (3) It is possible that REE-rich minor phases, that retain a pre-metamorphic history, are included in the garnet separates. Continued research is underway to provide a full explanation of the P-T-t evolution of the Svartberget garnet peridotite body.

1.8 Geological history

The data presented in this study allows part of the geological history of the UHP Fe-Ti peridotite-websterite body to be determined. The mineralogy and petrology of the Svartberget garnet peridotite body closely resembles other Fe-Ti type peridotites in the WGR (Schmidt, 1963; Carswell et al., 1983; Jamtveit, 1987b,a). These rocks

are believed to be formed from Proterozoic cumulates in the lower crust. The initial ratio of the peridotite mineral isochron (ϵNd of -3.6) suggests that these rocks had a prehistory of 1 Ga, consistent with a Proterozoic age. Nd model ages have a large spread, but most of them indicate a Proterozoic (1500-2500 Ma) age, which is in line with the other Fe-Ti type garnet peridotites. We believe there are three factors that contribute to the wide spread in Nd model ages (Fig. 1.8). Fractionation of garnet assemblages from a melt/fluid will lead to a marked fractionation of Sm/Nd leading to decoupling of the parent daughter ratio and the time integrated Nd isotope ratio. The significance of the Nd model ages of the websterite-garnetite assemblages with very variable garnet contents (5-100%), is therefore difficult to assess without detailed knowledge of their petrogenesis. In addition, the metamorphic formation of relatively garnet-rich and -poor peridotites will also cause redistribution of REE and potentially disruption of Nd model ages. The radiogenic Sr isotope ratios, coupled with the polyphase inclusions, suggest that the websterites were formed by volatile-rich melts that had interacted extensively with the continental crust. These melts would transport Nd derived from the Proterozoic crust leading to apparent Proterozoic ages and due to garnet fractionation a large scatter of the Nd model ages. We therefore follow previous workers in interpreting the Fe-Ti garnet peridotites as lower crustal cumulates formed in layered mafic igneous intrusions during the Proterozoic (Schmidt, 1963; Mørk, 1985a,b; Jamtveit, 1987b,a). We consider the fact that the polyphase solid inclusions are randomly located in garnet to be highly significant. The simplest interpretation is that inclusions crystallised synchronously with the garnet-websterites and garnetites under diamond facies UHP conditions. Alternatively they may have been introduced to existing minerals during UHP garnet growth. However, it is difficult to envisage how metamorphic reactions and mineral recrystallisation would not lead to the formation of inclusion trails. Therefore our favoured geological evolution of the Svartberget garnet peridotite body began with formation in the Proterozoic. During Scandian times volatile-rich melts/fluids infiltrated the garnet peridotite body during diamond facies UHPM forming garnet websterite/garnetite veins that trapped fluids that are preserved as polyphase solid inclusions. The melts were most likely C-O-H-rich 'fluids' that originate from crustal sources carrying large ion lithophile and highly incompatible elements (Rb, Th, LREE etc). We speculate that fracturing and vein emplacement were the result of local high fluid pressure caused by the dehydration of the Baltic plate during subduction.

1.9 Tectonic implications

The data presented in this paper suggest that the northern UHP domain in the WGR can be extended approximately 25 km northeastwards. Therefore the northern UHP domain in the WGR has a length of 75 km. The other two UHP domains in WGR are of comparable size. Although the three UHP domains are arbitrary grouping of UHPM rocks in the WGR of Norway (Fig. 1.1) the following question arises: Do they represent one individual large domain or several small subdomains. Resolution of this question has important implication for the processes responsible for the exhumation of the UHP domains. In the case of a single large UHP domain,

the domain might have returned to the surface buoyancy driven as a large coherent nappe (Ernst, 1973; Chemenda et al., 1995; Brueckner and Van Roermund, 2004). But in the case of small sub domains, the domains might have returned to the surface as small slivers, separated by thrusts. In this latter case, variation in exhumation and subduction rates and residence time may produce distinct P-T-t trajectories in the individual domains, while a coherent nappe will produce a coherent set of P-T-t trajectories. The present study establishes that the size and extent of the northern UHP domain is not completely known. Therefore more detailed mapping and subsequent P-T and geochemical analysis on neighbouring areas is required to reveal the size and inter-relationships of the UHP domains in the WGR. A major implication of this work is that the paragneissic basement of the WGR, regionally referred to as the Ulla Gneiss, has undergone UHPM (diamond grade). This conclusion is in strong contrast with the work of Terry and Robinson (2004) at the island of Fjørtoft. The latter authors recognised a major tectonic break on Fjørtoft between a northern UHP (diamond grade) segment and a southern Ulla-Gneiss-related terrane, metamorphosed at 2.0 GPa and 750-800° C. The present study indicates that the Ulla-Gneiss related unit was also metamorphosed at UHPM (diamond grade) conditions, leaving no evidence for a major tectonic break. Such a conclusion is also in agreement with the work of Carswell et al. (2006).

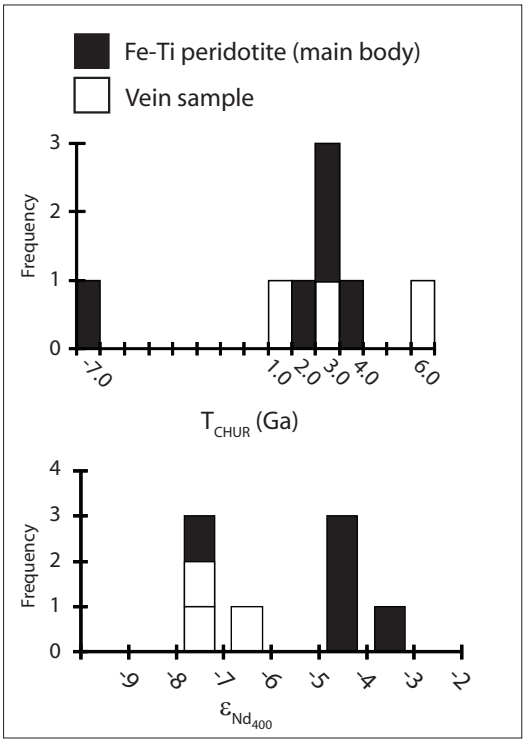

Figure 1.8: Diagrams of **(a)** Sm-Nd T_{CHUR} model ages and **(b)** Nd values at 400Ma BP from all samples

1.10 Conclusions

Lithological and structural field data combined with isotope geochemistry and geothermobarometry in the Bud-Tornes region of the WGR have led us to the following conclusions: A new occurrence of Fe-Ti type garnet peridotite, named Svartberget, lies along strike with other Fe-Ti type garnet peridotites. The occurrence of diamond and P-T estimates establish that the rocks have been at diamond grade UHP conditions. Consequently, the northern UHP domain in the Western Gneiss Region in Norway can be extended approximately 25 km towards the northeast. The Svartberget peridotite body was cross-cut by a network of garnet-websterites and garnetites. Textural and mineralogical evidence from polyphase solid inclusions, Sm-Nd whole rock and Sr-isotope data suggest that crustal derived C-O-H rich melts/fluids infiltrated the Svartberget body, probably during Caledonian subduction, forming a network of garnet websterite and garnetite veins with pronounced preferred orientations. Young Caledonian Sm-Nd garnet-clinopyroxene ages are either the result of REE-rich micro-inclusions that cannot be removed by leaching, or they represent a cooling age somewhat later than the UHPM, possibly the result of influx of pegmatite veins. The mineral ages do, however, demonstrate that the last metamorphic equilibration was associated with the Caledonian Orogeny. The initial ratio of the garnet peridotite mineral isochron implies a Proterozoic origin. However, the large range in Nd model ages from the peridotite body can be explained by the involvement of crustal derived (high $^{87}Sr/^{86}Sr$) C-O-H bearing melts/fluids, and or by garnet fractionation that disrupted the Sm-Nd isotope systematics. The present study shows that the size and extent of the northern UHP domain is not completely known. More detailed mapping and subsequent P-T and geochemical analysis on neighbouring areas is required to reveal the size and inter-relation- ships of the UHP domains in the WGR. This work is required to better understand the exhumation mechanisms of the UHP rocks.

1.11 Acknowledgements

We would like to thank the Faculty of Earth and Life Sciences at the VU in Amsterdam and the Faculty of Earth Sciences at the Utrecht University for providing the funding for this project and access to the laboratories at the two universities. The fieldwork was partly funded by a grant from the Dittmer fund of the VU. We thank Håkon Austrheim and Muriel Erambert at the University of Oslo for useful discussions and help on geothermobarometry. Two highly constructive reviews by Erling Ravna and Simon Cuthbert and editorial handling by Aberra Mogessie significantly improved the structure of this manuscript.

References

Andersen, T. B. (1998). Extensional tectonics in the Caledonides of southern Norway, an overview. *Tectonophysics*, 285(3-4):333–351.

Austrheim, H., Corfu, F., Bryhni, I., and Andersen, T. B. (2003). The Proterozoic Hustad igneous complex: a low strain enclave with a key to the history of the Western Gneiss Region of Norway. *Precambrian Research*, 120(1-2):149–175.

Brey, G. and Köhler, T. (1990). Geothermobarometry in Four-phase Lherzolites II. New Thermobarometers, and Practical Assessment of Existing Thermobarometers. *Journal of Petrology*, 31(6):1353–1378.

Brueckner, H. K. and Van Roermund, H. L. M. (2004). Dunk tectonics: A multiple subduction/eduction model for the evolution of the scandinavian caledonides.

Bryhni, I. (1989). Status of the supracrustal rocks in the Western Gneiss Region, S. Norway. In Gayer, R., editor, *The Caledonide Geology of Scandinavia*, pages 221–228. Graham & Trotman.

Bryhni, I., Austrheim, H., and Solli, A. (1989). Hustad berggrunnskart 1220 1.

Bryhni, I. and Sturt, B. A. (1985). Caledonides of southwestern Norway. In Gee, D. G. and Sturt, B. A., editors, *The Caledonide Orogen; Scandinavia and related areas*, volume 1, pages 89–107. John Wiley & Sons, Chichester, United Kingdom.

Bundy, F. P. (1980). The P, T phase and reaction diagram for elemental carbon. *Journal of Geophysical Research*, 85:6930–6936.

Carswell, D. A., Brueckner, H. K., Cuthbert, S. J., Mehta, K., and O'Brien, P. J. (2003a). The timing of stabilisation and the exhumation rate for ultra-high pressure rocks in the Western Gneiss Region of Norway. *Journal of Metamorphic Geology*, 21(6):601–612.

Carswell, D. A. and Harley, S. L. (1990). Mineral barometry and thermometry. In Carswell, D., editor, *Eclogite facies rocks*, pages 83–110. Blackie, Glasgow.

Carswell, D. A. and Harvey, M. A. (1982). The Intrusive History and Tectono-Metamorphic Evolution of the Basal Gneiss Complex in the Moldefjord Region, W Norway. *Journal of the Geological Society*, 139(May):368–368.

Carswell, D. A., Harvey, M. A., and Alsamman, A. (1983). The petrogenesis of contrasting Fe-Ti and Mg-Cr garnet peridotite types in the high-grade gneiss complex of Western Norway. *Bulletin De Minéralogie*, 106(6):727–750.

Carswell, D. A., Tucker, R. D., O'Brien, P. J., and Krogh, T. E. (2003b). Coesite micro-inclusions and the U/Pb age of zircons from the Hareidland eclogite in the Western Gneiss Region of Norway. *Lithos*, 67(3-4):181–190.

Carswell, D. A. and Van Roermund, H. L. M. (2005). On multi-phase mineral inclusions associated with microdiamond formation in mantle-derived peridotite lens at Bardane on Fjørtoft, west Norway. *European Journal of Mineralogy*, 17(1):31–42.

Carswell, D. A., van Roermund, H. L. M., and Wiggers de Vries, D. F. (2006). Scandian Ultrahigh-Pressure Metamorphism of Proterozoic Basement Rocks on Fjørtoft and Otrøy, Western Gneiss Region, Norway. *International Geology Review*, 48(11):957–977.

Chemenda, A. I., Mattauer, M., Malavieille, J., and Bokun, A. N. (1995). A Mechanism for Syn-Collisional Rock Exhumation and Associated Normal Faulting - Results from Physical Modeling. *Earth and Planetary Science Letters*, 132(1-4):225–232.

Cuthbert, S. J., Carswell, D. A., Krogh-Ravna, E. J., and Wain, A. (2000). Eclogites and eclogites in the Western Gneiss Region, Norwegian Caledonides. *Lithos*, 52(1-4):165–195.

Dobrzhinetskaya, L. F., Eide, E. A., Larsen, R. B., Sturt, B. A., Tronnes, R. G., Smith, D. C., Taylor, W. R., and Posukhova, T. V. (1995). Microdiamond in high-grade metamorphic rocks of the Western Gneiss Region, Norway. *Geology*, 23(7):597–600.

Dodson, M. H. (1973). Closure Temperature in Cooling Geochronological and Petrological Systems. *Contributions to Mineralogy and Petrology*, 40(3):259–274.

Droop, G. T. R. (1987). A General Equation for Estimating Fe^{3+} Concentrations in Ferromagnesian Silicates and Oxides from Microprobe Analyses, Using Stoichiometric Criteria. *Mineralogical Magazine*, 51(361):431–435.

Ellis, D. J. and Green, D. H. (1979). Experimental-Study of the Effect of Ca Upon Garnet-Clinopyroxene Fe-Mg Exchange Equilibria. *Contributions to Mineralogy and Petrology*, 71(1):13–22.

Ernst, W. G. (1973). Interpretative Synthesis of Metamorphism in Alps. *Geological Society of America Bulletin*, 84(6):2053–2078.

Ganguly, J. and Tirone, M. (1999). Diffusion closure temperature and age of a mineral with arbitrary extent of diffusion: theoretical formulation and applications. *Earth and Planetary Science Letters*, 170(1-2):131–140.

Ganguly, J., Tirone, M., and Hervig, R. L. (1998). Diffusion Kinetics of Samarium and Neodymium in Garnet, and a Method for Determining Cooling Rates of Rocks. *Science*, 281(5378):805–807.

Griffin, W. L., Austrheim, H., Brastad, K., Bryhni, I., Krill, A. G., Krogh, E. J., Mørk, M. B. E., Qvale, H., and Torudbakken, B. (1985). High-pressure metamorphism in the Scandinavian Caledonides. In Gee, D. G. and Sturt, B. A., editors, *The Caledonide Orogen; Scandinavia and related areas*, volume 2, pages 783–801. John Wiley & Sons, Chichester, United Kingdom.

Griffin, W. L. and Brueckner, H. K. (1985). Ree, Rb-Sr and Sm-Nd Studies of Norwegian Eclogites. *Chemical Geology*, 52(2):249–271.

Hacker, B., Root, D., Walsh, E., Young, D., and Mattinson, J. (2001). Recent progress on the Norwegian HP-UHP eclogites. *Abstract to UHPM Workshop at Waseda University, Japan*, 4B06:174.

Harley, S. L. (1984a). An Experimental-Study of the Partitioning of Fe and Mg between Garnet and Ortho-Pyroxene. *Contributions to Mineralogy and Petrology*, 86(4):359–373.

Harley, S. L. (1984b). The Solubility of Alumina in Orthopyroxene Coexisting with Garnet in FeO-MgO-Al_2O_3-SiO_2 and CaO-FeO-MgO-Al_2O_3-SiO_2. *Journal of Petrology*, 25(3):665–696.

Harley, S. L. and Green, D. H. (1982). Garnet Ortho-Pyroxene Barometry for Granulites and Peridotites. *Nature*, 300(5894):697–701.

Harvey, M. A. (1983). A geochemical and Rb-Sr study of the Proterozoic augen orthogneisses on the Molde peninsula, west Norway. *Lithos*, 16(4):325–338.

Hemingway, B. S., Bohlen, S. R., Hankins, W. B., Westrum, E. F., and Kuskov, O. L. (1998). Heat capacity and thermodynamic properties for coesite and jadeite, reexamination of the quartz-coesite equilibrium boundary. *American Mineralogist*, 83(5-6):409–418.

Hermann, J. (2003). Experimental evidence for diamond-facies metamorphism in the Dora-Maira massif. *Lithos*, 70(3-4):163–182.

Jamtveit, B. (1987a). Magmatic and Metamorphic Controls on Chemical Variations within the Eiksunddal Eclogite Complex, Sunnmore, Western Norway. *Lithos*, 20(5):369–389.

Jamtveit, B. (1987b). Metamorphic evolution of the Eiksunddal eclogite complex. Western Norway, and some tectonic implications. *Contributions to Mineralogy and Petrology*, 95(1):82–99.

Krabbendam, M. and Dewey, J. F. (1998). Exhumation of UHP rocks by transtension in the Western Gneiss Region, Scandinavian Caledonides. *Geological Society Special Publications*, 135:159–181.

Krill, A. G. (1980). Tectonics of the Oppdal area, central Norway. *Geologiska Föreningens i Stockholm Förhandlingar*, 102(4):523–530.

Krill, A. G. (1985). Relationships between the Western Gneiss Region and the Trondheim region; stockwerk-tectonics reconsidered. In Gee, D. G. and Sturt, B. A., editors, *The Caledonide Orogen; Scandinavia and related areas*, volume 1, pages 475–483. John Wiley & Sons, Chichester, United Kingdom.

Krogh, E. and Carswell, D. (1995). HP and UHP Eclogites and Garnet Peridotites in the Scandinavian Caledonides. In Coleman, R. and Wang, X., editors, *Ultrahigh Pressure Metamorphism*, Cambridge Topics in Petrology, pages 244–298. Cambridge University Press.

Krogh, E. J. (1977). Evidence of Precambrian continent-continent collision in Western Norway. *Nature*, 267(5606):17–19.

Krogh, E. J. (1988). The garnet-clinopyroxene Fe-Mg geothermometer - a reinterpretation of existing experimental data. *Contributions to Mineralogy and Petrology*, 99(1):44–48.

Krogh, T., Robinson, P., and Terry, M. (2003). Precise U-Pb zircon ages define 18 and 19 m.y. Subduction to uplift intervals in the Averøya-Nordøyane area, Western Gneiss Region. *NGU-report*, 2003-055:71–72.

Lee, H. Y. and Ganguly, J. (1988). Equilibrium Compositions of Coexisting Garnet and Orthopyroxene - Experimental Determinations in the System FeO-MgO-Al_2O_3-SiO_2, and Applications. *Journal of Petrology*, 29(1):93–113.

Mørk, M. B. E. (1985a). A Gabbro to Eclogite Transition on Flemsøy, Sunnmore, Western Norway. *Chemical Geology*, 50:283–310.

Mørk, M. B. E. (1985b). Incomplete High P-T Metamorphic Transitions within the Kvamsøy Pyroxenite Complex, West Norway - a Case-Study of Disequilibrium. *Journal of Metamorphic Geology*, 3(3):245–264.

Nickel, K. G. and Green, D. H. (1985). Empirical Geothermobarometry for Garnet Peridotites and Implications for the Nature of the Lithosphere, Kimberlites and Diamonds. *Earth and Planetary Science Letters*, 73(1):158–170.

O'Neill, H. S. C. (1980). Correction. *Contributions to Mineralogy and Petrology*, 72(3):337–337.

O'Neill, H. S. C. and Wood, B. J. (1979). Experimental-Study of Fe-Mg Partitioning between Garnet and Olivine and Its Calibration as a Geothermometer. *Contributions to Mineralogy and Petrology*, 70(1):59–70.

Powell, R. (1985). Regression Diagnostics and Robust Regression in Geothermometer Geobarometer Calibration - the Garnet Clinopyroxene Geothermometer Revisited. *Journal of Metamorphic Geology*, 3(3):231–243.

Råheim, A. and Green, D. H. (1974). Experimental Determination of the Temperature and Pressure Dependence of the Fe-Mg Partition Coefficient for Coexisting Garnet and Clinopyroxene. *Contributions to Mineralogy and Petrology*, 48:179–203.

Ravna, E. K. (2000). The garnet-clinopyroxene Fe_2-Mg geothermometer: an updated calibration. *Journal of Metamorphic Geology*, 18(2):211–219.

Ravna-Krogh, E. and Paquin, J. (2003). Thermobarometric methodologies applicable to eclogites and garnet ultrabasites. In Carswell, D. A. and Compagnoni, R., editors, *Ultrahigh Pressure Metamorphism*, volume 5 of *EMU Notes in Mineralogy*, pages 229–259. Eötvös University Press, Budapest.

Roberts, D. (2003). The Scandinavian Caledonides: event chronology, palaeogeographic settings and likely, modern analogues. *Tectonophysics*, 365(1-4):283–299.

Robinson, P. (1995). Extension of Trollheimen tectono-stratigraphic sequence in deep synclines near Molde and Brattvåg, Western Gneiss Region, Southern Norway. *Norsk Geologisk Tidsskrift*, 75(4):181–197.

Root, D. B., Hacker, B. R., Gans, P. B., Ducea, M. N., Eide, E. A., and Mosenfelder, J. L. (2005). Discrete ultrahigh-pressure domains in the Western Gneiss Region, Norway: implications for formation and exhumation. *Journal of Metamorphic Geology*, 23(1):45–61.

Sambridge, M. and Lambert, D. D. (1997). Propagating errors in decay equations: Examples from the Re-Os isotopic system. *Geochimica Et Cosmochimica Acta*, 61(14):3019–3024.

Schmidt, H. (1963). *Petrology and structure of the Eiksundal Eclogite Complex, Hareidlandet, Sunnmore, Norway*. Ph.d. thesis, Harvard University U.S.A.

Seranne, M. (1992). Late Paleozoic Kinematics of the Mre-Trondelag Fault Zone and Adjacent Areas, Central Norway. *Norsk Geologisk Tidsskrift*, 72(2):141–158.

Smith, D. C. (1984). Coesite in clinopyroxene in the Caledonides and its implications for geodynamics. *Nature*, 310(5979):641–644.

Stalder, P., Ulmer, P., Thompson, A. B., and Gunther, D. (2000). Experimental approach to constrain second critical end points in fluid/silicate systems: Near-solidus fluids and melts in the system albite-H_2O. *American Mineralogist*, 85(1):68–77.

Terry, M. P. and Robinson, P. (2003). Evolution of amphibolite-facies structural features and boundary conditions for deformation during exhumation of high- and ultrahigh-pressure rocks, Nordoyane, Western Gneiss Region, Norway. *Tectonics*, 22(4):1036, 10.1029/2001TC001349.

Terry, M. P. and Robinson, P. (2004). Geometry of eclogite-facies structural features: Implications for production and exhumation of ultrahigh-pressure and high-pressure rocks, Western Gneiss Region, Norway. *Tectonics*, 23(2):TC2001, 10.1029/2002TC001401.

Terry, M. P., Robinson, P., and Ravna, E. J. K. (2000). Kyanite eclogite thermobarometry and evidence for thrusting of UHP over HP metamorphic rocks, Nordøyane, Western Gneiss Region, Norway. *American Mineralogist*, 85(11-12):1637–1650.

Thöni, M. (2002). Sm-Nd isotope systematics in garnet from different lithologies (Eastern Alps): age results, and an evaluation of potential problems for garnet Sm-Nd chronometry. *Chemical Geology*, 185(3-4):255–281.

Torsvik, T. H., Smethurst, M. A., Meert, J. G., VanderVoo, R., McKerrow, W. S., Brasier, M. D., Sturt, B. A., and Walderhaug, H. J. (1996). Continental break-up and collision in the Neoproterozoic and Palaeozoic - A tale of Baltica and Laurentia. *Earth-Science Reviews*, 40(3-4):229–258.

Tveten, E., Lutro, O., and Thornes, T. (1998). *ÅLESUND, Geological map*. Norges geologiske undersøkelse.

Van Orman, J. A., Grove, T. L., Shimizu, N., and Layne, G. D. (2002). Rare earth element diffusion in a natural pyrope single crystal at 2.8 GPa. *Contributions to Mineralogy and Petrology*, 142(4):416–424.

Van Roermund, H. L. M., Carswell, D. A., Drury, M. R., and Heijboer, T. C. (2002). Microdiamonds in a megacrystic garnet websterite pod from Bardane on the island of Fjørtoft, western Norway: Evidence for diamond formation in mantle rocks during deep continental subduction. *Geology*, 30(11):959–962.

Van Roermund, H. L. M., Spengler, D., and Wiggers de Vries, D. (2005). Evidence for ultra-high pressure (UHP) metamorphism within Proterozoic basement rocks on Otrøy, Western Gneiss Region, Norway. *Mitteilungen der Österreichischen Mineralogischen Gesellschaft*, 150:159.

Van Straaten, B., Wiggers de Vries, D., Van Roermund, H., and Drury, M. (2003). A structural, metamorphic and geochronological study of eclogites and country rock gneisses from Otrøy (Moldefjord), WGR, Norway. *Norges Geologiske Undersøkelse, Trondheim*, Report 2003.055:155–156.

Vrijmoed, J., Smith, D. C., and Van Roermund, H. (in prep.). A new in-situ microdiamond locality in the Scandinavian Caledonides: Svartberget. *Terra Nova*.

Wells, P. R. A. (1977). Pyroxene Thermometry in Simple and Complex Systems. *Contributions to Mineralogy and Petrology*, 62(2):129–139.

Chapter 2

Raman confirmation of microdiamond in the Svartberget Fe-Ti type garnet peridotite, Western Gneiss Region, Western, Norway[1]

2.1 Abstract

Ultra-high pressure metamorphic rocks have been found worldwide. The volume and areal extent of an exhumed UHPM domain are important for understanding the geodynamic mechanisms responsible for the high pressure and relatively medium temperature conditions needed for their creation. We report here Raman microspectroscopical data that prove the existence of microdiamonds at the Svartberget Fe-Ti type peridotite locality in the Western Gneiss Region of Norway. Raman microscopy of two carbon microinclusions belonging to polyphase inclusion assemblages included in garnets from a garnet-phlogopite websterite vein yielded a sharp, narrow, intense peak at 1332 cm^{-1}, characteristic of diamond. The diamond is associated with polyphase solid inclusions possibly originating from supercritical, dense, H-C-N-O-F-P-S-Cl fluids. Lithological, textural and geochronological evidence points towards a Caledonian origin of the trapped fluid and subsequent diamond formation.

2.2 Introduction

Vestiges of ultra-high pressure metamorphism (UHPM) have been found in continental and oceanic rocks of different orogens worldwide (Van Roermund et al., 2005; Coleman and Wang, 1995; Carswell and Compagnoni, 2003). Indirect UHPM evidence comes from the application of geothermobarometric techniques (Lappin and Smith, 1978; Ravna-Krogh and Paquin, 2003) applied to UHPM mineral assemblages and directly from mineralogical indicators, such as coesite, diamond and majoritic

[1]Vrijmoed, J.C., D.C.Smith, H.L.M. van Roermund, 2008, *Terra Nova*, 20, 295-301

garnet (Chopin, 1984; Smith, 1984; Sobolev and Shatsky, 1990; Dobrzhinetskaya et al., 1995; Van Roermund and Drury, 1998; Nasdala and Massonne, 2000; Mposkos and Kostopoulos, 2001; Van Roermund et al., 2002; Godard et al., 2003). Nevertheless, the mechanisms responsible for the formation, preservation and exhumation of UHPM rocks in orogens are still not fully understood.

The volume and spatial distribution of UHPM rocks within UHPM terranes including the observed contrast in metamorphic grade between rocks that contain UHPM minerals and adjacent country rocks that do not contain them, have led to different explanations concerning the origin, emplacement and preservation of these rocks. To explain the occurrence, volume and areal extent of UHPM rocks in the Western Gneiss Region (WGR), the following mechanisms that assume a continental subduction scenario have been proposed: (a) the existence of major and/or minor post-UHPM tectonic contacts such as nappes and/or tectonic melanges (Lappin and Smith, 1978; Smith, 1984, 1988; Wain, 1997; Cuthbert et al., 2000; Terry and Robinson, 2003, 2004), or (b) the presence of fluids and/or deformation leading to differential prograde or retrograde reactions and differences in reaction-kinetics between rock types (Austrheim et al., 1997; Cuthbert et al., 2000; Wain et al., 2001; Carswell and Cuthbert, 2003; Cuthbert and Carswell, 2003). Hypotheses that do not necessarily involve continental subduction may involve local/regional (tectonic) overpressure in rocks (Smith, 1984; Mancktelow, 1993; Petrini and Podladchikov, 2000). It is considered here that the volume and areal extent of UHPM domains within a single metamorphic terrain are thus important parameters to determine as they can modify or identify the locations of 'inferred' or observed tectonic contacts, the relations between fluids and UHPM, and/or the scales at which continental crust subduction or (tectonic) overpressure might act.

Here we report Raman data that confirm the previously reported, but not proven, presence of microdiamonds at the Svartberget UHPM locality, in the WGR of Norway (Vrijmoed et al., 2006). Microdiamond confirmation is consistent with the results of Vrijmoed et al. (2006) that the volume and areal extent of the northern UHPM domain of the WGR (Fig. 2.1) are considerably expanded eastwards and, following the reasoning in the paragraph above, the new microdiamond finding will put important constraints on the models described above.

2.3 Ultra-high pressure in the WGR

The WGR represents a window in the Scandinavian Caledonides where Scandian reworked, high grade gneissic rocks of Proterozoic age, presumably belonging to the Baltic Plate, are exposed. In addition, variable amounts of metadolerites, amphibolites, marbles, granulites, anorthosites, eclogites and peridotites occur. The Scandian event in the Caledonides is associated with collision between the continents Baltica and Laurentia around 430-390 Ma ago. A majority opinion today is that in the WGR, this continental collision is associated with subduction of Baltica below Laurentia and associated HP/UHP metamorphism now recorded dominantly in (ultra)-mafic rocks of the WGR. UHPM data in north-east Greenland have given rise to the proposal of scenarios involving intracratonic subduction (Gilotti and Mcclelland, 2007).

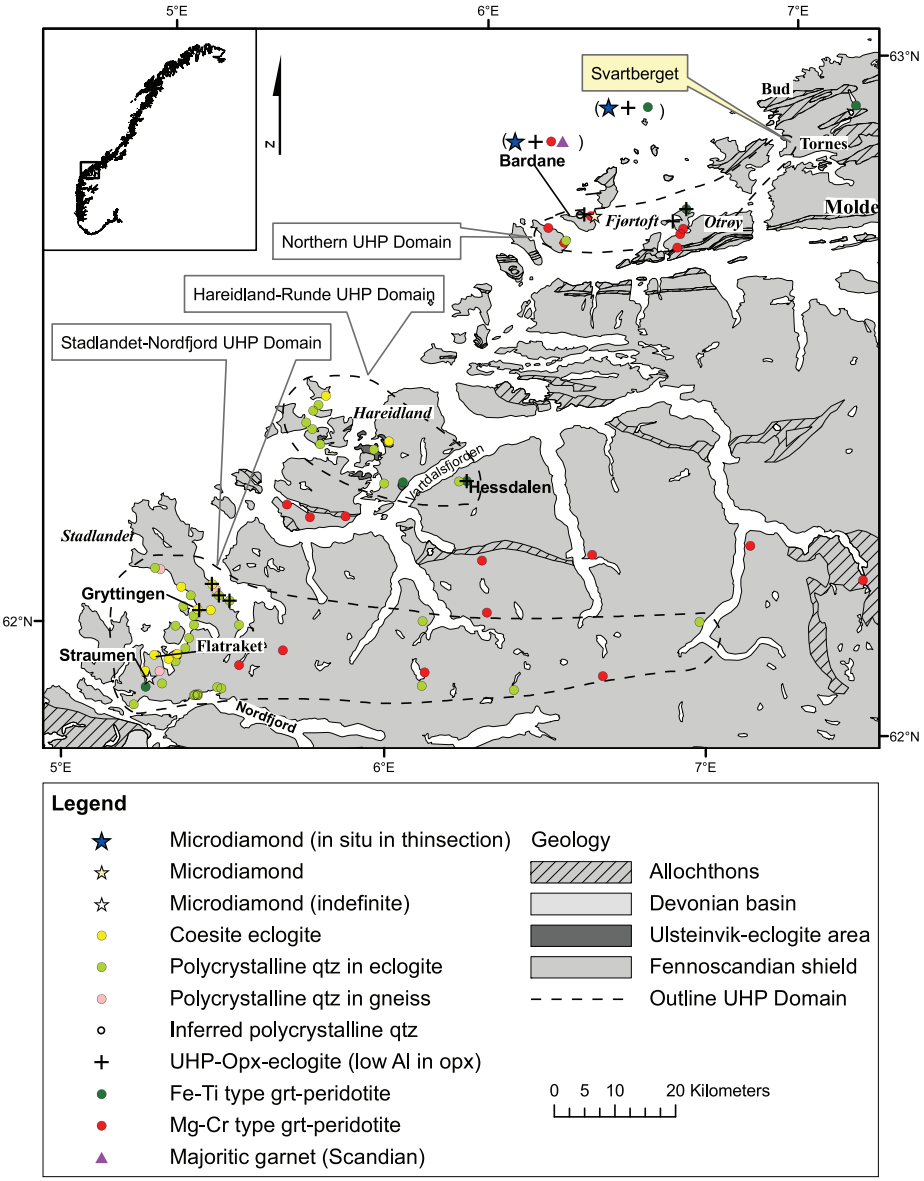

Figure 2.1: Map of UHPM findings in Norway and the deduced UHPM domains (either entirely of UHPM rocks or areas of non-UHPM gneiss in which individual UHPM rocks are localised) (compiled from Wain, 1997; Cuthbert et al., 2000; Terry et al., 2000; Carswell et al., 2003; Root et al., 2005; Spengler, 2006). Low-Al-in opx: $Al_2O_3 < 0.5$-0.6 (wt %).

The first indirect evidence for UHPM, but certainly not universally accepted at that time, in the WGR was presented by Lappin and Smith (1978) who used geothermobarometric techniques based on the very low Al-content of orthopyroxene coexisting with garnet within the Gryttingen and other opx-eclogites, followed by Lappin and Smith (1981) who developed a new magnesite + diopside = dolomite + enstatite geothermobarometer. Direct mineralogical evidence for UHPM was subsequently provided by Smith (1984) who found coesite in an adjacent eclogite pod at Gryttingen (Fig. 2.1). Subsequently, coesite was found by Smith (1985) in the Straumen eclogite, in and around Flatraket (Wain, 1997; Cuthbert et al., 2000; Wain et al., 2000), in Hareidlandet (Hacker et al., 2001; Carswell et al., 2003) and Root et al. (2005). In addition, evidence elsewhere for the former existence of coesite was proposed by (Smith, 1984, 1988) and reported in the Flatraket area by Wain (1997) and Wain et al. (2000). Cuthbert et al. (2000) reported polycrystalline quartz (PCQ) in Hareidlandet as well as Root et al. (2005), Terry et al. (2000) reported possible PCQ on Fjørtoft mentioned earlier by Cuthbert et al. (2000). Walsh and Hacker (2004) expanded the southernmost UHP domains towards the east with findings of PCQ inclusions (Fig. 2.1).

The first microdiamonds in the WGR were found in continental, Caledonian reworked, felsic gneisses on the island of Fjørtoft by Dobrzhinetskaya et al. (1995) (Fig. 2.1). These yellow diamonds were recovered using a total rock digestion process, but other research teams using similar techniques on the same rocks could not find any diamond. This cast sincere doubts on their true occurrence until Van Roermund et al. (2002) reported the first microdiamonds within their textural context in a thin section from a garnet websterite from the same island. The microdiamonds were found in polyphase solid inclusion assemblages within spinel that were included in garnet and dated by the Sm-Nd technique by Brueckner et al. (2002) to be 'near' Scandian in age (518 ± 78 Ma). In the classical Stadlandet UHPM area (Fig. 2.1), Godard et al. (2003) also reported microdiamond in a thin section from the Straumen coesite-kyanite-eclogite pod of Smith and Lappin (1989).

Overall, the evidence points towards a Scandian origin of the diamonds in the WGR. Presently, three distinct 'UHPM domains' have been defined, predominantly along the NW margin of the WGR

(Root et al., 2005; Carswell et al., 2006). However, a crucial but quite unsolved problem is to what extent can one deduce UHPM in intervening gneisses that show no evidence of UHPM; one can 'argue' for (Van Roermund et al., 2005; Carswell et al., 2006; Scambelluri et al., 2008) or against (Lappin and Smith, 1978; Smith, 1995), but one cannot 'prove it'. Thus, an UHPM domain (Fig. 2.1) is a geological province where UHPM rocks can and do outcrop, without implying if all the intervening rocks experienced UHPM or not.

Our presently identified microdiamonds form also part of polyphase solid inclusion assemblages in garnet crystals of the Svartberget garnet-peridotite/websterite body in West Norway. This type of rock is classified by Carswell et al. (1983) as Fe-Ti type peridotite, having protoliths presumably formed as part of mafic layered intrusions in the lower crust in mid(?)-Proterozoic times, in contrast to the Mg-Cr type peridotites such as the microdiamond- (and majoritic garnet)-bearing Bardane peridotite discussed above, which is presumably directly derived from the subcontinental lithospheric mantle (SCLM). The present confirmation of microdiamonds in

the presumed Fe-Ti type peridotite suggests that the microdiamonds in both peridotite types are of Scandian (Caledonian) age. The Svartberget peridotite/websterite body is described in more detail by Vrijmoed et al. (2006).

2.4 Methods

Preparation of the thin sections for Electron Microprobe (EMP) analysis was performed at the Geological Technical Laboratory, Vrije Universiteit, Amsterdam. The desired rock sample was cut down to a slice of 0.5 cm thick, followed by polishing with silicon carbide. Subsequently, the rock slice was polished with high quality diamond paste fabricated by the department itself (grain size between 2-4 μm), followed by polishing with 1 μm grain-size diamond paste, down to a thickness of 25 μm. The polished section was then cleaned thoroughly with ethanol and left overnight in petroleum ether to remove the last contaminants. The thin sections were coated with carbon for Scanning Electron Microscopy (SEM) and EMP analysis.

Electron Microprobe analyses were performed with the JEOL JXA-8600 Superprobe at Utrecht University, the Netherlands. Operating conditions were 15 kV accelerating voltage, a 1 μm beam size and a beam current of 20 nA. SEM analyses were performed at EMSA, Utrecht University, the Netherlands. Mineral phases were identified using energy dispersive X-ray spectrometry (EDS).

Raman spectra were obtained at the 'Laboratoire Franais de Gemmologie' at the 'Chambre de Commerce et d'Industrie de Paris' using a Renishaw inVia Raman Microscope to identify the elemental carbon as diamond. The operational conditions of Raman point analyses were: 100x objective; green laser 514.5 nm Ar+, laser power 10-100% = 5-50 mW, laser impact size 1 μm, grating 1800, spectral range 100-4000 cm^{-1}, 'synchroscan' scanning technique, counting time 10-100s x 3-5 accumulations. Raman mapping was performed with the same instrument and analytical conditions except for: laser power 100% = 50 mW, spectral range 100-1800 cm^{-1}, counting time 20s x 1 accumulation, rectangle 30 μm (X) x 16 μm (Y), step 0.8 μm in both directions.

2.5 Results

We sampled coarse-grained garnet-websterite veins that crosscut the Svartberget Fe-Ti type garnet peridotite body. One thin section (sample h in Fig. 3 of Vrijmoed et al. (2006)) contained two microdiamonds, which were detected by combining Electron Microscopy and Raman Microscopy (RM). The microdiamonds were detected in this sample in two different polyphase solid inclusion assemblages in garnet. Polyphase solid inclusions are numerous in our samples and are similar to observed and well-studied samples from other localities and rock types (Stöckhert et al., 2001; Van Roermund et al., 2002; Carswell and Van Roermund, 2005). Photomicrographs and backscattered electron (BSE) images (Fig. 2) show some of the polyphase solid inclusions (inclusion 1 and 2) in garnet that contain microdiamond. The inclusions consist of diamond, semi-amorphous carbon, Al-Mg-Fe-oxide, Fe-Pb-sulphides, Y-phosphate, Al-silicate, garnet, amphibole and chlorite (the mineral species is not known for some of these phases). SEM and EMP analyses of the diamonds could

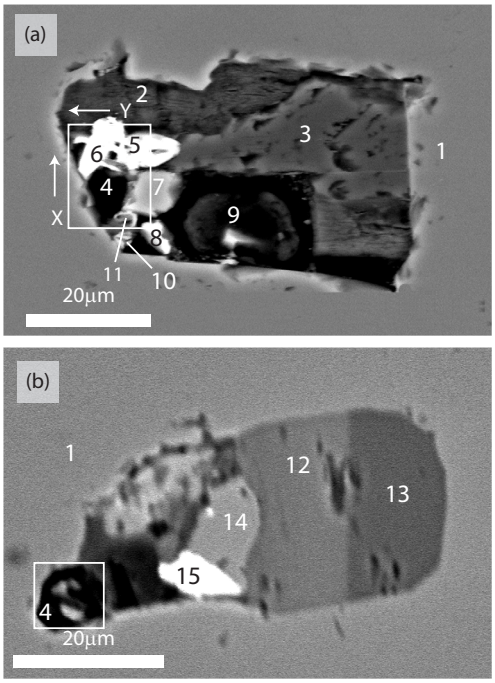

Figure 2.2: **(a)** SEM BSE image of inclusion 1. Rectangle indicates location of Raman map in Fig. 2.3a. **(b)** Microprobe BSE image of inclusion 2. Rectangle indicates location of Raman map in Fig. 2.3b. Legend: 1) garnet; 2) chlorite; 3) Al-silicate; 4) diamond; 5) galena; 6) haematite; 7) Al-spinel; 8) Y-phosphate; 9-10) Fe-oxide; 11) amphibole; 12) chlorite; 13) Al-Fe-Mg oxide; 14) Fe-sulphide.

only identify the presence of carbon, and secondary electron (SE) images verified that they did not present a hole in the thin section. RM of the carbon inclusions yielded a sharp, narrow, intense (>70 000 counts) peak at 1331-1332 cm^{-1}, uniquely characteristic for diamond (Fig. 3a). A weaker, wider peak at approximately 1600 cm^{-1} clearly represents the coexistence of some highly disordered graphite (=semi-amorphous carbon). The Fe-oxide (no. 6 in Fig. 2) is clearly identified by RM as hematite.

After mapping the whole spectral range, Raman maps were acquired of the signal-to-baseline intensity in the spectral zone 1325-1338 cm^{-1} that, with the 514.5 nm laser, cuts out the G band of graphite at 1580 cm^{-1} and cuts out all of the weak D1 band of graphite around 1350 cm^{-1}, as this is treated as eliminated baseline (Fig. 4b). A total of 819 full spectra were obtained to acquire maps for inclusion 1. They show the spatial XY extent of the garnet, diamond, hematite, carbon and chlorite near the surface of the thin section (Fig. 4a-e). The diamond zone is at least 5 μm in diameter, but there may be two grains. It appears larger in the map ($\pm$10 μm) as some Raman signal from diamond is reflected through the neighbouring phases; the same phenomenon occurs with all the species, which therefore overlap on the maps. Diamond spectra were also found below the garnet-surface when focusing slightly below the surface of the thin section. Raman spectra for semi-amorphous carbon (G band wide and G intensity about twice the D1 intensity) were found mostly between the hematite and the chlorite, but some occur on the left side of the diamond (Fig. 4d); no ordered graphite (G band narrow and D1 band weak or inexistent) was detected.

For the diamond in inclusion 2, a total of 45 spectra were obtained to acquire a

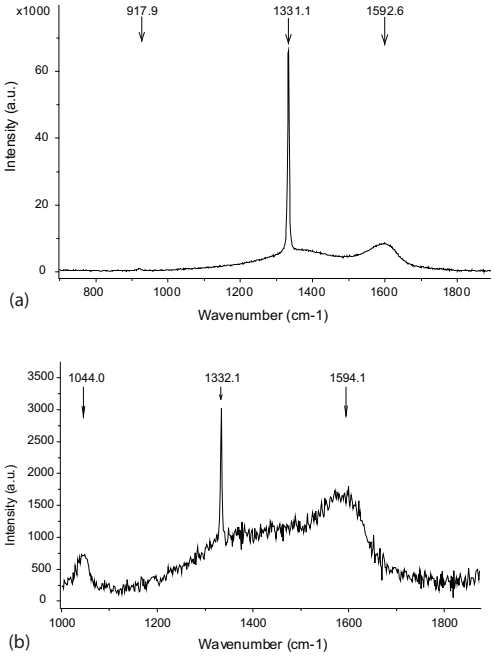

Figure 2.3: (a) A Raman spectrum from inclusion 1 (Fig. 2.2a) showing a sharp unequivocal diamond band at 1331 cm^{-1} with some highly disordered graphite G band at 1593 cm^{-1} (very wide) along with its even wider band D1 (1250-1450 cm^{-1}) and also the 916 cm^{-1} band of garnet; raw untreated data except for a linear baseline subtraction. Haematite coexists with carbon in other nearby spectra. **(b)** The Raman spectrum from the very edge of inclusion 2 (Fig. 2.2b) showing a sharp unequivocal diamond band at 1332 cm^{-1} with some highly disordered graphite G band at 1594 cm^{-1} (very wide) along with its even wider D1 band (1230-1490 cm^{-1}) and also the 1044 cm^{-1} band of garnet; raw untreated data except for a linear baseline subtraction. Dolomite coexists with carbon in other nearby spectra.

small map. It shows only one pixel yielding an excellent spectrum for diamond (Fig. 3b); thus, this diamond is much smaller than the mapping step of 1.5 μm as its Raman intensity was not picked up in adjacent pixels. There are many semi-amorphous carbon spectra with the D1: G ratio of band intensities varying enormously from 1 to 0. Dolomite also coexists in the mapped zone of this polyphase inclusion.

2.6 Discussion

We feel confident that the discovered microdiamonds are natural because of the facts that (i) the size of the diamond in inclusion 1 is larger than that of the diamonds used to polish the sample, combined with the very small probability of leaving any traces of contamination during preparation of the sample, (ii) there is no textural evidence of scraping of the thin section surface that would be expected, if a polishing diamond had been thrust into the rock surface, (iii) the diamond spectra found slightly below the surface of the thin section, (iv) the location of the diamonds in C-O-H bearing mineral assemblages defined by polyphase solid inclusions, and (v) the geothermobarometric P-T estimates yielding 5.5 GPa at 800 ° C (Vrijmoed et al., 2006) that indicate diamond grade UHPM conditions. The coexistence of highly oxidized hematite with highly reduced carbon is not an evidence for contamination because of disequilibrium redox conditions as, on the basis of crystal-chemical parameters, hematite + carbon could be the stable equivalent of magnetite + CO2 at UHPM conditions (Smith, 2008). This also conveniently explains why elemental carbon can exist at UHPM.

Polyphase solid inclusions have been found in relation with microdiamond before

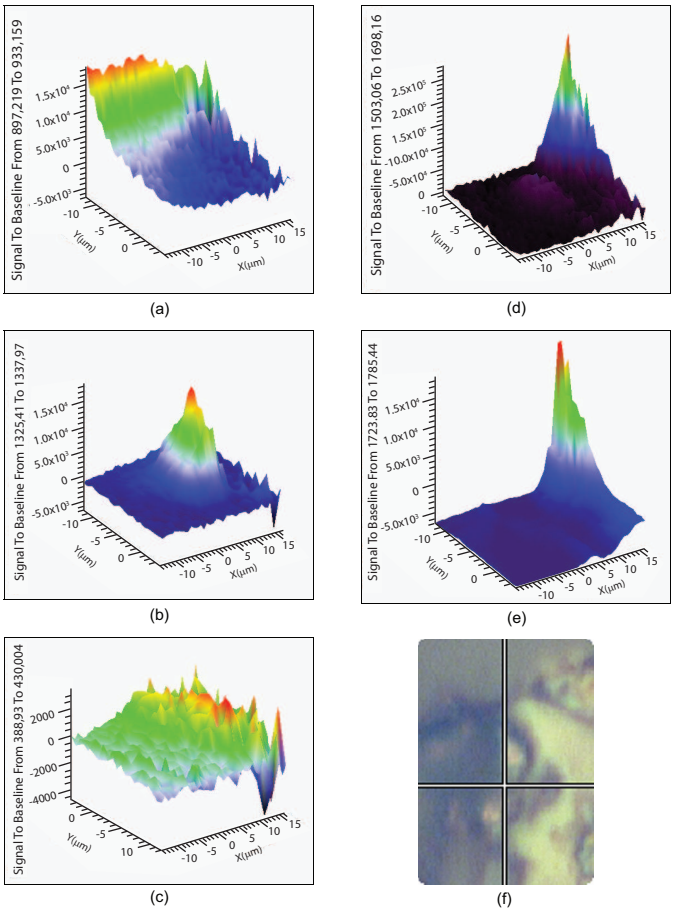

Figure 2.4: Raman microspectrometrical XY maps of the top left part of inclusion 1 (NB the images are rotated 90° with respect to the outlined area in Fig. 2.2a). 'Rainbow' colours indicate signal-to-baseline values that are the integrated surface area between the signal and the baseline within the selected cursors, i.e. intensity of the spectral zone (in arbitrary units) corresponding to the vertical axis Z. **(a)** Raman map of the bands II, III & IV of garnet (897-933 cm^{-1}) such that the edge of the inclusion is mapped in the top left corner. **(b)** Raman map of the 1324-1340 cm^{-1} zone of diamond excluding the D1 band of graphite; the 'mountain' reveals a roughly spherical distribution of Raman intensity collected from diamond to the right of the centre. **(c)** Raman map of the 410 cm^{-1} band of haematite showing highest intensities on the right of the diamond. **(d)** Raman map of the 1503-1698 cm^{-1} zone of semi-amorphous carbon showing some presence on the left of the diamond, but most on the right next to the chlorite. **(e)** Raman map of a highly-fluorescent baseline that corresponds to the presence of chlorite in the top right corner. **(f)** Reflected light image of the central part of the Raman map (about 15 μm high x 10 μm across) taken whilst setting up the mapping. The cross hair intersection lies exactly at the centre of the diamond distribution in map (b) and one can see two whitish areas of diamond at least 2 μm wide on each side of the cross hairs, bright yellow haematite on the right, fuzzy yellow chlorite at top right and bottom right, grey garnet at top, and a fuzzy dark area on the left that corresponds to laser damage made during an earlier Raman attempt by another establishment with too much laser power.

(Stöckhert et al., 2001; Van Roermund et al., 2002; Carswell and Van Roermund, 2005) and were interpreted to be crystallized from a supercritical dense 'COH' fluid. The relationship between supercritical dense COH fluids and microdiamond associated with polyphase solid inclusions including metal sulphides has been studied experimentally (Dobrzhinetskaya et al., 1995; Hwang et al., 2003). Stöckhert et al. (2001) argued for the coexistence of metastable phases in polyphase solid inclusions. Possibly metastable semi-amorphous carbon (highly disordered graphite) coexisting with diamond is common in UHPM rocks in Kazakhstan (Smith et al., 2004). Thermodynamic data on COH fluids (more probably H-C-N-O-F-P-S-Cl fluids with cations like Pb and Y; see Fig. 2 legend) are still scarce and it is therefore impossible yet to give correct thermodynamic predictions for the formation of polyphase solid inclusions. The microdiamonds that we found form part of polyphase solid inclusion assemblages in garnet, which are in textural equilibrium with clino- and orthopyroxene at Svartberget, yielding diamond-grade UHPM P-T conditions. Based on the similarities with other findings cited above the microdiamonds described in this paper are most probably also formed from trapped supercritical fluids in garnet. The new data thus present a petrogenetical feature that needs to be evaluated in all tectonic modelling of the WGR. Several debatable geodynamical aspects are all concerned and will no doubt be developed at length in future papers by ourselves and other researchers as several alternative hypotheses are still open (e.g. crustal vs. mantle protoliths, in situ vs. foreign introduction, depth of subduction, geochronological contradictions).

2.7 Conclusion

Raman microspectrometrical data confirm the presence of microdiamond in the garnet-websterite in the Fe-Ti type Svartberget peridotite. According to Vrijmoed et al. (2006), the garnets in which the diamond-bearing inclusions occur, combined with clinopyroxene crystals, yield Scandian (Caledonian) metamorphic Sm-Nd cooling ages thus arguing for a Scandian origin of the garnet and hence of the trapped microdiamond. The microdiamond is intimately related to polyphase solid inclusions that seem to have formed from supercritical H-C-N-O-F-P-S-Cl metal-bearing fluids. Fully understanding the detailed origin and formation of microdiamond and associated minerals in such polyphase solid inclusions requires great advances over present-day calculations of the thermodynamics of supercritical multicomponent fluids in confined and open systems. These data provide an important new data item that needs to be taken into consideration in all geodynamic modelling of the WGR, modelling that is enriched, although not solved, by the recognition of these diamonds.

2.8 Acknowledgements

Wynanda Koot and the rest of the staff of the Geological Technical Laboratory at the Vrije Universiteit in Amsterdam are thanked for important work and discussions concerning the preparation of the thin sections. The authors are particularly grateful to Heja Garcia-Guillerminet of the 'Laboratoire Français de Gemmologie'

at the 'Chambre de Commerce et d'Industrie de Paris' for providing access to their inVia Raman spectrometer. Gareth Davies and the Department of Petrology at the Vrije Universiteit in Amsterdam kindly provided the opportunity and funding for fieldwork and sample collection. Brit Sundsbø generously helped with accommodation during the fieldwork in the area. The reviewer's detailed comments were very helpful in improving the manuscript.

References

Austrheim, H., Erambert, M., and Engvik, A. K. (1997). Processing of crust in the root of the Caledonian continental collision zone: The role of eclogitization. *Tectonophysics*, 273(1-2):129–153.

Brueckner, H. K., Carswell, D. A., and Griffin, W. L. (2002). Paleozoic diamonds within a Precambrian peridotite lens in UHP gneisses of the Norwegian Caledonides. *Earth and Planetary Science Letters*, 203(3-4):805–816.

Carswell, D. A. and Compagnoni, R. (2003). Introduction with review of the definition, distribution and geotectonic significance of ultrahigh pressure metamorphism. In Carswell, D. A. and Compagnoni, R., editors, *Ultrahigh Pressure Metamorphism*, volume 5 of *EMU Notes in Mineralogy*, pages 3–9. Eötvös University Press, Budapest.

Carswell, D. A. and Cuthbert, S. J. (2003). Ultrahigh pressure metamorphism in the Western Gneiss region of Norway. In Carswell, D. A. and Compagnoni, R., editors, *Ultrahigh Pressure Metamorphism*, volume 5 of *EMU notes in Mineralogy*, pages 51–73. Eötvös University Press, Budapest.

Carswell, D. A., Harvey, M. A., and Alsamman, A. (1983). The petrogenesis of contrasting Fe-Ti and Mg-Cr garnet peridotite types in the high-grade gneiss complex of Western Norway. *Bulletin De Minéralogie*, 106(6):727–750.

Carswell, D. A., Tucker, R. D., O'Brien, P. J., and Krogh, T. E. (2003). Coesite micro-inclusions and the U/Pb age of zircons from the Hareidland eclogite in the Western Gneiss Region of Norway. *Lithos*, 67(3-4):181–190.

Carswell, D. A. and Van Roermund, H. L. M. (2005). On multi-phase mineral inclusions associated with microdiamond formation in mantle-derived peridotite lens at Bardane on Fjørtoft, west Norway. *European Journal of Mineralogy*, 17(1):31–42.

Carswell, D. A., van Roermund, H. L. M., and Wiggers de Vries, D. F. (2006). Scandian Ultrahigh-Pressure Metamorphism of Proterozoic Basement Rocks on Fjørtoft and Otrøy, Western Gneiss Region, Norway. *International Geology Review*, 48(11):957–977.

Chopin, C. (1984). Coesite and pure pyrope in high-grade blueschists of the Western Alps - a first record and some consequences. *Contributions to Mineralogy and Petrology*, 86(2):107–118.

Coleman, R. G. and Wang, X. (1995). Overview of the geology and tectonics of UHPM. In Coleman, R. and Wang, X., editors, *Ultra-High Pressure Metamorphism (UHPM)*, pages 1–32. Cambridge University Press, Cambridge.

Cuthbert, S. J. and Carswell, D. A. (2003). The HP-UHP transition in the Nordfjord-Stadlandet region, Western Gneiss Complex, Norway. *NGU-report*, 2003.055:39–40.

Cuthbert, S. J., Carswell, D. A., Krogh-Ravna, E. J., and Wain, A. (2000). Eclogites and eclogites in the Western Gneiss Region, Norwegian Caledonides. *Lithos*, 52(1-4):165–195.

Dobrzhinetskaya, L. F., Eide, E. A., Larsen, R. B., Sturt, B. A., Tronnes, R. G., Smith, D. C., Taylor, W. R., and Posukhova, T. V. (1995). Microdiamond in high-grade metamorphic rocks of the Western Gneiss Region, Norway. *Geology*, 23(7):597–600.

Gilotti, J. A. and Mcclelland, W. C. (2007). Characteristics of, and a tectonic model for, Ultrahigh-Pressure metamorphism in the overriding plate of the Caledonian orogen. *International Geology Review*, 49(9):777–797.

Godard, G., Smith, D. C., and Thouvenin, C. (2003). Microdiamond within zircon in thin section in the Straumen coesite-kyanite-eclogite pod, Norway. *NGU-report*, 2003.055:54.

Hacker, B., Root, D., Walsh, E., Young, D., and Mattinson, J. (2001). Recent progress on the Norwegian HP-UHP eclogites. *Abstract to UHPM Workshop at Waseda University, Japan*, 4B06:174.

Hwang, S. L., Shen, P. Y., Yui, T. F., and Chu, H. T. (2003). Metal-sulfur-COH-silicate fluid mediated diamond nucleation in Kokchetav ultrahigh-pressure gneiss. *European Journal of Mineralogy*, 15(3):503–511.

Lappin, M. A. and Smith, D. (1981). Carbonate, silicate and fluid relationships in eclogites, Selje District and environs, SW Norway. *Trans. Roy. Soc. Edinburgh*, 72:171–193.

Lappin, M. A. and Smith, D. C. (1978). Mantle-Equilibrated Ortho-Pyroxene Eclogite Pods from Basal Gneisses in Selje-District, Western Norway. *Journal of Petrology*, 19(3):530–584.

Mancktelow, N. S. (1993). Tectonic Overpressure in Competent Mafic Layers and the Development of Isolated Eclogites. *Journal of Metamorphic Geology*, 11(6):801–812.

Mposkos, E. D. and Kostopoulos, D. K. (2001). Diamond, former coesite and supersilicic garnet in metasedimentary rocks from the Greek Rhodope: a new ultrahigh-pressure metamorphic province established. *Earth and Planetary Science Letters*, 192(4):497–506.

Nasdala, L. and Massonne, H. J. (2000). Microdiamonds from the Saxonian Erzgebirge, Germany: in situ micro-Raman characterisation. *European Journal of Mineralogy*, 12(2):495–498.

Petrini, K. and Podladchikov, Y. (2000). Lithospheric pressure-depth relationship in compressive regions of thickened crust. *Journal of Metamorphic Geology*, 18(1):67–77.

Ravna-Krogh, E. and Paquin, J. (2003). Thermobarometric methodologies applicable to eclogites and garnet ultrabasites. In Carswell, D. A. and Compagnoni, R., editors, *Ultrahigh Pressure Metamorphism*, volume 5 of *EMU Notes in Mineralogy*, pages 229–259. Etvs University Press, Budapest.

Root, D. B., Hacker, B. R., Gans, P. B., Ducea, M. N., Eide, E. A., and Mosenfelder, J. L. (2005). Discrete ultrahigh-pressure domains in the Western Gneiss Region, Norway: implications for formation and exhumation. *Journal of Metamorphic Geology*, 23(1):45–61.

Scambelluri, M., Pettke, T., and van Roermund, H. L. M. (2008). Majoritic garnets monitor deep subduction fluid flow and mantle dynamics. *Geology*, 36(1):59–62.

Smith, D. (1995). Chlorite-Rich Ultramafic Reaction Zones in Colorado Plateau Xenoliths - Recorders of Sub-Moho Hydration. *Contributions to Mineralogy and Petrology*, 121(2):185–200.

Smith, D. (2008). Raman confirmation of haematite leads to a new (U)HPM indicator paragenesis : haematite + carbon. *Book of Abstracts: GeoRaman '08: 8th International Conference on Raman Spectroscopy Applied to the Earth Sciences - Sensu Latu*.

Smith, D. C. (1984). Coesite in clinopyroxene in the Caledonides and its implications for geodynamics. *Nature*, 310(5979):641–644.

Smith, D. C. (1985). Coesite in the Straumen eclogite pod, Norway. *Terra Cognita*, 5:226–227.

Smith, D. C. (1988). A review of the peculiar mineralogy of the "Norwegian coesite-eclogite province", with crystal-chemical, petrological, geochemical and geodynamical notes and an extensive bibliography. In Smith, D. C., editor, *Eclogites and Eclogite-Facies Rocks*, volume 12 of *Developments in Petrology*, pages 1–206. Elsevier, Amsterdam.

Smith, D. C., Godard, G., Dobrzhinetskaya, L., Green, H., and Belleil, M. (2004). A preliminary comparative Raman mapping study of contrasting zircon/diamond/graphite relations at Kokchetav, Kazakhstan. In Fredericks, P. M., Frost, R., and Rintoul, L., editors, *Proceedings, XIXth International Conference on Raman Spectroscopy*, pages 562–563. Csiro publishing, Queensland, Australia.

Smith, D. C. and Lappin, M. A. (1989). Coesite in the Straumen kyanite-eclogite pod, Norway. *Terra Nova*, 1(1):47–56.

Sobolev, N. V. and Shatsky, V. S. (1990). Diamond Inclusions in Garnets from Metamorphic Rocks - a New Environment for Diamond Formation. *Nature*, 343(6260):742–746.

Spengler, D. (2006). *Origin and evolution of deep upper mantle rocks from Western Norway* . Doctoral, Utrecht University.

Stöckhert, B., Duyster, J., Trepmann, C., and Massonne, H. J. (2001). Microdiamond daughter crystals precipitated from supercritical COH plus silicate fluids included in garnet, Erzgebirge, Germany. *Geology*, 29(5):391–394.

Terry, M. P. and Robinson, P. (2003). Evolution of amphibolite-facies structural features and boundary conditions for deformation during exhumation of high- and ultrahigh-pressure rocks, Nordoyane, Western Gneiss Region, Norway. *Tectonics*, 22(4):1036, 10.1029/2001TC001349.

Terry, M. P. and Robinson, P. (2004). Geometry of eclogite-facies structural features: Implications for production and exhumation of ultrahigh-pressure and high-pressure rocks, Western Gneiss Region, Norway. *Tectonics*, 23(2):TC2001, 10.1029/2002TC001401.

Terry, M. P., Robinson, P., and Ravna, E. J. K. (2000). Kyanite eclogite thermobarometry and evidence for thrusting of UHP over HP metamorphic rocks, Nordøyane, Western Gneiss Region, Norway. *American Mineralogist*, 85(11-12):1637–1650.

Van Roermund, H. L. M., Carswell, D. A., Drury, M. R., and Heijboer, T. C. (2002). Microdiamonds in a megacrystic garnet websterite pod from Bardane on the island of Fjørtoft, western Norway: Evidence for diamond formation in mantle rocks during deep continental subduction. *Geology*, 30(11):959–962.

Van Roermund, H. L. M. and Drury, M. R. (1998). Ultra-high pressure (P > 6 GPa) garnet peridotites in Western Norway: exhumation of mantle rocks from > 185 km depth. *Terra Nova*, 10(6):295–301.

Van Roermund, H. L. M., Spengler, D., and Wiggers de Vries, D. (2005). Evidence for ultra-high pressure (UHP) metamorphism within Proterozoic basement rocks on Otrøy, Western Gneiss Region, Norway. *Mitteilungen der Österreichischen Mineralogischen Gesellschaft*, 150:159.

Vrijmoed, J. C., Van Roermund, H. L. M., and Davies, G. R. (2006). Evidence for diamond-grade ultra-high pressure metamorphism and fluid interaction in the Svartberget Fe-Ti garnet peridotite-websterite body, Western Gneiss Region, Norway. *Mineralogy and Petrology*, 88(1-2):381–405.

Wain, A. (1997). New evidence for coesite in eclogite and gneisses: Defining an ultrahigh-pressure province in the Western Gneiss region of Norway. *Geology*, 25(10):927–930.

Wain, A., Waters, D., Jephcoat, A., and Olijynk, H. (2000). The high-pressure to ultrahigh-pressure eclogite transition in the Western Gneiss Region, Norway. *European Journal of Mineralogy*, 12(3):667–687.

Wain, A. L., Waters, D. J., and Austrheim, H. (2001). Metastability of granulites and processes of eclogitisation in the UHP region of western Norway. *Journal of Metamorphic Geology*, 19(5):607–623.

Walsh, E. O. and Hacker, B. R. (2004). The fate of subducted continental margins: Two-stage exhumation of the high-pressure to ultrahigh-pressure Western Gneiss Region, Norway. *Journal of Metamorphic Geology*, 22(7):671–687.

Chapter 5

An alternative model for ultra-high pressure in the Svartberget Fe-Ti garnet-peridotite, Western Gneiss Region, Norway.[1]

5.1 abstract

The previously reported 'Fe-Ti type' garnet-peridotite is located in the northern part of the well known ultra-high pressure (UHP) area of the Western Gneiss Region (WGR) in Norway. Primary spinel stable up to only 2.0 GPa at 800 °C coexists with Caledonian ultra-high pressure (4.0 GPa at 800 °C) grt-cpx-opx-ol assemblages in the Svartberget garnet-peridotite. The body is cut by a conjugate set of metasomatic fractures filled dominantly with diamond bearing garnet-phlogopite-websterite (5.5 GPa at 800 °C) and garnetite. Single zircon U-Pb dating suggest metamorphic growth of zircon in the garnetite at 397.2 ± 1.2 Ma, either coinciding or predating an initial phase of leucosomes formation at 397-391 Ma. Field observations, major and trace elements, mineral-chemistry, polyphase inclusions including microdiamond, coupled with $^{87}Sr/^{86}Sr$ ratios in clinopyroxene and whole rock ranging from 0.73 to 0.74, suggest that the Svartberget garnet-peridotite was infiltrated by melts/fluids from the host rock gneiss during the Caledonian UHP event. Present observations in the WGR document a regional metamorphic gradient increasing towards the NW, and structures in the field can account for the exhumation of the (U)HP rocks from 2.5 to 3 GPa. Assuming lithostatic pressures the diamond-bearing Svartberget peridotite body must have come from a burial depth of more than 150 km. However there is a lack of observable structures in the field to explain exhumation from extreme UHP conditions (5.5 GPa or more) to normal HP-UHP conditions (2.5-3GPa), which are common pressures calculated from eclogites in western parts of the WGR.

[1] Vrijmoed, J. C., Podladchikov, Y. Y., Andersen, T. B. (accepted), An alternative model for ultra-high pressure in the Svartberget Fe-Ti garnet-peridotite, Western Gneiss Region, Norway, European Journal of Mineralogy (special volume IGC33)

Because of the regional and mostly coherent metamorphic gradient across the WGR terrain it is difficult to account for local extreme pressure excursions such as documented from within the Svartberget peridotite. We introduce here a conceptual model to explain the main features of the Svartberget body. During burial and heating rocks surrounding the peridotite start to melt, but surrounding non-molten rocks confine the space and pressure builds up. When pressure is high enough conjugate brittle shear fractures develop in the peridotite. Melt (or supercritical fluid) that has the same pressure (5.5 GPa) as the surrounding gneiss can flow in as soon as fractures propagate into the peridotite. This supercritical fluid is now highly reactive and metasomatism takes place at UHP conditions along the fractures capturing microinclusions of diamond while growing. Finally the lithosphere holding the overpressured gneiss constrained breaks due to formation of large scale fractures in the crust and decompression melting starts. Modelling using finite element method (FEM) shows that melting of the gneiss results in pressure variations when gneiss is ten times weaker than surroundings and peridotite enclave. These pressure variations are qualitatively similar to observations in the field. Pressures of several GPa can be potentially build up, and maintained on the geological time scale, by localised partial melting.

5.2 Introduction

The problem of exhumation of ultra-high pressure rocks in the Western Gneiss Region in Norway has been challenging since the first UHP discoveries in the WGR (Smith, 1984). The WGR is well known for its occurrences of HP to UHP rocks, mainly found as eclogite and peridotite boudins and lenses and more rarely within felsic gneisses. The HP-UHP metamorphism (HPM-UHPM) was associated with the continental collision between Baltica and Laurentia around 400 Ma ago (Torsvik et al., 1996). Present observations document a regional metamorphic gradient increasing towards the NW (Labrousse et al., 2004), and structures in the field can account for the exhumation of the (U)HP rocks from 2.5 to 3 GPa. Three distinct 'UHPM domains' have been identified, predominantly along the NW margin of the WGR (Root et al., 2005). The UHP locality in the northernmost UHPM domain,

Figure 5.1: (a) Map of West Norway showing the WGR, intact Proterozoic basement with cover and Caledonian nappes (Lower, Middle and Upper Allochthon) and Devonian old red sandstone basins on top. The area that is overprinted by Caledonian HP and UHP metamorphism is indicated by thick grey line. The thick black line indicates the location of major extensional contacts and outlines approximately the WGR. Domains in which UHP evidence is documented are outlined by thin black lines along the westcoast. Light grey line indicates location of the profile below (modified after Tucker et al., 2004). **(b)** Profile through the southern part of the WGR showing the main structures and distances between major contacts. It shows how the intact Proterozoic basement in the east is overlain by Caledonian nappes more to the west and ultimately is overprinted by HP metamorphism. In the east separated by major extensional contacts (thick black lines) the Caledonian nappes with Devionan basins on top are shown. From this figure it can be concluded that the structures can explain a vertical distance of maximal 70 km including 10 km erosion for the first appearance of eclogites in the east. More to the north structures might explain a maximum depth of 90 km.

called Svartberget, is an Fe-Ti type garnet-peridotite that is crosscut by Caledonian phl-grt-websterite and garnetite veins. Peak P-T estimates for the crosscutting veins reach about 5.5 GPa at a temperature of 800 °C, supported by the presence of microdiamond (Vrijmoed et al., 2008).

Assuming lithostatic pressures the diamond-bearing rocks at Svartberget in the northernmost UHP domain of the WGR must have come from a burial depth of

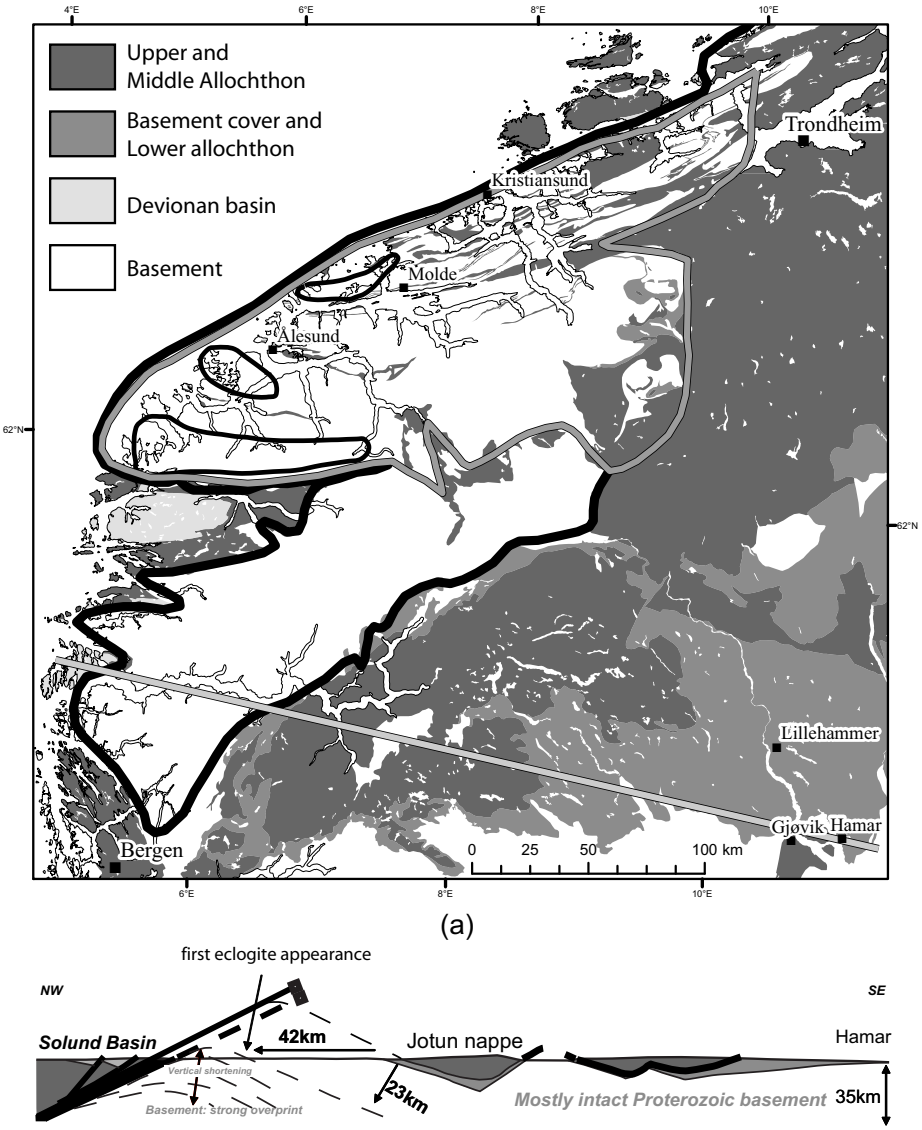

Figure 5.1

more than 150 km. Advanced numerical and analogue models exist to explain how UHP rocks can be created at great depth and be exhumed to the surface (Gerya et al., 2002). These models are capable to explain the path that UHP rocks traveled and its present final position of UHP domains at the surface. However there is a lack of observable structures in the field to explain exhumation from extreme UHP conditions (5.5 GPa or more) to normal HP-UHP conditions (2.5-3GPa), which are common pressures calculated from eclogites in western parts of the WGR. Because of the regional and mostly coherent metamorphic gradient across the WGR terrain it is difficult to account for local extreme pressure excursions such as documented from within the Svartberget peridotite. We discuss a completely different conceptual model and present results of calculations using FEM to check the feasibility of our conceptual model.

A profile in the southern part of the WGR is shown in Fig. 5.1. To the east we have the Proterozoic intact Baltica basement with the Caledonian nappes on top separated from the basement by major extensional structures. Going to the west the first HP rocks in the form of eclogites are found 42 km away from the extensional contact between the Jotun nappe. Based on field measurements the vertical distance between the nappes and the first eclogites is 23 km. Assuming a hinterland dip of 30 to 60 degrees during the Caledonian collison a vertical distance of 26.5-46 km can be reached. Allowing for a conservative 10 km of erosion the present geometry suggests original crustal thicknesses to be 58.5 km to a maximum of 70 km for the first appearance of eclogites. Eclogite facies temperature estimates are around 650-700 °C and give a reasonable geotherm between 9-12 °C/km. The HP rocks to the north are positioned structurally below the rocks to the south where the profile was shown. Going towards the coast structures are positioned deeper than 70 km reaching a depth of about 90 km. This estimate already stretches the observed structural data and we take therefore 90 km as the maximum depth estimated from structural reconstructions.

In this paper we will focus our study on the Svartberget peridotite body that yield P-T estimates in crosscutting grt-phl-websterite veins of 5.5 GPa at 800 °C (Vrijmoed et al., 2006). Assuming lithostatic pressures and an average rock density of 3000 kg/m^3 this would indicate that the Svartberget rocks were at a depth of 165 km. This depth is not supported by structural field data and we therefore consider an alternative. The alternative is to consider the possibility of having variations in pressure rather than a continuous homogeneous pressure gradient from surface to depth. Pressure variations must have existed on the grain scale to preserve coesite in strong host minerals such as garnet and zircon (O'Brien and Ziemann, 2008; Perrillat et al., 2003; Zhang, 1998; Ye et al., 2001). Also on a larger scale for example in volcanic systems it seems possible that the lithosphere is able to sustain pressures above lithostatic long enough to be recorded in minerals (Blundy et al., 2006). This leads us to the interesting idea that perhaps such a situation in which pressures, considerably higher than lithostatic might be sustained on a time scale that allows minerals to record these pressures. This might solve the discrepancy between the depth estimated by assuming lithostatic pressure and the lack of structures in the field to account for burial to the large depths. It has been stated before that in confined space pressures derived from inclusions may not have depth significance (Zhang, 1998). Our idea is that partial melting of felsic gneiss in

a confined space is a possible mechanism to account for the UHP and large pressure variations recorded in the Svartberget peridotite located in the WGR. This concept has also been proposed for UHP rock in Greenland (Dabrowski et al., 2008; Hartz et al., 2007). After introducing the available data on the Svartberget peridotite we propose a model to explain the data and combine this with numerical modelling to test the feasibility of the conceptual model.

5.3 Data

The Svartberget peridotite is crosscut by a conjugate set of fractures along which a metasomatic column developed due to the infiltration of supercritical fluids from the surrounding gneisses at UHP conditions at the end of the Caledonian Orogeny. The data presented before in this thesis will be shortly repeated below to facilitate the explanation of our model.

5.3.1 Field

Aerial photographs and field measurements reveal that the dominant fractures crosscutting the Svartberget peridotite form a conjugate set indicative of brittle deformation. Figure 5.2 shows a map of structures, an aerial photograph and stereographic projection of measured fracture planes. The aerial photograph is an orthophoto which means that the distances and angles are corrected for distortion due to the angle at which the photo was taken. It can be seen from the photograph that the Svartberget peridotite is broken in pieces and many of the fractures cut eachother with a 60 ° angle. A detailed mapping was done by measuring all pieces and blocks of the peridotite and for suitable fracture planes orientation and dip were measured. The strike of these fracture planes is shown in Fig. 5.2a and the azimuth and dip are presented in a stereographic projection in Fig. 5.2c. The angle between the averages of the two dominant groups of fractures is 55 °. From the aerial photo and field measurements it is clear there is also a minor amount of fractures oriented differently (plotted grey in Fig. 5.2c).

The lithology in the fractures is typically diamond-grade phl-grt-websterite with a core of garnetite (Fig. 5.3). This applies to all fractures shown in Fig. 5.2c. More detailed observations reveal a total of 11 different lithological zones along the fractures and contacts between the individual zones are sharp (Vrijmoed, 2008). Field observations, major and trace elements, mineral-chemistry, polyphase inclusions including microdiamond, coupled with $^{87}Sr/^{86}Sr$ ratios in clinopyroxene and whole rock ranging from 0.73 to 0.74, suggest that the Svartberget grt-peridotite was infiltrated by melts/fluids from the host rock gneiss during the Caledonian UHP event. Peak P-T estimates for grt-websterite samples yield 5.5 GPa at 800 °C based on the Al-in opx barometer of Brey and Köhler (1990) and microinclusions of diamond were found by Vrijmoed et al. (2008). The peridotite has low pressure primary spinel stable up to a pressure of 2.0 GPa at a temperature of 800 °C preserved while geothermobarometry on opx-grt-cpx assemblages yield pressures around 4.0 GPa and temperatures around 800 °C. This issue will discussed in a future paper (Vrijmoed, 2009, in prep.) where it is suggested, based on field evidence, that pres-

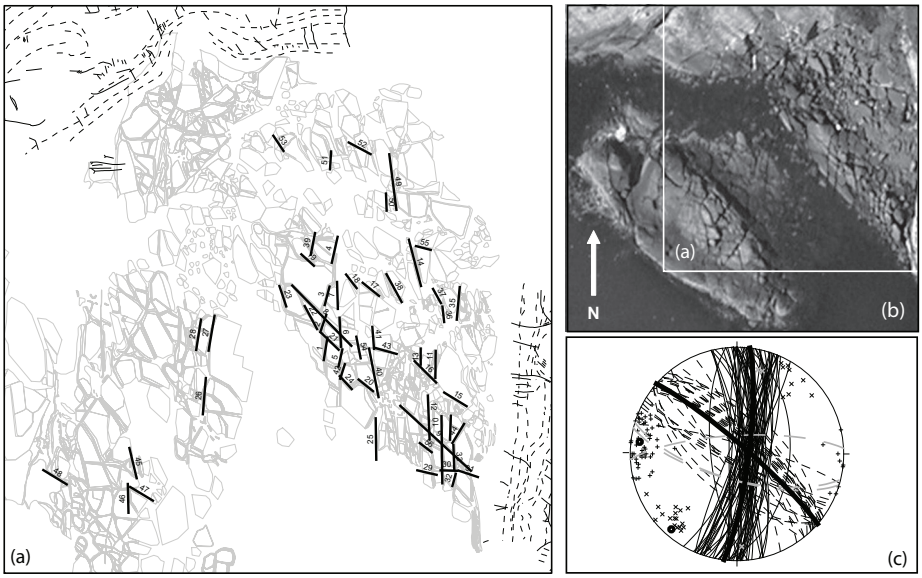

Figure 5.2: (a) Structural map showing representative measurements of the fractures crosscutting the Svartberget peridotite. Numbers are for identification of the fractures. The background light grey lines show outlines of individual peridotite blocks and veins in fractures. Thin black lines indicate late brittle fractures (joints) and foliation in surrounding gneiss is indicated by thin black broken lines. The regular pattern characteristic of conjugate sets of fractures can already be seen from the outlines of mapped blocks, aerial photograph shown in **(b)** and selected measured fractures highlighted in black. **(c)** Orientation of selected measured fractures in (a) plotted as poles and great circles in a stereographic projection. Thick black lines show the average of two major fracture sets (thin black lines: fractures 1-7,10-14,25-28,32-36,39-42,46,49,51,54 and thin black broken lines: fractures 8,9,15-22,24,47,52,55,56) and their poles in filled black circles. A minor fracture set is also shown in light grey broken lines (fractures 29-31). The figures show how the two main sets of fractures form a conjugate pair that is characteristic for brittle shear fractures.

sure variations may have existed during UHPM. Here we will provide a concept of a mechanism behind such pressure variations. The main observations that are important for this paper is that the phl-grt-websterites in the fractures yield much higher pressure estimates than the peridotite, which itself contains remnants of early low pressure spinel.

Migmatitic quartzo-feldspathic biotite-amphibole gneisses surround the peridotite. These are ductily deformed with abundant leucosomes and eclogite-amphibolite boudins (Fig. 5.3). Leucosomes are present as slivers several cm thick on a small scale throughout the whole extend of the outcrop up to 50 cm wide layer on the scale of several tens of meters. The composition of the leucosomes and melanosomes in the gneiss is typical for migmatites formed during the partial melting of metapelites by comparison with well-known examples of migmatites (Bea et al., 1994). Sillimanite and occassionally tiny garnets can be observed in the gneiss.

5.3.2 Timing

Garnet-clinopyroxene mineral pairs yield a Sm-Nd cooling age of 393 ± 3 Ma for the peridotite and 381 ± 6 Ma for the websterite suggesting that the grt-cpx assemblages in the Svartberget body formed during the UHPM of the Caledonian Orogeny. Details of the dating are discussed in (Vrijmoed et al., 2006). The grt-cpx mineral separates were taken from the same samples that were used for the P-T estimates and that yielded UHPM conditions.

There is a number of steps that can be recognized within the present database of ages (Vrijmoed et al., 2009, in prep.): metamorphic growth of zircon in the garnetite at 397 ± 1.2 Ma, either coinciding or predating an initial phase of leucosomes formation (397.4 ± 1.1 or 391.0 ± 1.0), formation or equilibration of garnet and pyroxene in peridotites and crystallization of pegmatite cores, rutile and monazite at 393-388 Ma, and late stages of activity at around 380 Ma.

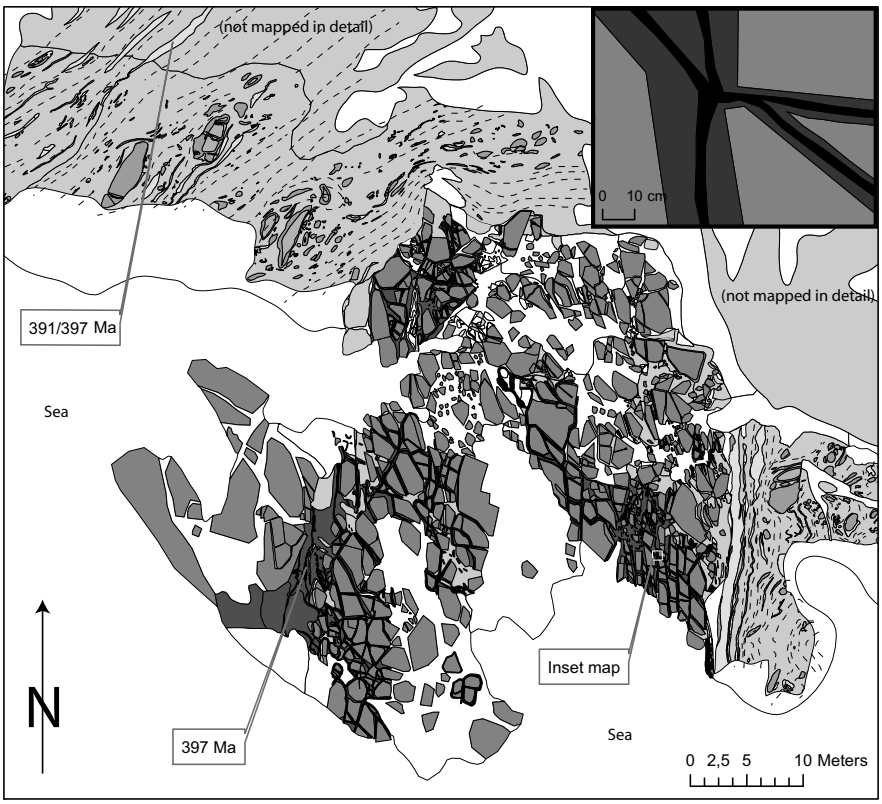

Figure 5.3: Geological map of the Svartberget peridotite and surrounding felsic gneiss showing only the major zones of the veins in the conjugate fractures. In the peridotite: Grey colours = peridotite; dark grey = grt-phl-websterite; black = garnetite. In surrounding area: light grey = migmatite; medium grey = amphibolitic migmatitic felsic gneiss; grey = eclogite; dark grey = amphibolite. Inset shows a detail of the relation of peridotite with crosscutting veins in the fractures. Ages point to location of zircon samples.

5.3.3 Melt infiltration and metasomatism

Field relations suggest that metasomatic reactions took place along the fractures with the peridotite. Whole rock XRF measurements were performed on the various altered peridotite blocks and the crosscutting websterites. The whole rock samples of altered peridotite blocks and individual zones in the fractures were compared to the least altered peridotite for mass balance. Mass balance calculations show a gain in Si, Al, Na, K, Rb, Ba, Sr, Y and Zr and loss of Fe, Mg, Ca, Sc, Zn, V, Cr, Cu and Ni in websterites with respect to most pristine wall rock samples of the peridotite indicating metasomatism of the Svartberget peridotite.

Sr isotopes in grt, cpx and whole rock of the veins and peridotite have a crustal signature matching the Sr isotopes in the gneiss, indicating that melts from the gneiss infiltrated the peridotite. Measured $^{87}Sr/^{86}Sr$ ratios were calculated back to 400 Ma, the time of the Caledonian UHP event. Initial $^{87}Sr/^{86}Sr$ values start from elevated values about 0.723 in most pristine peridotite samples and show an increasing trend up to ~ 0.743 in most altered samples in veins. All intials are about ten times higher than would be expected from a mafic-ultramafic rock. Whole rock samples from leucosomes and gneiss yield Sr initial values around 0.75 and are the

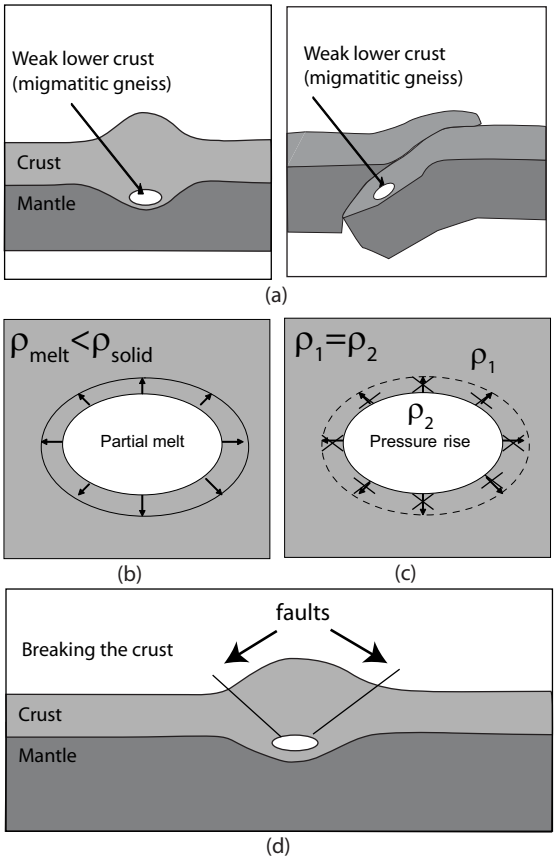

Figure 5.4: Figures showing the conceptual model discussed in this study. **(a)** Initial situation in which rocks from the lower crust are buried due to continental collision. It is reasonable to assume that not the whole crust that gets heated by burial will melt. So we consider that certain areas start producing partial melt which could happen both in a classical continental thickening scenario or a continental subduction scenario. **(b)** During this melting the rocks will have to expand because the density of melt will be lower than that of solid. **(c)** Because surrounding rocks are not melting the melting area is now confined to a certain volume, therefore the rocks will not be able to melt as much as they would in unconfined space. As a result the pressure in the melting area has to rise. **(d)** The pressure will rise up to a point where the rocks that formed the container break due to formation of large scale faults. When the pressure is released extensive decompression melting can take place.

most likely source for the crustal signature of Sr in the peridotite.

5.4 Conceptual model

The essence of our conceptual model is that a volume increasing reaction (partial melting of the gneiss) takes place in a space with a confined volume held by a container (the lithosphere). The result of such a reaction is an increase in pressure. The pressure is released as soon as the space is not confined anymore (i.e. when the container breaks). In the following section we will explain this for a general case and apply it to the case of the Svartberget peridotite.

5.4.1 Melting in confined space

Commonly when two continents collide a thickened crust develops with a mountain belt on top and a root below to maintain isostacy. During this process crustal rocks are being buried as the crust thickens. The lower crust consist of different material both ortho- and paragneiss. When rocks become metamorphosed during the burial partial melting in pelitic gneiss is likely to occur above a certain temperature. It is however not likely that the whole lithosphere starts melting. Thus a situation develops in which partial melting starts in certain volumes of rock surrounded by non-molten rocks. This situation is illustrated in Fig. 5.4a. The partially molten area is surrounded by solid rocks. Partially molten gneiss will have a lower density than solid rocks and will need to expand as a result of the melting (Fig. 5.4b). However the rocks that are not melting will not expand and a space problem develops. Therefore the melting region can not expand and instead it will rise the pressure (Fig.5.4c). Although the surrounding rocks of the lower crust might be relatively weak the upper crust and upper mantle confine the space and act as a container. When lithosphere scale fractures develop, for example extensional faults, this container breaks and pressure will be released Fig. 5.4d.

Melting in a confined space can be understood from a simple binary solid solution system which can be approximated by ideal solutions. For more complex multicomponent systems such as pelitic gneiss the thermodynamics is more complicated but the principle is the same. In Fig. 5.6 a P-T diagram of volume and melt percentage is shown for the Fo-Fa binary system. Consider what happens when temperature increases up to a point where melting starts. First volume will expand gently due to thermal expansion, until the rocks reach the solidus. At this point volume increases more rapidly and if the volume is confined the rock will stay on equal volume lines (isochores). When temperature keeps rising the rock will follow a path on an isochore increasing in T and inevitably also in P. From the P-T diagram where melt percentage is contoured it can be seen that isopleths of melt directly follow isochores, which means that melt percentage will not increase during such an isochoric melting process.

5.4.2 Application to Svartberget

The available whole rock, geochronological and isotope data from the Svartberget peridotite body suggest that the rocks were in a situation where surrounding gneis-

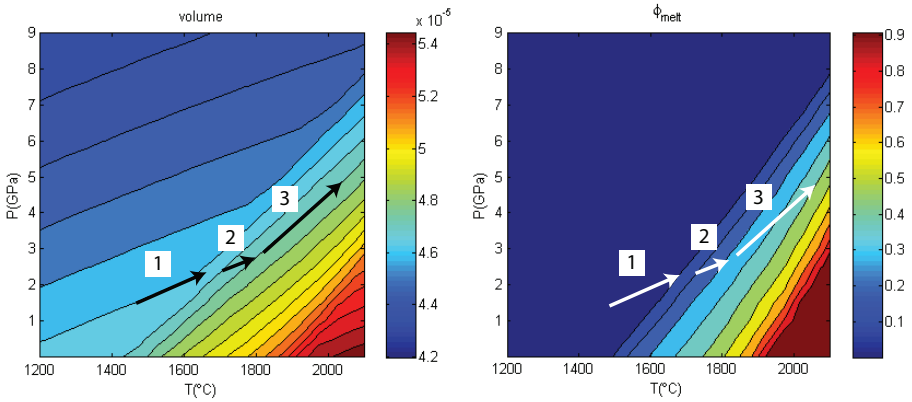

Figure 5.5: Concept of melting in a confined space for a simple binary ideal system as an example. **(a)** P-T diagram showing the volume of a system consisting of pure olivine calculated from the thermodynamic database of Holland and Powell (1998), assuming ideal mixing for both solid and liquid. Below a certain temparature (depending on P) the diagram shows gently dipping slopes of equal volume (isochores) in P-T space. This represents the increase in volume due to thermal expansion and the decrease in volume due to increase in P. Above this certain temperature isochores become much steeper which means that with increasing temperature a much stronger increase in volume takes place. This is the result of melting as can be seen in a plot of melt percentage in Fig. (b). The arrows indicate a hypothetical P-T path. First dry rocks that approache the solidus (arrow 1). Above the solidus the system starts to produce some melt (step 2) but now imagine that the volume is constrained. Then it has to follow lines of equal volume (step 3) and if temperature keeps increasing with the same amount the pressure suddenly increases much more than before. **(b)** The same P-T path is drawn on top of a diagram showing the fraction of melt. It can be seen that melting is greatly reduced while the rocks are constrained. Because rocks are never perfectly incompressible it is still possible to accommodate some melting.

sic rocks started melting during the Caledonian orogeny. Therefore the concept explained in the previous section can be applied to the rocks at Svartberget. We start the conceptual model at the point where rocks are buried to 70 km as can be constructed from structural data in the southern part of the WGR (Fig. 5.1). The

Figure 5.6: Conceptual model accounting for observed features in Svartberget. **(a)** Initial stage where the Svartberget body is enclosed in basement gneiss of the WGR somewhere in the lower crust.**(b)** During burial and heating rocks surrounding the peridotite start to melt, but surrounding non-molten rocks confine the space and pressure builds up **(c)** The small amount of interstitial melt that accumulates between grains adjacent to the peridotite lower the yield strength of the peridotite Fig. 5.7. **(d)** The lowering of the yield strength causes the rock to reach the brittle fracture criterion and conjugate brittle shear fractures develop **(e)** As soon as fracture propagate into the peridotite melt (or supercritical fluid) that has the same pressure (5.5 GPa) as the surrounding gneiss can flow in. This supercritical fluid is now highly reactive and metasomatism takes place at UHP conditions along the fractures capturing microinclusions of diamond while growing. **(f)** Finally the lithosphere holding the overpressured gneiss constrained breaks due to formation of large scale fractures in the crust and decompression melting starts and now that the gneiss is not constrained to a certain volume it can flow ductily and it is highly unlikely that any UHP mineral survived in such a deforming fluid rich environment.

strong peridotite is included in the weak gneiss of the lower crust which in itself is sandwiched between the upper crust and mantle (Fig. 5.6a).

The Svartberget rocks are situated in the structurally lowest part in the north of the WGR and are likely to have been buried deeper, perhaps as deep as 90 km. During this burial the rocks will cross the melting boundary from 700 to 800 °C (Hermann and Spandler, 2008) and melting in the confined space will rise the pressure up to 5.5 GPa (Fig. 5.6b). The peridotite is strong and holds its original low pressures.

The melt that is formed in the gneiss will be present between the mineral grains at a very high pressure and exert a pressure on the peridotite (Fig. 5.6c). Figure 5.7

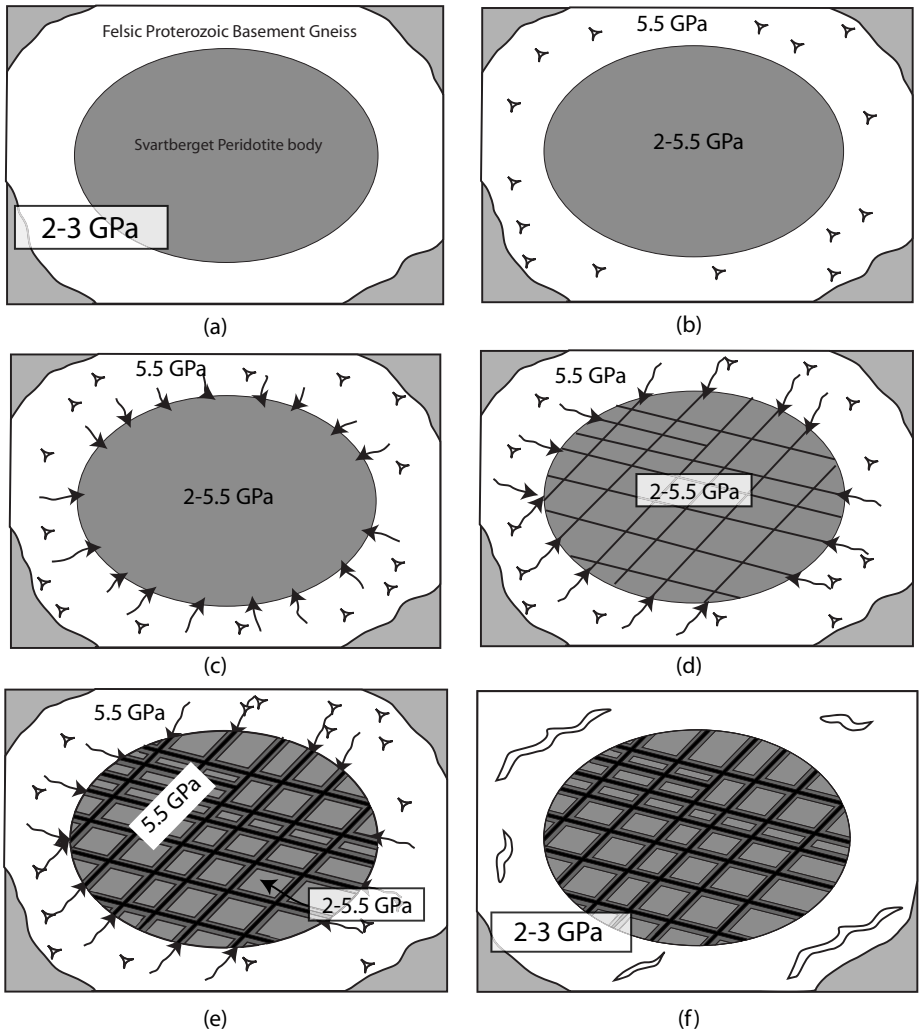

Figure 5.6

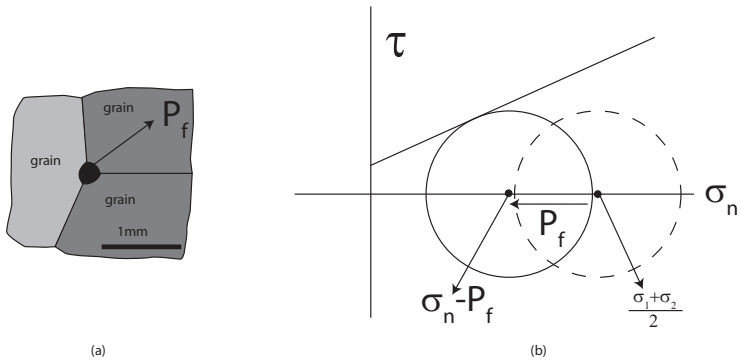

Figure 5.7: This figure illustrates how fracturing initiates at the contact of gneiss and peridotite **(a)** A melt pocket (black) situated between grains of peridotite and gneiss with a high pressure lowers in that point the yield strength of the material. **(b)** This figure illustrates how the state of stress at the location of melt shifts and hits the brittle failure envelope. As soon as this happens a fracture propagates into the peridotite and melt can percolate in, lowering the yield strenght again and the fracture can propagate further. This is likely to happen along the whole boundary between gneiss and peridotite. (P_f = fluid (melt) pressure; σ_n = normal stress; σ_1 = principal stress 1; σ_2 = principal stress 2; τ = shear stress)

is an enlargement of the situation on the boundary between gneiss and peridotite. A sketch of the state of stress of the peridotite is visualised by the Mohr circle in Fig. 5.7a.

The pressure of the melt or fluid (P_f) will lower the strength of the peridotite resulting in a shift of the Mohr circle to the left where it meets the brittle failure criterium. The fracture set that develops is a conjugate set having 60 ° angles (Fig. 5.6d). These fractures provide a pathway for the supercritical fluids to infiltrate the peridotite and metasomatise the rock to form a metasomatic column consisting mainly of phl-grt-websterites and garnetite (Fig. 5.6e). Because these supercritical fluids are physically connected to the gneiss and have the high pressures (5.5 GPa) diamond-grade conditions will be recorded in the websterites. The blocks of peridotite that are not broken will maintain their original pressure due to their strength.

Finally when for example extensional structures form in the orogen the container will break. When this happens the pressures are released and decompression melting takes place (5.6f). Now that the gneiss is not constrained to a certain volume anymore it will start to deform ductily more heavily and together with all the fluids released from dehydration reactions retrogression in the gneiss is quick and destroys any record of UHP. The release of such a highly pressurised unit of rocks is a potentially good exhumation mechanism, very similar to but perhaps less catastrophic than volcanic eruptions.

A summary of the conceptual model for the Svartberget peridotite is given in Fig. 5.9.

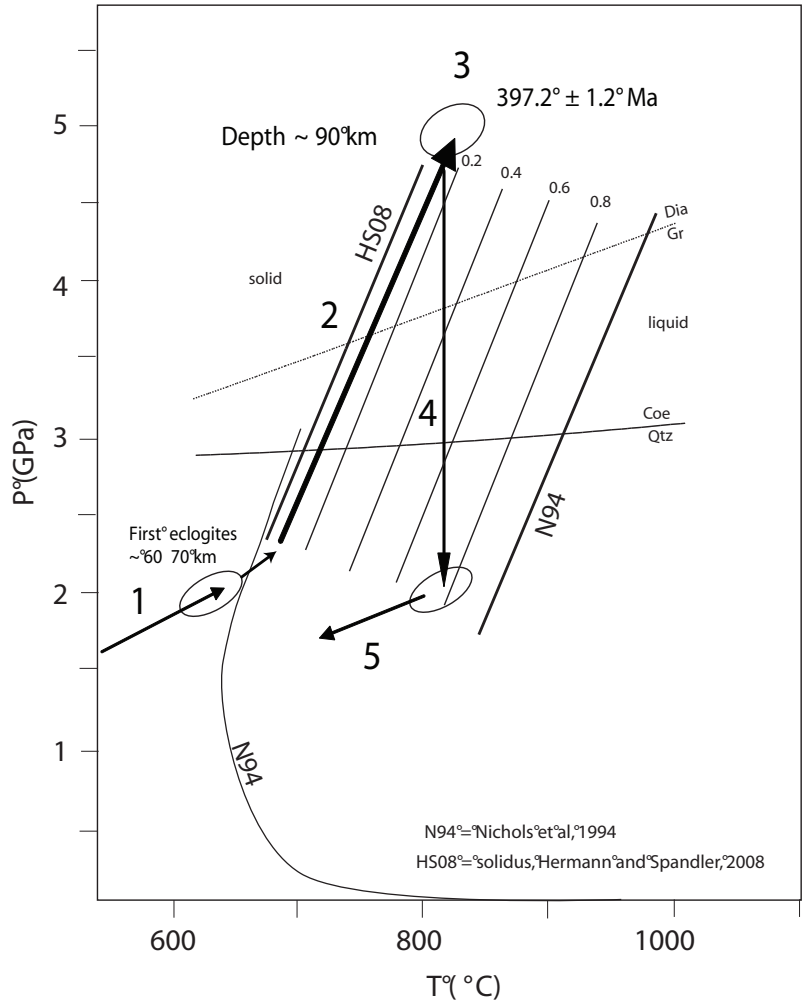

Figure 5.8: Summary of the conceptual model displayed in P-T space. The P-T trajectory is shown with arrows 1 to 5. In the first stage of collision rocks become buried and in the south of the WGR reached a depth of 60-70 in agreement with structural field reconstructions. In the north of the WGR rocks are positioned structurally below this and reached a depth of 90 km at the most. However during this path the gneiss surrounding the Svartberget peridotite started melting in a confined space and followed approximately the melt isopleths. During this process the pressures increased up to 5.5 GPa where fractures in the peridotite developed and metasomatism took place including the precipitation of diamond. Then the confined space was broken and pressure was released (arrow 4) resulting in extensive melting and new zircon growth in leucosomes. Finally the rocks were exhumed at 5 along the observed structures in the field. Dia-Gr and Coe-Qtz equilibrium lines, isopleths of melt (near vertical thin black lines taken from Hermann and Spandler (2008) (HS08 = solidus taken from Hermann and Spandler (2008)) N94 = liquidus taken from (Nichols et al., 1994); sol = solid; liq = liquid). Ages are single zircon U-Pb data for garnetite at 3 and leucosome at 4

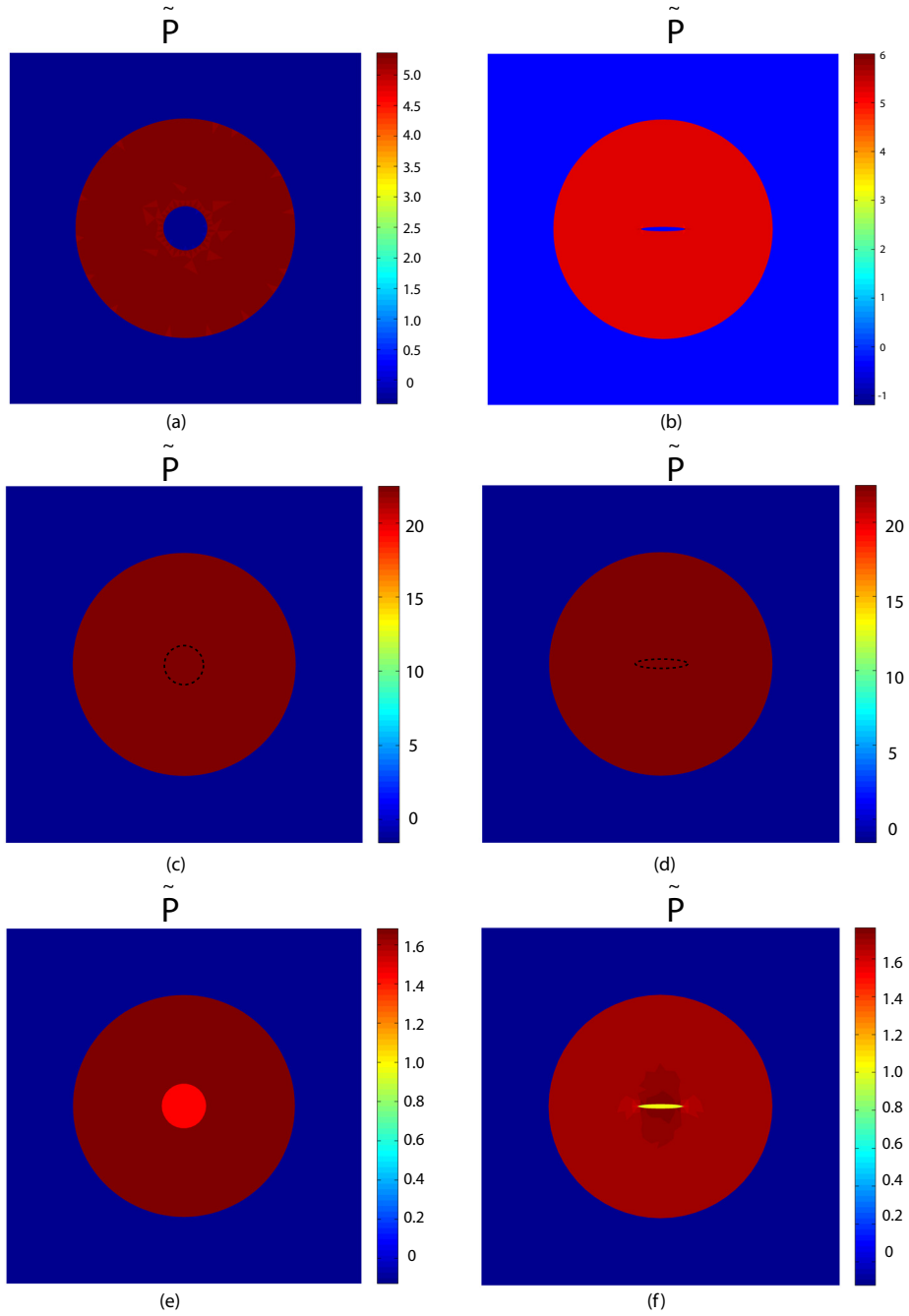
P̃
5.0
4.5
4.0
3.5
3.0
2.5
2.0
1.5
1.0
0.5
0
(a)
P̃
6
5
4
3
2
1
0
-1
(b)
P̃
20
15
10
5
0
(c)
P̃
20
15
10
5
0
(d)
P̃
1.6
1.4
1.2
1.0
0.8
0.6
0.4
0.2
0
(e)
P̃
1.6
1.4
1.2
1.0
0.8
0.6
0.4
0.2
0
(f)

Figure 5.9

5.5 Numerical test

To understand how a system will behave mechanically in a setting as described above we conducted numerical tests using FEM. We found that pressure variations are expected in the case when gneiss starts melting while it is enclosed in a ten to hundred times stronger container and has a peridotite enclave with the same strength as the container. Intuitively it might be expected that a peridotite enclave enclosed in pressurised confined melting gneiss would experience the same pressures as the gneiss. However the results of our mechanical modelling show that in this case pressures in the expanding gneiss are highest, while pressures in the peridotite are much lower than in the gneiss but still higher than in the containing lithosphere. Our results are discussed in more detail in the rest of this section.

5.5.1 Methods

We use a 2D FEM code written in Matlab with triangular elements having three nodes and one integration point. The mesh is generated using the mesh generator 'Triangle' (Shewchuk, 2005). The system of equations that we solve consist of the stress balance equations and a rheology law, either completely elastic (Hook's law) or viscous (Newton's law) including thermal strain that results from melting in a confined space. We use a setup with three nested cilinders that can be given different material properties. The outermost cilinder is our analogue for the lithosphere or the container, the middle cilinder simulates the migmatitic gneiss and the innermost cilinder is analogue to the peridotite. The outermost boundary of the outermost cilinder is fixed so it does not expand. The middle cilinder is expanding due to a rise in temperature. The shape of the peridotite can be varied. Results of systematic variations of the parameters are documented below.

5.5.2 Results

Results are shown in Fig. 5.9 and described below. The results are presented as colour coded 2D plots zoomed in on the area of interest (the boundaries of the

Figure 5.9: Results of the 2D FEM calculations plotted for dimensionless pressure. **(a)** In this case we calculated the pressures with equal strength of migmatitic gneiss, peridotite and non-molten containing lithosphere. The figure shows that the partially molten gneiss has a high overpressure while the peridotite and containing lithosphere have the same pressure and are hardly affected by the melting in the gneiss. **(b)** The same parameters as in (a) but only with a different shape of peridotite. It can be seen that there is no significant effect on the pressure distribution (N.B. colours are different but values are the same) **(c)** This figure shows the result for the case that the migmatitic gneiss is 10^5 times weaker than the peridotite and surrounding lithosphere. It can be seen that pressures are very high in the migmatitic gneiss and equally high in the peridotite and low in the surrounding lithosphere. **(d)** The same result as in (c) is obtained for different aspect ratios. **(e)** These results show the case where the migmatitic gneiss is ten times weaker than the lithosphere and peridotite. Here highest pressures are obtained in the migmatitic gneiss and lowest pressures in the surrounding lithosphere and intermediate pressures (but higher than the surrounding lithosphere) in the peridotite. **(f)** The same parameters are applied for this figure, but a different aspect ratio which results in higher pressure in the peridotite and slightly heterogeneous pressure distribution in the migmatitic gneiss.

outermost cilinder are far away). The colours correspond to values of a dimensionless pressure ($\tilde{P}$) for a Poisson's ratio of 1/3 :

$$\tilde{P} = \frac{\beta \Delta P}{\alpha \Delta T} \tag{5.1}$$

Where α = thermal expansion coefficient, β = compressibility, and the ΔP and ΔT are the increments of pressure and temperature during the process. If we rearrange this, we get an expression similar to the relation between pressure and temperature in a confined space derived given in Turcotte and Schubert (2002) (p. 172, Eq. 4-180):

$$\Delta P = \tilde{P} \frac{\alpha}{\beta} \Delta T \tag{5.2}$$

The exception is that the equation given here above includes the dimensionless pressure that we calculated. Our calculations can also be used for purely viscous rocks under the condition that the total strain during a given increase in temperature is the same. This is the case for our model, because the strain is a result of the melting reaction and is therefore the same in both viscous and elastic cases. Then the equation can we rewritten as:

$$\Delta P = \tilde{P} \eta \alpha \frac{\Delta T}{\Delta t} \tag{5.3}$$

Known values from literature can be substituted for α (thermal expansion coefficient) and η (viscosity) over a given temperature interval ΔT during a given period in time Δt to obtain the corresponding pressure increase ΔP. In the purely elastic case we can use equation 5.2. In that case ΔP will represent the total pressure increase starting from zero pressure.

When the strength of the container, gneiss and peridotite are all equal overpressure builds up in the gneiss and the container and peridotite have the same pressure. Figure 5.9a and b show the results of the calculations in the case of equal strengths of all three units for a spherically and elliptically shaped peridotite respectively. This situation produces large overpressures in the gneiss but the pressures in the peridotite are the same as in the container. However, felsic gneiss with hydrous minerals in the lower crust is likely to be much weaker than the upper crust and mantle or ultramafic rocks such as peridotite.

If the gneiss is five orders of magnitude weaker than the peridotite and container large overpressures are obtained in the gneiss and equally high overpressures are obtained for any shape of peridotite. The results are shown in Fig. 5.9c and d for different geometries. This case is more realistic in the sense that now the gneiss is weaker than the container and peridotite. But it does not explain how pressures in the peridotite can be lower than in the fractures that were inferred to have the same pressure as the gneiss.

If the gneiss is ten times weaker than the peridotite and container the pressure in the gneiss is highest, while the pressure of the peridotite is higher than the container. This situation is probably the most realistic of the three presented here because the gneiss is not likely to be five orders of magnitude weaker than the other rocks. In this case we can explain the pressure variations that we observe in the field.

5.6 Discussion

Whether the overpressure resulting from the melting in a confined space is a plausible mechanism to account for the UHP in the Svartberget peridotite depends on how much pressure the container can hold before it breaks and the magnitude of the pressure that can be obtained from the melting reaction. Further questions that will be addressed here are what rocks in the field may represent the container, if the melt reaction would increase the volume and whether the Svartberget rocks are a unique case.

With the modelling results presented in Fig. 5.9 it is now possible to estimate the pressures that will be generated using estimated values for the individual parameters of the dimensionless pressure. A typical value of β for rocks is $1{\cdot}10^{-11}$ (Turcotte and Schubert, 2002). The thermal expansion coefficient can be obtained from the solidus and liquidus in P-T space, for example from the diagram in Hermann and Spandler (2008) and Fig. 5.8. Reading the values from the diagram combined with the densities of the solid and liquid we can use the expression below to calculate α:

$$\alpha = \frac{1}{V_{ref}} \frac{(V_{new} - V_{ref})}{(T_{new} - T_{ref})} \tag{5.4}$$

We can obtain volumes per unit mass from the densities ($V = 1/\rho$). As an approximation we using density of granite and granite melt, 2650 kg/m^3 (Turcotte and Schubert, 2002) and 2290 kg/m^3 (Bass, 1995) to calculate V_{ref} and V_{new}, respectively. Although the densities change with pressure and temperature this is not a significant change and serves as a good approximation. Reading from the diagram the temperature T_{ref} at the solidus and T_{new} at the liquidus we obtain using equation (5.4) $\alpha \pm 6.79{\cdot}10^{-4}$.

The pressure would increase by 12.2 GPa during an increase in temperature of 100 °C in the purely elastic case (using equation 5.2. In the purely viscous case we can, under certain assumptions, replace the compressibility by viscosity/time and use equation 5.3. The time here corresponds to the time it takes to melt the rocks up to a specified amount. It can be easily seen that the bigger the time is, or the slower it melts, the smaller the resulting overpressure is. Using viscosities of 10^{22} the overpressure reached by melting within 10 000 years is 3.9 GPa and for 100 000 years is about 0.39 GPa. During this period it is likely that there is enough time to form UHP minerals.

The arguments used here for the existence of a container that confines the space in which melting takes place are straightforward. It is unrealistic to have the whole lithosphere molten, consequently if rocks become subject to partial melting they will always be surrounded by non-molten rocks. If the melting reaction comes with an increase in volume then the rocks will expand while the non-molten rocks will not and will act as a container. In order to sustain pressure difference of 1-2 GPa the container must have sufficient strength, i.e. to be able to hold differential stresses of similar magnitude. Laboratory experiments confirm that rocks of all major compositions may sustain differential stresses up to 1-1.5 GPa (e.g. Renshaw and Schulson, 2007). However, it is commonly believed that the differential stress level is low (significantly less than a 0.1 GPa) in the Earth's mantle and lithosphere at much larger time and length scales. This can be due to strength of the rocks lower than

extrapolated from laboratory measurements or lack of the mechanism able to generate high stresses. Seismologists report earthquakes stress drops in subduction settings up to 0.25 GPa (Kanamori, 1994), which represents the lower bound of the maximum stress (Scholz, 2004). Geological records suggest 0.5-0.6 GPa stress drop (Andersen et al., 2008; Trepmann and Stöckhert, 2003) indicating that the maximum stress must have been higher and agrees well with estimations of the stress drop presented in John et al. (2009). Indeed, recent field data from Andersen et al. (2008) on pseudotachylytes in Corsica indicate both that upper mantle lithospheric rocks in fact could sustain high differential stresses (Andersen et al., 2008) and that high differential stresses were generated. High loading rates may be related to the 100 year earthquake cycles or any other high frequency dynamics of the subduction zone factory (Kelemen and Hirth, 2007). But even on the slow rates of deformation ($1{\cdot}10^{-14}$ s^{-1}) numerical experiments show need for the maximum stress of 1-1.5 GPa to initiate an unstable earthquake-like deformation mode (Kelemen and Hirth, 2007). Trepmann and Stöckhert (2001) interpreted microstructural evidences in an eclogite-facies metagranite to be produced by differential stresses from 0.5 to up 1.0-2.0 GPa. To conclude, high stress levels up to 1 GPa may much more often reachable in natural settings than previously anticipated.

Even if the non-molten rocks immediately surrounding the partially molten gneiss were too weak at 800 °C they still form part of the lithosphere and must have had a strong crust on top and an upper mantle below. The alternative is that we had a crustal asthenosphere and crustal isostacy in which everything in the lower crust is in lithostatic equilibrium. Since field gravity measurements in 1851 it has been clear that mountains have roots and the first level of isostacy is in the mantle. Therefore it means that lithospheric rocks are strong enough to hold undulations of both topography and Moho (the upper and low parts of the container) for considerable geological time. According to the classic 'rheology independent Jeffreys argument' (Kanamori, 1979) the differential stress averaged over 100 km thickness of the lithosphere must be at the level of 0.1 GPa to support the mountains and their roots. John et al. (2009) reasoned that if concentrated to a 10 km stress guide within an otherwise weak plate boundary or to a similar size strong (cold) block of rock acting as a stress concentrator the stress level may reach the level of 1.0 GPa needed for failure even in their most simple simulations (0.1 GPa x 100 km /10km = 1 GPa). A similar argument can be suggested in 3D. For example, a strong exhuming block of lithosphere of 50 km lateral and crossectional extend within a 500 km long very weak (< 0.1 GPa) plate boundary having high mountains (e.g. Andes) would concentrate 2 GPa stresses (0.1 Gpa x 500/50 x 100 km /50km = 2 GPa). To conclude, an ability of rocks to hold differential stress levels up to 2 GPa is required to sustain topography of mountains and their roots, esspecially if significant part of the lithosphere is weakened by melting or any other mechanism along the weak plate boundary.

Large pressure variations can be sustained in inclusions in mechanically strong minerals such as garnet (Chopin, 1984; Van der Molen and Van Roermund, 1986; Chopin, 2003; O'Brien and Ziemann, 2008; Perrillat et al., 2003; Zhang, 1998; Ye et al., 2001), but may be suspected to drop dramatically in polycrystalline rocks. However, laboratory measurements on the rheology of eclogite show that the strength of such rocks is a simple mechanical mixture of the pure endmembers

garnetite and weaker omphacitite rather than a dramatically weaker rock type (Jin et al., 2001). If garnet can sustain 1-2 GPa overpressure and the mixture of garnet and cpx rheologically is not orders of magnitude weaker it seems plausible that pressure variations can be sustained also on the larger scale.

From a field geology perspective it might be questioned what rocks represent the container (referred to here as containing lithosphere occassionally). In the WGR there are many differences in amount of migmatisation of the gneisses and the Svartberget peridotite is located in an area that shows some of the most migmatised rocks equivalent to local units such as the Ulla Gneiss (Terry and Robinson, 2003). In contrast to those rocks, there are low-strain Proterozoic plutonic granitic rocks to the north at Drøga and Hustad (Austrheim et al., 2003) and relatively low strain rapakivi type augen orthogneiss near Molde to the south of the Svartberget gneisses (Harvey, 1983). These rocks are situated structurally above and below the migmatitic Svartberget gneiss (Ulla gneiss) and could possibly represent the container, which now is broken and will not form a coherent closed seal anymore. It must be noted here though that it is possible that late transverse movement associated with movement along the Møre Trøndelag Fault Zone (MTFZ) (Seranne, 1992) might have offset rock units in this area out of its original context. Possible thrust movement of the rock units is yet unconstrained in this area as it is difficult to identify major tectonic contacts. It is thus still possible that the rocks were approximately in their original context and their relative low grades of migmatisation and deformation might indicate their relative strength as a container.

Another immediate question to the concept presented here is whether the melt that forms has a higher or lower density (i.e. whether it is expanding or contracting). Depending on fluid-absent or fluid-present melting conditions the volume of melt is respectively larger or smaller than volume of the solid (Clemens and Droop, 1998). On the other hand, melt (or fluid) is more compressible than solid, so density crossovers are expected at higher pressures. For the case of the Svartberget conceptual model starting at 2-3 GPa it is likely to have fluid-absent melting condition and still far away from the density inversion where melt becomes heavier than solid (Suzuki and Ohtani, 2003). It can also be inferred from the positive slope of the experimentally derived melt isopleths in Fig. 5.8.

In the conceptual model described above the fracturing in the Svartberget peridotite is a result of lowering of the yield strength of the peridotite by pore fluid (melt) pressure. The same might happen on the side of the container and as such the boundaries of the container will be moving at the speed of the propagation of this fracture front. It is likely that it will take longer to break through the whole pile of rocks above and below than through than to fracture a small peridotite enclave.

Although a common consensus exists about the deep origin of the UHPM (Green, 2005) and several conceptual and sophisticated numerical models of deep continental subduction exist (Gerya et al., 2008; Hacker, 2007; Brueckner and Van Roermund, 2004), the problem remains that structures in the field only show the last part of the exhumation from the large depths derived from a lithostatic pressure assumption. The structural geology of the Western Alps has been studied in detail and reconstructions along several profiles through that part of the orogen that is famous for its coesite discovery in the Dora Maira massif (Chopin, 1984) are often insufficient to explain the exhumation of the coesite bearing rocks from depths of 100 km (Platt,

1986; Wheeler, 1991; Avigad et al., 2003; Ford et al., 2006). Or some reconstructions show that rocks might have been at greater depth than inferred from its P-T estimates, in other words they did not record the (U)HP and may have escaped through a subduction channel (Michard et al., 2004).

In addition, many UHP rocks are situated in a similar setting as the Svartberget peridotite, where UHP eclogites or peridotites are surrounded by migmatitic gneiss that show no signs of UHPM. The Alpe Arami garnet-peridotite massif in the central Alps displays UHP mineralogy while the surrounding, kyanite-bearing Lepontine gneisses display evidence of partial melting, but lack mineralogic relics indicative of UHPM and presents a problem of active research (Ernst and Liou, 2008).

If structural reconstructions in UHP areas cannot account for the amount of burial needed to explain lithostatic pressures or lack of fluids (Austrheim, 1987) and sluggish kinetics did not seem to be the problem then it might be worth investigating a possible explanation as we propose here for the Svartberget peridotite.

5.7 Conclusion

From the first order quantifications presented in this paper we can conclude that melting of gneiss in the weak lower crust can result in significant overpressures that are sustainable on the geological time scale.

Melting of gneiss in confined space where the gneiss is weaker than its container and inclusions provides a mechanism for pressure variations in rocks.

We can therefore conclude that the model of melting gneiss in confined space is a possible mechanism to account for the pressure variations and UHP metamorphism in the Svartberget peridotite.

5.8 Acknowledgements

This project was funded by the Norwegian Research Council as part of the funding of Physics of Geological Processes (PGP) for the PhD of J.C.Vrijmoed. We thank all PGP people for extensive discussions, in particular Nina Simon and Timm John. Marcin Dabrowski kindly provided help with the numerical modelling.

References

Andersen, T., Mair, K., Austrheim, H., Podladchikov, Y. Y., and Vrijmoed, J. C. (2008). Stress release in exhumed intermediate and deep earthquakes determined from ultramafic pseudotachylyte. *Geology*, 36(12):995–998.

Austrheim, H. (1987). Eclogitization of Lower Crustal Granulites by Fluid Migration through Shear Zones. *Earth and Planetary Science Letters*, 81(2-3):221–232.

Austrheim, H., Corfu, F., Bryhni, I., and Andersen, T. B. (2003). The Proterozoic Hustad igneous complex: a low strain enclave with a key to the history of the Western Gneiss Region of Norway. *Precambrian Research*, 120(1-2):149–175.

Avigad, D., Chopin, C., and Le Bayon, R. (2003). Thrusting and extension in the southern dora-maira ultra-high-pressure massif (Western alps): View from below the coesite-bearing unit. *Journal of Geology*, 111(1):57–70.

Bass, J. D. (1995). Elasticity of Minerals, Glasses, and Melts. *Mineral physics and Crystallography*, AGU Reference Shelf 2:45–63.

Bea, F., Pereira, M. D., and Stroh, A. (1994). Mineral Leucosome Trace-Element Partitioning in a Peraluminous Migmatite (a Laser Ablation-Icp-Ms Study). *Chemical Geology*, 117(1-4):291–312.

Blundy, J., Cashman, K., and Humphreys, M. (2006). Magma heating by decompression-driven crystallization beneath andesite volcanoes. *Nature*, 443(7107):76–80.

Brey, G. and Köhler, T. (1990). Geothermobarometry in Four-phase Lherzolites II. New Thermobarometers, and Practical Assessment of Existing Thermobarometers. *Journal of Petrology*, 31(6):1353–1378.

Brueckner, H. K. and Van Roermund, H. L. M. (2004). Dunk tectonics: A multiple subduction/eduction model for the evolution of the scandinavian caledonides.

Chopin, C. (1984). Coesite and pure pyrope in high-grade blueschists of the Western Alps - a first record and some consequences. *Contributions to Mineralogy and Petrology*, 86(2):107–118.

Chopin, C. (2003). Ultrahigh-pressure metamorphism: tracing continental crust into the mantle. *Earth and Planetary Science Letters*, 212(1-2):1–14.

Clemens, J. D. and Droop, G. T. R. (1998). Fluids, P-T paths and the fates of anatectic melts in the Earth's crust. *Lithos*, 44(1-2):21–36.

Dabrowski, M., Podladchikov, Y. Y., and Hartz, E. H. (2008). Migmatization induced overpressure, East Greenland case study. *Geophysical Research Abstracts*, 10:EGU2008–A–11303.

Ernst, W. G. and Liou, J. G. (2008). High- and ultrahigh-pressure metamorphism: Past results and future prospects. *American Mineralogist*, 93(11-12):1771–1786.

Ford, M., Duchene, S., Gasquet, D., and Vanderhaeghe, O. (2006). Two-phase orogenic convergence in the external and internal SW Alps. *Journal of the Geological Society*, 163:815–826.

Gerya, T. V., Perchuk, L. L., and Burg, J. P. (2008). Transient hot channels: Perpetrating and regurgitating ultrahigh-pressure, high-temperature crust-mantle associations in collision belts. *Lithos*, 103(1-2):236–256.

Gerya, T. V., Stöckhert, B., and Perchuk, A. L. (2002). Exhumation of high-pressure metamorphic rocks in a subduction channel: A numerical simulation. *Tectonics*, 21(6):1056.

Green, H. W. (2005). Psychology of a changing paradigm: 40+ years of high-pressure metamorphism. *International Geology Review*, 47(5):439–456.

Hacker, B. R. (2007). Ascent of the ultrahigh-pressure Western Gneiss Region, Norway. In Cloos, M., Carlson, W. D., Gilbert, M. C., Liou, J. G., and Sorensen, S. S., editors, *Convergent Margin Terranes and Associated Regions: A Tribute to W. G. Ernst*, volume 419 of *Geological Society of America Special Paper*, pages 1–14. Geological Society of America, USA.

Hartz, E. H., Podladchikov, Y. Y., and Dabrowski, M. (2007). Tectonic and reaction overpressures: Theoretical models and natural examples. *Geophysical Research Abstracts*, 9:EGU2007–A–10430.

Harvey, M. A. (1983). A geochemical and Rb-Sr study of the Proterozoic augen orthogneisses on the Molde peninsula, west Norway. *Lithos*, 16(4):325–338.

Hermann, J. and Spandler, C. J. (2008). Sediment melts at sub-arc depths: An experimental study. *Journal of Petrology*, 49(4):717–740.

Holland, T. J. B. and Powell, R. (1998). An internally consistent thermodynamic data set for phases of petrological interest. *Journal of Metamorphic Geology*, 16(3):309–343.

Jin, Z. M., Zhang, J., Green, H. W., and Jin, S. (2001). Eclogite rheology: Implications for subducted lithosphere. *Geology*, 29(8):667–670.

John, T., Medvedev, S., Rüpke, L. H., Andersen, T., Podladchikov, Y. Y., and Austrheim, H. (2009). Self-localizing thermal runaway as a mechanism for intermediate deep focus earthquakes. *Nature Geoscience*, in press.

Kanamori, H. (1979). Physics of the earth's interior, Proceedings of the International School of Physics Enrico Fermi, Course LXXVIII. *Varenna on Lake Como, Villa Monastero*, 23rd July-4th August:531–555.

Kanamori, H. (1994). Mechanics of Earthquakes. *Annual Review of Earth and Planetary Sciences*, 22:207–237.

Kelemen, P. B. and Hirth, G. (2007). A periodic shear-heating mechanism for intermediate-depth earthquakes in the mantle. *Nature*, 446(7137):787–790.

Labrousse, L., Jolivet, L., Andersen, T., Agard, P., Maluski, H., and Schärer, U. (2004). Pressure-temperature-time-deformation history of the exhumation of ultra-high-pressure rocks in the Western Gneiss Region, Norway. *Geol. Soc. Am., Special Paper*, 380:155–183.

Michard, A., Avigad, D., Goffe, B., and Chopin, C. (2004). The high-pressure metamorphic front of the south Western Alps (Ubaye-Maira transect, France, Italy). *Schweizerische Mineralogische Und Petrographische Mitteilungen*, 84(3):215–235.

Nichols, G. T., Wyllie, P. J., and Stern, C. R. (1994). Subduction Zone-Melting of Pelagic Sediments Constrained by Melting Experiments. *Nature*, 371(6500):785–788.

O'Brien, P. J. and Ziemann, M. A. (2008). Preservation of coesite in exhumed eclogite: insights from Raman mapping. *European Journal of Mineralogy*, 20:827–834.

Perrillat, J. P., Daniel, I., Lardeaux, J. M., and Cardon, H. (2003). Kinetics of the Coesite-Quartz Transition: Application to the Exhumation of Ultrahigh-Pressure Rocks. *Journal of Petrology*, 44(4):773–788.

Platt, J. P. (1986). Dynamics of Orogenic Wedges and the Uplift of High-Pressure Metamorphic Rocks. *Geological Society of America Bulletin*, 97(9):1037–1053.

Renshaw, C. E. and Schulson, E. M. (2007). Limits on rock strength under high confinement. *Earth and Planetary Science Letters*, 258(1-2):307–314.

Root, D. B., Hacker, B. R., Gans, P. B., Ducea, M. N., Eide, E. A., and Mosenfelder, J. L. (2005). Discrete ultrahigh-pressure domains in the Western Gneiss Region, Norway: implications for formation and exhumation. *Journal of Metamorphic Geology*, 23(1):45–61.

Scholz, C. H. (2004). *The mechanics of earthquakes and faulting (2nd edition)*. Cambridge University Press, Cambridge, UK.

Seranne, M. (1992). Late Paleozoic Kinematics of the Mre-Trondelag Fault Zone and Adjacent Areas, Central Norway. *Norsk Geologisk Tidsskrift*, 72(2):141–158.

Shewchuk, J. R. (2005). Triangle 1.6. In *http://www.cs.cmu.edu/ quake/triangle.html*. Internet.

Smith, D. C. (1984). Coesite in clinopyroxene in the Caledonides and its implications for geodynamics. *Nature*, 310(5979):641–644.

Suzuki, A. and Ohtani, E. (2003). Density of peridotite melts at high pressure. *Physics and Chemistry of Minerals*, 30(8):449–456.

Terry, M. P. and Robinson, P. (2003). Evolution of amphibolite-facies structural features and boundary conditions for deformation during exhumation of high- and ultrahigh-pressure rocks, Nordoyane, Western Gneiss Region, Norway. *Tectonics*, 22(4):1036, 10.1029/2001TC001349.

Torsvik, T. H., Smethurst, M. A., Meert, J. G., VanderVoo, R., McKerrow, W. S., Brasier, M. D., Sturt, B. A., and Walderhaug, H. J. (1996). Continental break-up and collision in the Neoproterozoic and Palaeozoic - A tale of Baltica and Laurentia. *Earth-Science Reviews*, 40(3-4):229–258.

Trepmann, C. and Stöckhert, B. (2001). Mechanical twinning of jadeite - an indication of synseismic loading beneath the brittle-plastic transition. *International Journal of Earth Sciences*, 90(1):4–13.

Trepmann, C. A. and Stöckhert, B. (2003). Quartz microstructures developed during non-steady state plastic flow at rapidly decaying stress and strain rate. *Journal of Structural Geology*, 25(12):2035–2051.

Tucker, R. D., Robinson, P., Solli, A., Gee, D. G., Thorsnes, T., Krogh, T. E., Nordgulen, Ø., and Bickford, M. E. (2004). Thrusting and extension in the scandian hinterland, Norway: New U-Pb ages and tectonostratigraphic evidence. *American Journal of Science*, 304(6):477–532.

Turcotte, D. L. and Schubert, G. (2002). *Geodynamics (Second Edition)*. Cambridge University Press, Cambridge.

Van der Molen, I. and Van Roermund, H. L. M. (1986). The Pressure Path of Solid Inclusions in Minerals - the Retention of Coesite Inclusions during Uplift. *Lithos*, 19(3-4):317–324.

Vrijmoed, J., Smith, D. C., and Van Roermund, H. (2008). Raman Confirmation of Microdiamond in the Svartberget Fe-Ti type garnet peridotite, Western Gneiss Region, Western Norway. *Terra Nova*, 40:295–301.

Vrijmoed, J. C. (2008). Stop 10.1. Diamond-bearing Svartberget olivine-websterite. In Robinson, P., Roberts, D., and D., G., editors, *A tectonostratigraphic transect across the central Scandinavian Caledonides, Part II Preliminary*, volume 2008.064, pages 2–5. Norges geologiske undersøkelse, Trondheim.

Vrijmoed, J. C. (2009). Pressure variations during ultra-high pressure metamorphism from single grain up to outcrop scale? *in preparation*.

Vrijmoed, J. C., Austrheim, H., John, T., R., H., Davies, G. R., and Corfu, F. (2009). Metasomatism of the ultra-high pressure Svartberget Fe-Ti type garnet-peridotite, Western Gneiss Region, Norway. *in preparation*.

Vrijmoed, J. C., Van Roermund, H. L. M., and Davies, G. R. (2006). Evidence for diamond-grade ultra-high pressure metamorphism and fluid interaction in the Svartberget Fe-Ti garnet peridotite-websterite body, Western Gneiss Region, Norway. *Mineralogy and Petrology*, 88(1-2):381–405.

Wheeler, J. (1991). Structural Evolution of a Subducted Continental Sliver - the Northern Dora Maira Massif, Italian Alps. *Journal of the Geological Society*, 148:1101–1113.

Ye, K., Liou, J. B., Cong, B., and Maruyama, S. (2001). Overpressures induced by coesite-quartz transition in zircon. *American Mineralogist*, 86:1151–1155.

Zhang, Y. (1998). Mechanical and phase equilibria in inclusion-host systems. *Earth and Planetary Science Letters*, 157:209–222.

Appendix A

Supplementary

A.1 Geological map

See inside back cover.

A.2 Table

	First session				Second session				Long term error (%)			
Standard	AGV-1	BCR-2	BHVO-2	GSP-1	AGV-1	BCR-2	BHVO-2	GSP-1	AGV-1	BCR-2	BHVO-2	GSP-1
Major elements (weight percentage)												
SiO_2	59.57	53.64	48.95	66.92	59.36	53.66	48.93	66.79	<1	<1	<1	<1
TiO_2	1.05	2.23	2.69	0.65	1.05	2.23	2.69	0.65	<1	<1	<1	<1
Al_2O_3	17.28	13.42	13.37	15.01	17.19	13.42	13.38	15.00	<1	<1	<1	<1
$Fe_2O_3^T$	6.74	13.60	12.08	4.20	6.72	13.62	12.10	4.19	<1	<1	<1	<1
MnO	0.10	0.19	0.17	0.04	0.10	0.20	0.17	0.04	<1	<1	<1	<1
MgO	1.46	3.50	7.07	0.92	1.46	3.50	7.06	0.92	<1	<1	<1	<1
CaO	4.97	7.05	11.22	1.99	4.95	7.06	11.23	1.99	<1	<1	<1	<1
Na_2O	4.25	3.11	2.18	2.75	4.22	3.11	2.16	2.74	<1	<1	<1	<1
K_2O	2.96	1.77	0.51	5.48	2.95	1.77	0.51	5.47	<1	<1	<1	<1
P_2O_5	0.50	0.35	0.26	0.28	0.50	0.35	0.26	0.28	<1	<1	<1	<1
Trace elements (ppm)												
Rb	68.35	49.49	9.35	256.13	68.27	49.60	9.53	256.44	1.31	3.07	-5.53	1.10
Ba	1196.77	657.71	63.03	1282.00	1199.89	660.49	63.64	1278.76	-2.32	-3.47	-47.88	-2.19
Sr	655.48	347.97	396.85	231.53	654.45	347.63	397.39	231.88	-1.00	0.59	1.89	-0.86
Pb	36.37	12.61	4.36	53.53	36.27	13.08	4.51	53.60	-2.45	12.34	n.d.	-3.14
Y	19.55	38.84	27.70	26.24	19.52	38.60	27.71	26.42	-2.48	4.57	6.63	-0.85
Sc	14.36	30.47	35.30	7.18	15.46	33.41	36.48	7.49	22.85	-5.43	9.54	8.22
Zr	228.66	189.60	172.39	504.14	228.72	189.79	172.87	506.42	0.02	0.32	-0.82	-4.65
Nb	15.20	12.39	18.83	28.90	15.15	12.52	18.98	28.94	0.42	n.d.	3.51	2.70
Ga	19.76	21.57	21.12	21.17	19.82	21.43	21.13	21.02	-0.52	-6.72	-3.46	-8.62
Zn	89.11	124.10	103.57	102.25	89.32	124.07	103.37	102.23	0.95	-2.48	0.34	-1.78
V	119.92	406.81	319.89	49.49	121.74	405.47	319.45	49.82	0.47	-2.38	-0.02	-6.42
Cr	9.86	15.55	296.31	11.40	9.57	15.25	296.10	10.93	-6.14	-20.83	5.19	-13.85
Cu	72.20	16.71	127.55	37.56	72.38	16.87	127.40	36.95	19.65	-12.82	0.28	13.15
Ni	14.99	9.63	124.16	7.38	14.89	9.50	124.28	6.93	-4.02	n.d.	3.37	-13.29
La	38.88	23.93	11.36	141.95	39.33	24.20	11.74	141.96	3.43	-6.57	-19.88	-22.11
Nd	27.17	26.30	26.02	150.39	29.24	26.86	25.83	152.51	-3.82	0.61	1.39	-21.33
Sm	5.10	5.87	5.65	23.88	5.82	6.10	5.79	24.32	3.24	-4.60	-3.53	26.35
Yb	1.81	4.33	3.66	1.51	1.38	3.69	4.17	1.01	-20.70	-5.36	88.07	-34.20

Table A.1: Results of standards measured during the two XRF sessions and errors of these standards based on long term reproducibility at the Faculty of Earth and Life Sciences, Vrije Universiteit, Amsterdam

Appendix B

Metasomatic zoning

B.1 Introduction

Metasomatism is usually used to describe metamorphism in an open system. This definition is so general that we need to specify it a bit more. When to call processes metasomatic depends really on the point of reference or what we define as the system. Suppose we consider the whole lower crust as our system. No matter how much of material is mobilized and redistributed this will not be defined as metasomatism as long as there is no material transferred across the boundaries of our system. In contrast if we look at the scale of single minerals and we consider metamorphic reactions there needs to be transfer of elements between grains so if an individual mineral is considered to be the system then we are dealing with metasomatism everywhere in the lower crust. So the definition used here is that if during metamorphism of our system material has been transported across the boundaries of our system we are dealing with metasomatism. Similar reasoning is given by Thompson (1959) in his introduction.

In this study we will look at infiltration of material dissolved in a fluid by porous flow perpendicular to a fracture. Our system is defined as the porous medium and the infiltrating material originates from outside the system. Thus we are dealing with metasomatism. The methods will be directly applied to a peridotite body enclosed in felsic gneisses of the Western Gneiss Region (WGR) in Norway.

B.2 Methods

B.2.1 Transport

Material or components are brought into our system dissolved in a fluid by means of advection and simultanously concentrations in the fluid can diffuse according to Fick's law. The complete balance equation for the concentration in the fluid and respectively solid reads (appendix C.1.1 lines 11-12 show the laws before substituting fluid and solid subscripts):

$$\frac{\partial \phi \rho_f c_f}{\partial t} + \frac{\partial \phi \rho_f c_f v_f}{\partial x} + D_{c_f} \frac{\partial^2 c_f}{\partial x^2} = Q_{c_f} \tag{B.1a}$$

$$\frac{\partial \left(1-\phi\right) \rho_s c_s}{\partial t} + \frac{\partial \left(1-\phi\right) \rho_s c_s v_s}{\partial x} + D_{c_s} \frac{\partial^2 c_s}{\partial x^2} = Q_{c_s} \tag{B.1b}$$

where c_f and c_s are the concentrations in the fluid and solid respectively, D_c is the diffusion coefficient, v_f and v_s are the velocities of fluid and solid, and Q_{c_f} and Q_{cs} are sources for the concentration of fluid and solid. Concentrations are conserved if $Q_{c_f} = -Q_{c_s}$ which can be thought of as how fast concentrations from the solid are entering the fluid during ion exchange reactions or vice versa (appendix C.1.1 line 22). The mass balance laws similarly look like:

$$\frac{\partial \phi \rho_f}{\partial t} + \frac{\partial \phi \rho_f v_f}{\partial x} = Q_{\rho_f} \tag{B.2a}$$

$$\frac{\partial \left(1-\phi\right) \rho_s}{\partial t} + \frac{\partial \left(1-\phi\right) \rho_s v_s}{\partial x} = Q_{\rho_s} \tag{B.2b}$$

Here the source terms $Q_{\rho f}$ and $Q_{\rho s}$ represent how mass is transferred from the solid to the fluid or vice versa. This can be thought of as melting due to change in pressure or temperature. Again to conserve mass we need to have $Q_{\rho_f} = -Q_{\rho_s}$ (appendix C.1.1 line 23). First, let us ignore the diffusion in the fluid and solid, which would be justified in the case that diffusion is much slower than the advection. We can recognise in the concentration balance the mass balance laws and by substituting the mass balance laws (equation (B.2)) we can simplify the concentration balance laws (appendix C.1.1 line 14-19):

$$\rho_f \phi \frac{\partial c_f}{\partial t} + \rho_f \phi v_f \frac{\partial c_f}{\partial x} = Q_{c_f} - c_f Q_{\rho_f} \tag{B.3a}$$

$$\rho_s \left(1-\phi\right) \frac{\partial c_s}{\partial t} + \rho_s \left(1-\phi\right) v_s \frac{\partial c_s}{\partial x} = Q_{c_s} - c_s Q_{\rho_s} \tag{B.3b}$$

We will keep the porosity constant, assuming that replacement of minerals proceeds without changing the porosity significantly in the process. We consider a situation in which the solid does not to move ($v_s = 0$). Summing up the balance equations for the concentration in fluid and solid the total concentration balance equation become then much simpler (appendix C.1.1 line 26-34):

$$\rho_f \phi \left(\frac{\partial c_f}{\partial t} + v_f \frac{\partial c_f}{\partial x} \right) + \rho_f \left(1-\phi\right) \left(\frac{\partial c_s}{\partial t} \right) = \left(c_s - c_f\right) Q_\rho \tag{B.4}$$

If the porosity is small the amount of the component in the fluid is also small and may be neglected for simplicity. We assume densities of solid and liquid and the velocity of the fluid to be constant which means that Q_ρ is zero (no melting or crystallisation, and equal P and T). Then we include the density in the concentration by defining the concentration as c/ρ and we end up with the simple form equivalent to equation 2 in Guy (1993):

$$\frac{\partial c_s}{\partial t} = -\phi \; v_f \frac{\partial c_f}{\partial x} \tag{B.5}$$

B.2.2 Metasomatic fronts

To study the evolution of metasomatic fronts it is not enough to just transport material into a rock. We need to consider reaction with the rock or interaction between the fluid and the solid which it infiltrates. This section introduces reaction to the equation (B.5) which makes it possible to solve the equation and discusses the evolution of metasomatic fronts.

Equation (B.1b) has two unknowns c_f and c_s and to find a solution to the equation we need another equation. From equilibrium thermodynamics we can get a relation between the fluid and solid concentrations at equilibrium:

$$c_f = f(c_s) \tag{B.6}$$

An example of such a relation is given here:

$$c_f = K_D c_s^n \tag{B.7}$$

where K_D represents the distribution coefficient between the solid and liquid. If $n = 1$ then the solid solutions are treated as ideal (Korzhinskii, 1970). Following Henry's law this can be applied to trace elements. Deviations from ideal behaviour can be made by introducing exponents above or below one. With a relation like (B.7) we can solve the equations numerically for example in Matlab. An example code is shown in appendix C.2.1 where line 24 represents equation (B.7) and line 25 is equivalent to (B.5).

The following explanation by Guy (1993) is very helpful to understand how the relationships of c_s with c_f may lead to the formation of reaction fronts. He shows that straight lines ($n = 1$) in c_s-c_f diagrams or isotherms with a constant slope just move all concentrations from an initial concentration profile at the same speed along with the infiltrating fluid. In contrast, curved isotherms cause different concentrations to move with different speeds resulting in a distortion of the shape of the initial concentration profile. The same has been shown nicely by Fletcher and Hofmann (1974). This can be understood if we subsitute c_f into (B.5). Using the chain rule of differentiation [1] (B.5) becomes:

$$\frac{\partial c_s}{\partial t} = -\phi \, v_f \, \frac{\partial c_f}{\partial c_s} \frac{\partial c_s}{\partial x} \tag{B.8}$$

If ϕ and v_f remain constant the formation of fronts can be predicted from the slope $(\partial c_f / \partial c_s)$ of the isotherms because the gradient in concentration is multiplied by the slope of the isotherm in (B.8) similar to ϕ and v_f. For example downward curving isotherms ($n > 1$) have larger slopes for high concentration than for low concentrations and consequently high concentrations will travel faster relative to low concentrations. Depending on existing gradients in concentration (negative versus positive gradients) an increase or decrease of these gradients will occur. The opposite will happen with isotherms curving upward ($n < 1$). Figure B.1 shows an example of the effect of different isotherms in the case of a sinosoidally curved initial concentration profile decreasing in concentration in the direction of fluid infiltration. In the case of the upward curved isotherm ($n = 0.5$) the low concentrations move

[1] $y(u(x))' = y(u)' \cdot u(x)'$, in this case: $y = c_f$ and $u = c_s$

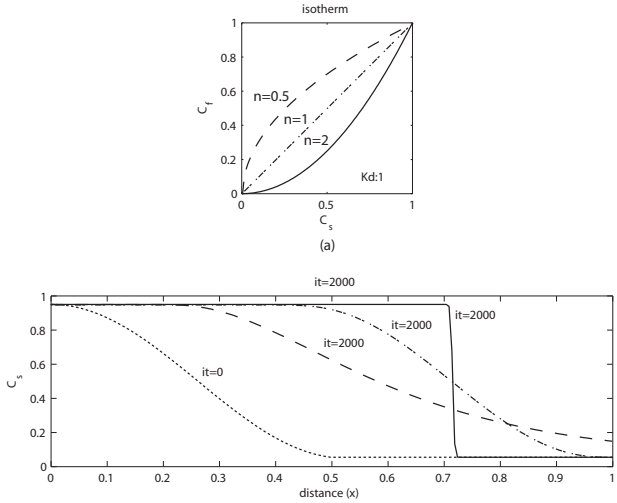

Figure B.1: (a) Three different isotherms with constant Kd and different exponent (n = power). (b) Calculated profiles for c_s after some time (2000 timesteps) for the corresponding isotherms in Fig (a). The initial profile of c_s is shown by the dotted line. Curves for are produced with the code in appendix C.2.1 by changing only the parameter pow in line 7 of the code (n in Fig. (a)).

faster than the high concentrations leading to a decrease in sharpness of concentration profile. For the linear isotherm the shape of the initial profile is maintained while being advected by the fluid. Only in the case of the downward curved isotherm ($n = 2$) where high concentrations move faster than low concentrations and a sharp front forms.

Fletcher and Hofmann (1974) analysed the effect of different shapes of isotherms including miscibility-gaps on concentration profiles in the case of combined diffusion-infiltration. The reader is referred to the original paper by Fletcher and Hofmann (1974) for further discussion. Isotherms describing the relation between c_s and c_f can only account for (metasomatic or replacement) fronts within rocks consisting of a mineral of variable composition or consisting of different minerals of variable composition that can be expressed with the same component as explained by Korzhinskii (1970) in his Fig. 3.

However in the description of of Thompson (1959) about metasomatic zoning we can read that metasomatic fronts can also be produced with pure minerals. We can use a titration method to do this. Titration is a common laboratory method of quantitative chemical analysis that is used to determine the unknown concentration of a known reactant. One adds a reagent of known concentration to a known reactant of unknown concentration and by reading the amount added until saturation one can determine the concentration of the reactant. This is possible when the chemical reaction and its equilibrium constant are known. Imagine for example a rock consisting of salt that has a saturated solution of water in its pores. In such a situation nothing will happen, the salt is in equilibrium with the water as it cannot dissolve more salt in it. As soon as we add fresh water to the system the pore solution

becomes undersaturated and some salt can dissolve. From experiments or theory we know the equilibrium conditions and we can determine the deviation from equilibrium which is the difference between the added fresh water and the equilibrium concentration of salt. We can then determine the amount of salt to be dissolved until saturation. Assuming local equilibrium the salt is immediately dissolved at the contact between fresh water and salt. Therefore we will always obtain a sharp reaction front with a titration method.

B.2.3 Multi-component, multi-phase systems

Rocks are usually multi-phase (or -mineralic) and multi-component systems and it is therefore interesting and more realistic to consider what would happen in the case of having more phases and components. This can quickly get complex and we to reduce complexity assume for the moment pure phases (i.e. minerals of fixed composition). Fletcher and Vidale (1976) have shown an example of how to treat a multi-component, multi-phase metasomatic system for fixed P-T and fixed solid compositions with a titration method and this is reproduced below.

For the transport we use a dimensionless version of equation (B.5) including diffusion, which is equivalent to equation 10 from Fletcher and Hofmann (1974) except for the usage of an isotherm (appendix C.2.2 lines 58-59):

$$\frac{\partial c_f}{\partial t} = D\frac{\partial^2 c_f}{\partial x^2} - q\frac{\partial c_f}{\partial x} \tag{B.9}$$

Suppose we have a rock that has four minerals in it. Muscovite (mu), sanidine (san), anorthite (an) and quartz (q). The rock has a porosity (which is low) and a chlorine fluid fills the porosity. The fluid in the pores is in equilibrium with the solid. We can write three equations for this system.

$$KAl_3Si_3O_{10}(OH)_2 + 6\,SiO_2 + 2\,KCl \longleftrightarrow 3\,KAlSi_3O_8 + 2\,HCl \tag{B.10a}$$
$$mu + 6\,q + 2\,c_{2_f} \longleftrightarrow 3\,san + 2\,c_{1_f} \tag{B.10b}$$

$$CaAl_2Si_2O_8 + 4\,SiO_2 + 2\,KCl \longleftrightarrow 2\,KAlSi_3O_8 + CaCl_2 \tag{B.11a}$$
$$an + 4\,q + 2\,c_{2_f} \longleftrightarrow 2\,san + c_{3_f} \tag{B.11b}$$

$$3\,CaAl_2Si_2O_8 + 2\,KCl + 4\,HCl \longleftrightarrow 2\,KAl_3Si_3O_{10}(OH)_2 + 3\,CaCl_2 \tag{B.12a}$$
$$3\,an + 2\,c_{2_f} + 4\,c_{1_f} \longleftrightarrow 2\,mu + 3\,c_{3_f} \tag{B.12b}$$

The equilibrium constants are just given by the products divided by reactants (law of mass action) of the aqueous species because the solids are pure phases and have concentrations equal to 1. The equilibrium constant for reaction (B.10) is reduced here to exclude the stoichiometric coefficients, for simplicity. So we write the equilibrium constants like this:

$$K_1 = \frac{[HCl]}{[KCl]} \tag{B.13a}$$

$$K_2 = \frac{[CaCl_2]}{[KCl]^2} \tag{B.13b}$$

$$K_3 = \frac{[CaCl_2]^3}{[KCl]^2[HCl]^4} \tag{B.13c}$$

where:

$$[HCl] = \frac{[HCl]}{[HCl][KCl]\ 2[CaCl_2]} \tag{B.14a}$$

$$[KCl] = \frac{[KCl]}{[HCl][KCl]\ 2[CaCl_2]} \tag{B.14b}$$

$$[CaCl_2] = \frac{[CaCl_2]}{[HCl][KCl]\ 2[CaCl_2]} \tag{B.14c}$$

In fact K_3 can be formed from K_1 and K_2:

$$\frac{{K_2}^3}{{K_1}^4} = \frac{[CaCl_2]^3}{[KCl]^2[HCl]^4} \tag{B.15}$$

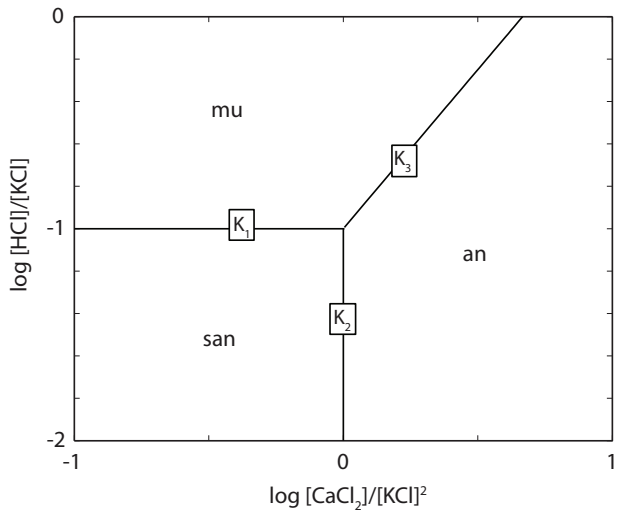

Figure B.2: Isothermal equilibrium diagram for the system an-san-mu-q (q is everywhere present).

We can visualise our system using the balanced reactions and values for the equilibrium constants in a concentration-concentration plot (Fig. B.2). From the plot we can see that mu, san and an (+ q) form an invariant assemblage. Use of the phase rule provides zero degrees of freedom (p=5, c=3) and hence the fluid composition

in equilibrium with the rock is also fixed. We can calculate the equilibrium values for the fluid in equilibrium with the rock using reaction (B.13a) and (B.13b) and the assumption that the chlorinity is constant in the system:

$$[HCl] + [KCl] + 2\,[CaCl_2] = 1 \tag{B.16}$$

We can initialise volume proportions of the solids and then calculate the amount of solid in mol/cm^3 by using the molar weights and density of the solids (appendix C.2.2 lines 9-19). With the calculated equilibrium concentrations we can intialise our system starting completely in equilibrium (appendix C.2.2 lines 38-41). Then we specify boundary conditions by solving equations (B.13a), (B.13b) and (B.16) simultaneously using different equilibrium constants (we choose a point on the equilibrium diagram) and set this as the boundary condition. This means that we have defined the incoming fluid composition (appendix C.2.2 lines 42-45).

So we have initialised the starting conditions now: a rock with 4 minerals, everywhere in equilibrium with a pore fluid and on the left boundary we start infiltrating with a fluid that is out of equilibrium with the rock. As soon as the new fluid meets the invariant mineral assemblage it disturbs the equilibrium. But exactly at this front a new equilibrium is established (local equilibrium). The incoming fluid deviates from the equilibrium value by Δc_f (appendix C.2.2 line 64).

$$\Delta c_{f_i} = c_{f_i} - c_{f_{eq_i}} \tag{B.17}$$

Exactly this amount can be used to establish how much of each phase will be dissolved or precipitated by using the chemical reactions. First we set up a system of equations by using a factor that determines the progress of the reaction f_r. Then we write balanced equations for each Δc_f. We do this by looking at the chemical reactions and counting the amount of moles of every concentration that would be gained or lost if the reaction goes to completion (to the right). For example for [HCl] (Δc_{1_f}) reaction (B.10) would give 2 moles from reaction (B.11) [HCl] is absent and from reaction (B.12) we would lose 4 moles of [HCl].

$$\Delta c_{1_f} = 2f_1 - 4f_3 \tag{B.18a}$$
$$\Delta c_{2_f} = -2f_1 - 2f_2 - 2f_3 \tag{B.18b}$$
$$\Delta c_{3_f} = f_2 + 3f_3 \tag{B.18c}$$

However, this system of equations has no solution because equation (B.18c) is dependent (Determinant = 0). So we just need equations (B.18a) and (B.18b) (appendix C.2.2 lines 66-67):

$$\Delta c_{1_f} = 2\,f_1 \tag{B.19a}$$
$$\Delta c_{2_f} = -2\,f_1 - 2\,f_2 \tag{B.19b}$$

Then we recalculate the moles in the reaction to mol/cm^3 by multiplying the Δc_{i_f} by porosity(ϕ) and the chlorinity ($[Cl]$) (appendix C.2.2 line 65), which are both assumed to be constant.

$$\Delta c_{1_f}[Cl]\,\phi = 2\,f_1 \tag{B.20a}$$
$$\Delta c_{2_f}[Cl]\,\phi = -2\,f_1 - 2\,f_2 \tag{B.20b}$$

We solve it for f (appendix C.2.2 line 68):

$$f_1 = 1/2\,\Delta c_{1_f}[Cl]\,\phi \tag{B.21a}$$
$$f_2 = -1/2\,\Delta c_{2_f}[Cl]\,\phi - 1/2\,\Delta\left(c_{1_f}\right)[Cl]\,\phi \tag{B.21b}$$

Now that we have found the reaction parameters we can also find how much of each solid will be produced as a result of the value of Δc_f. We simply use the stoichiometry of the reactions for this in the same way as we set up the system of equations (B.19). For example we would lose 1 mole of muscovite if equation (B.10) would go to completion, we would gain 3 moles of sanidine from equation (B.10) and 2 moles from equation (B.11), etc.

$$\Delta mu = -f_1 \tag{B.22a}$$
$$\Delta san = 3\,f_1 + 2\,f_2 \tag{B.22b}$$
$$\Delta an = -f_2 \tag{B.22c}$$
$$\Delta q = -6\,f_1 - 4\,f_2 \tag{B.22d}$$

Once have found all increments for fluid compositions (from transport) and all solid increments using the equilibrium equations we can update the solids by adding the increments (appendix C.2.2 lines 69-73). We must set the fluid composition to the equilibrium value before going to the next time step (appendix C.2.2 line 74).

The procedure described above holds only for the invariant point when all three solids are present (appendix C.2.2 line 63). If one of the solids completely disappears the fluid composition will be located on one of the univariant lines, which means that only one of the three reactions that we defined for the system takes place at the same time. Then we need to switch on a different calculation for each univariant line. We start with the reaction that has no muscovite (reaction 2). Here we use a somewhat different approach than in the invariant case. We cannot pinpoint the equilibrium fluid compositions because one of them is allowed to vary. This time we have to split the new c_f into the one from transport (c_{f_t}) and the one that is not known from the reaction (c_{f_r}).

$$c_{f_{new}} = c_{f_{t_i}} + \Delta c_{f_{r_i}} \tag{B.23}$$

We substitute the $c_{f_{new}}$ in to the equilibrium constant of the reaction of interest, for example for the muscovite-out reaction (B.11) (appendix C.2.2 lines 77-89).

$$K_2 = \frac{c_{3_f} + \Delta c_{3_f}}{\left(c_{2_f} + \Delta c_{2_f}\right)^2} \tag{B.24}$$

The next step is to bring back the number of unknowns to one by expressing the others in terms of one of them. For reaction (B.11) we can see that the moles of

[$CaCl_2$] and [KCl] are in equilibrium in the proportion 2:1. Therefore we can express [$CaCl_2$] (c_{3_f}) in the following way:

$$\Delta c_{3_f} = -1/2\,\Delta c_{2_f} \tag{B.25}$$

We substitute this in equation (B.24) and solve for the Δc_{2_f}.

$$\Delta c_{2_f} = -1/4\,\frac{4\,K_2 c_{2_f} + 1 - \sqrt{8\,K_2 c_{2_f} + 1 + 16\,K_2 c_{3_f}}}{K_2} \tag{B.26}$$

Finally we need to find the Δ's of the solids making use of equation (B.26):

$$\Delta an = 1/2\,\Delta c_{2_f}[Cl]\,\phi \tag{B.27a}$$
$$\Delta san = \Delta c_{2_f}[Cl]\,\phi \tag{B.27b}$$
$$\Delta q = 2\,\Delta c_{2_f}[Cl]\,\phi \tag{B.27c}$$

The other univariant lines work the same, although the sanidine-out (reaction(B.12)) is more challenging as it becomes a sixth order polynomial. For simplicity we truncate this after the second order and solve a normal quadratic formula (appendix C.2.2 lines 109-112). This seems to work fine in the san-mu-an-q case.

B.3 Application to a peridotite enclosed in felsic gneiss

B.3.1 Data

We will now apply the same method to rocks of the Western Gneiss Region at the Svartberget locality. This locality is situated along the coast south of the village Bud, north of Molde in West-Norway. At this locality a peridotite body is exposed within felsic migmatitic gneiss (Vrijmoed et al., 2006). This peridotite body is cut by a network of veins. These veins may consist up to 11 different zones each having sharp lithological boundaries. The zones get increasingly richer in crustal material compared to the peridotite. We can group these zones based on chemical similarity using whole rock data and mass balance on the different groups confirms the enrichment in crustal components. Two of these groups (A and B) are altered wall rocks and group C represent websterite veins while the innermost zone are mainly garnetites. From mass balance on these groups we see an increasing gain of SiO_2 CaO and Al_2O_3. Trace element data show a strong increase in Zr and Sr isotopes also show a gradient in radiogenic Sr from wall rock to veins. These data suggest that the infiltrating fluids or melts originated from the surrounding gneiss into the fractures of the peridotite. For simplicity we consider only non-hydrous pure minerals (opx=en-cpx=di-grt=py-ol=fo) in the modelling. The wall rock and altered wall rock (groups A and B) all have opx-cpx-grt-ol, the websterite veins (group C) have opx-grt-cpx and the garnetites have only grt (and some opx). These three groups are the main zones that we can model using the method described in the previous section.

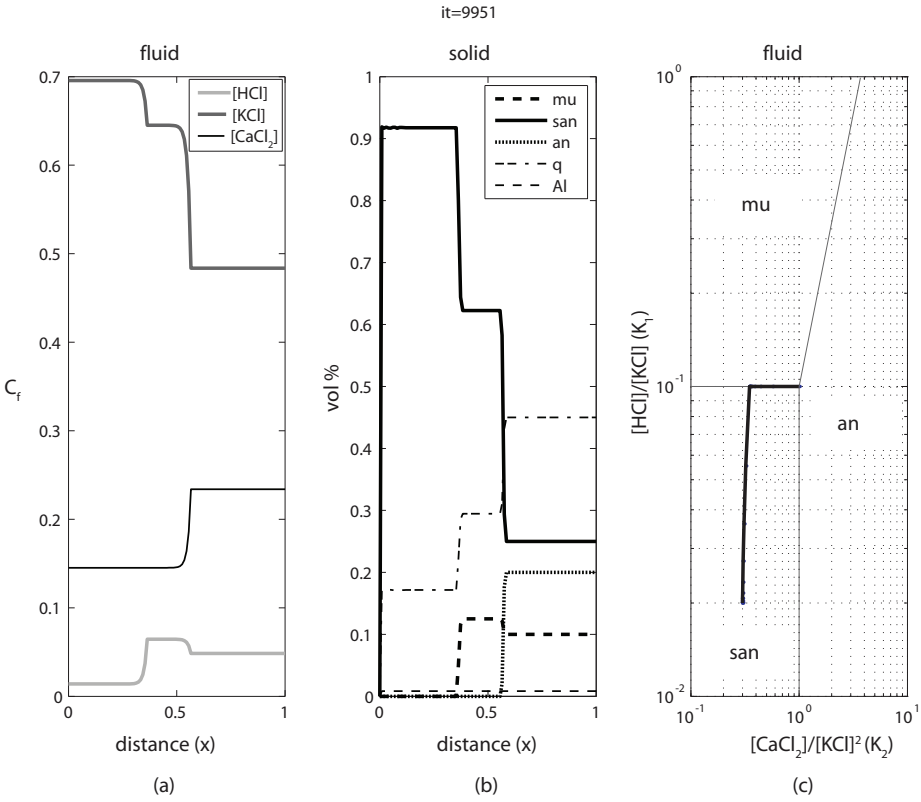

Figure B.3: Result of metasomatism after some time. A final zone of sanidine is inequilibrium with the incoming fluid. An intermediate zone is formed due to the presence of muscovite. This zone represents the univariant line.

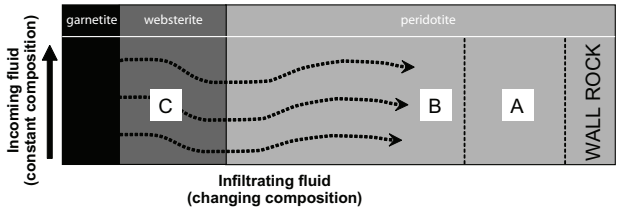

Figure B.4: Schematic representation of the metasomatic zoning in the Svartberget peridotite. The three main zones that are reproduced by modelling described in the text are indicated by the grey shading and simply called garnetite, websterite and peridotite. The chemically distinct groups wall rock, A, B, C and garnetite mentioned in the text are also indicated. From left to right they show a decreasing gain of SiO_2 CaO and Al_2O_3 with respect to the wall rock

B.3.2 Modelling

We take the wall rock as our initial rock which starts to be infiltrated with melts from the gneiss through fractures. We assume a continuous supply of melts in the fractures and melts percolate into the wall rock perpendicular to the fractures. We

can therefore represent the problem in 1D (Fig. B.4). The first thing to expect if olivine rocks are infiltrated with Si-rich fluids is that olivine reacts to form opx and if Ca accompanies Si it starts to form cpx. If Al was in the fluids then garnet could also form. Finally we can also have grt reacting to cpx with addition of Si and Ca and release of Al. All reactions are of course reversible if the right liquid composition is provided. These relations can (for pure phases) be expressed like this:

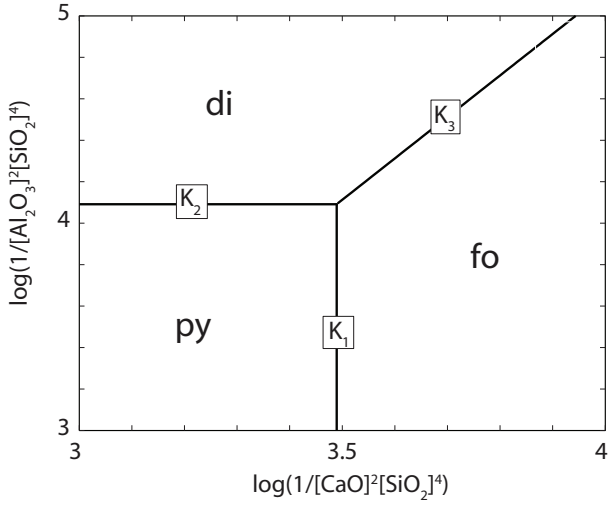

Figure B.5: Equilibrium phase diagram constructed with reactions (B.28),(B.29) and (B.30).

$$\begin{aligned} 2\,Mg_2SiO_4 \;+\; 4\,SiO_2 \;+\; 2\,CaO &\longleftrightarrow Mg_2Si_2O_6 \;+\; 2\,CaMgSi_2O_6 && \text{(B.28a)}\\ 2\,ol(fo) \;+\; 4\,c_{1_f} \;+\; 2\,c_{2_f} &\longleftrightarrow opx(en) \;+\; 2\,cpx(di) && \text{(B.28b)} \end{aligned}$$

$$\begin{aligned} 4\,Mg_2SiO_4 \;+\; 4\,SiO_2 \;+\; 2\,Al_2O_3 &\longleftrightarrow 2\,Mg_3Al_2Si_3O_{12} \;+\; Mg_2Si_2O_6 && \text{(B.29a)}\\ 4\,opx(en) \;+\; 4\,c_{1_f} \;+\; 2\,c_{3_f} &\longleftrightarrow 2\,grt(py) \;+\; opx(en) && \text{(B.29b)} \end{aligned}$$

$$2\,Mg_3Al_2Si_3O_{12} \;+\; 4\,SiO_2 \;+\; 4\,CaO \longleftrightarrow 4\,CaMgSi_2O_6 \;+\; Mg_2Si_2O_6 \;+\; 2\,Al_2O_3 \quad \text{(B.30a)}$$

$$2\,grt(py) \;+\; 4\,c_{1_f} \;+\; 4\,c_{2_f} \longleftrightarrow 4\,cpx(di) \;+\; opx(en) \;+\; 2\,c_{3_f} \quad \text{(B.30b)}$$

We can write the equilibrium constants for the first and second reaction and express the third with the other two:

$$K_1 = \frac{1}{[CaO]^2[SiO_2]^4} \tag{B.31a}$$

$$K_2 = \frac{1}{[SiO_2]^4[Al_2O_3]^2} \tag{B.31b}$$

$$K_3 = \frac{K_1^2}{K_2} \tag{B.31c}$$

Then we obtain a similar plot as for the san-mu-an system (Fig. B.5).

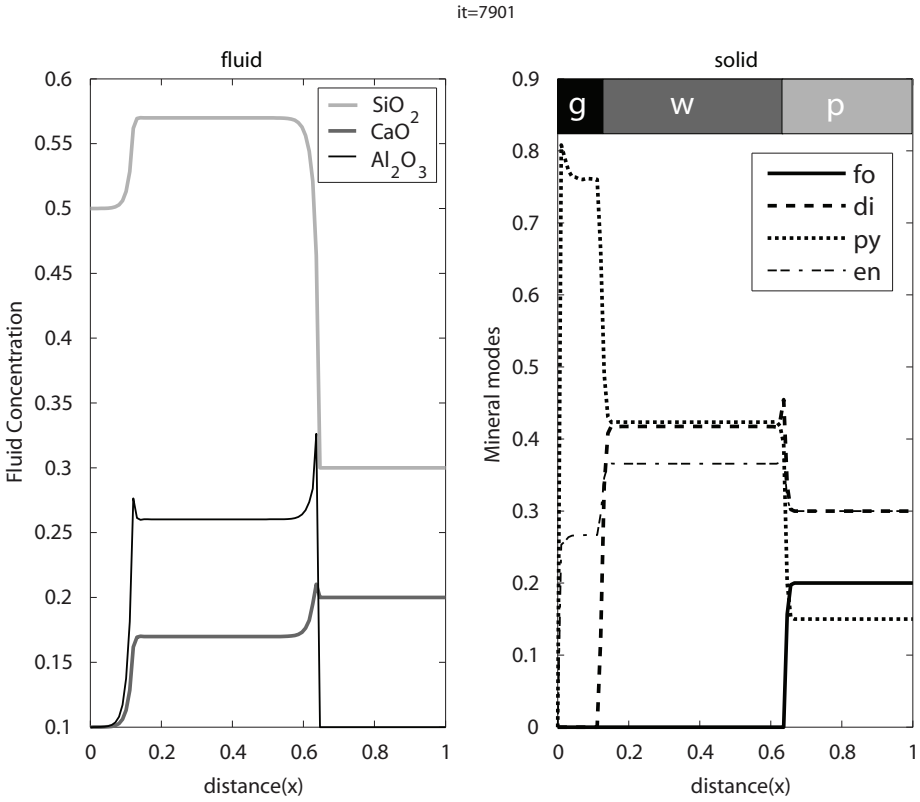

Figure B.6: Results of the metasomatic modelling reproduce the main zoning that can be observed in the field (indicated with the grey shaded bar on the top of the solid graph, g=garnetite, w=websterite,p=peridotite)

The rest of the procedure is the same (see appendix C.2.3). If the incoming fluid concentration plots in the field of garnet relatively more close to the K_2 equilibrium line than to the K_1 line in Fig. B.5 we will obtain the result as seen from the field: a wall rock with ol-cpx-opx-grt a zone with grt-cpx-opx and a zone with grt and opx (Fig. B.5).

References

Fletcher, R. and Hofmann, A. (1974). Simple models of diffusion and combined infiltration-diffusion metasomatism. In Hofmann, A., Giletti, B., Yoder, Jr., H., and Yund, R., editors, *Geochemical transport and kinetics*, volume 634, pages 243–259. Carnegie Institution of Washington Publication.

Fletcher, R. and Vidale, R. (1976). Analysis of infiltration metasomatism in a multicomponent chemical system. *EOS, Transactions American Geophysical Union*, 57(12):1015.

Guy, B. (1993). Mathematical Revision of Korzhinskii Theory of Infiltration Metasomatic Zoning. *European Journal of Mineralogy*, 5(2):317–339.

Korzhinskii, D. S. (1970). *Theory of metasomatic zoning*. Clarendon Press, Oxford.

Thompson, Jr., J. B. (1959). Local Equilibrium in Metasomatic Processes. In Abelson, P. H., editor, *Researches in Geochemistry*, volume 1, pages 427–457. John Wiley and Sons, Inc., New York.

Vrijmoed, J. C., Van Roermund, H. L. M., and Davies, G. R. (2006). Evidence for diamond-grade ultra-high pressure metamorphism and fluid interaction in the Svartberget Fe-Ti garnet peridotite-websterite body, Western Gneiss Region, Norway. *Mineralogy and Petrology*, 88(1-2):381–405.

Appendix C

Codes

C.1 Maple code

C.1.1 Derivation of transport equation

```
[> restart:
[> # Definitions
[> Rho   := rho(t,x):
[> C     := c(t,x):
[> V     := v(t,x):
[> Phi   := phi(t,x):
[> q[m]  := 0:
[> # General conservation law
[> BL    := Diff(M,t) + Diff(M*V+q[sub],x) = Q[sub]:
[> # Mass balance and concentration balance
[> BL_m  := convert(subs({M=Rho*Phi,sub=m},BL),diff):
[> BL_c  := convert(subs({M=Rho*C*Phi,sub=c},BL),diff):
[> # Substitute the mass balance in concentration balance
[> BL_c  := simplify(BL_c-BL_m*C):
[> # Split balance laws for fluid and solid
[> BL_cf := subs({v=v[f],c(t,x)=c[f](t,x),rho=rho[f],Q[c]=Qc[f],
                  Q[m]=Qm[f]},BL_c):
[> BL_cs := subs({v=v[s],c(t,x)=c[s](t,x),rho=rho[s],phi=(1-phi),
                  Q[c]=Qc[s],Q[m]=Qm[s]},BL_c):
[> BL_Ct := BL_cf+BL_cs:
[> # Conserve sources of fluid and solid
[> Qc[s] := -Qc[f]:
[> Qm[s] := -Qm[f]:
[> # Total concentration balance law
[> BL_C  := collect(simplify(BL_Ct),Qm[f]):
[> # Assumptions
[> v[s](t,x)   := 0:
[> rho[f](t,x) := rho[f]:
[> rho[s](t,x) := rho[s]:
[> v[f](t,x)   := v[f]:
```

```
31 [> phi[f](t,x) := rho[f]:
32 [> Qm[f]       := 0:
33 [> # Simplified concentration balance equation
34 [> BL_C;
```

C.2 Matlab code

C.2.1 Metasomatic fronts (using isotherm)

```
clear,clf
% Physics
Lx    = 1;
vf    = 10000;
phi   = 0.1;
Kd    = 1;
pow   = 2;
% The isotherm just for plotting
C_si  = 0:0.01:1;
C_fi  = Kd*C_si.^(pow);
% Numerics
nt    = 2000;
nx    = 200;
dx    = Lx/(nx-1);
x     = 0:dx:Lx;
dt    = 0.45*dx/vf;
% Initialisation;
C_s           = 0.45*cos(6*x)+0.5;
C_s(nx/2:end) = 0.055;
C_s_ini       = C_s;
% Processing
for it = 1:nt
    % The physics equations
    C_f         = Kd*C_s.^(pow);
    C_s(2:end) = C_s(2:end) - phi*vf*diff(C_f)/dx*dt;
    % Fix numerical trouble
    C_f0       = find(C_f<0);
    C_f(C_f0) = 0;
    C_s0       = find(C_s<0);
    C_s(C_s0) = 0;
    % Postprocessing
    subplot(211),plot(C_si,C_fi),...
        title('isotherm'),...
        text(0.7,0.1,['Kd:',num2str(Kd)]), ...
        xlabel('C_s'),ylabel('C_f'),axis square
    subplot(212),plot(x,C_s,x,C_s_ini), ....
        axis([0 Lx 0 1]), ...
        title(['it=', num2str(it)]), ...
        xlabel('distance (x)'),ylabel('C_s')
    drawnow
end
```

C.2.2 Multicomponent metasomatism (san-an-mu-qtz)

```
clear,clf
% Metasomatism in the sanidine–muscovite–anorthite system
%(after Ray Fletcher)
% physics
L      = 1;   % length of the domain
D      = 1;   % diffusion coefficient
q      = 100; % fluid flux
phi    = 0.1; % porosity
%        [mu     san  an     qtz];
modes  = [0.1    0.25  0.2  0.45];
%        [K      Ca     Al    Si     O      H];
MW     = [39.098 40.078 26.98 28.085 15.999 1];
rho    = [2.88   2.56 2.75 2.65 ];
stoich = [1 0 3 3 12 2;
          1 0 1 3  8 0;
          0 1 2 2  8 0;
          0 0 0 1  2 0];
molw   = stoich*MW';
molcm3 = rho'./molw;
solids = molcm3.*modes';
% chemistry
K1   = 0.1;
K2   = 1;
K    = [K1 K2 (K2^3)/(K1^4)];    % equilibrium constants
Cl   = 5e-3;       % chlorinity
Ki   = [0.02 0.3]; % incoming fluid composition
% numerics
nx   = 100;        % number of grid points
dx   = L/(nx-1);   % step in x direction
x    = 0:dx:L;     % x-array
nt   = 10000;      % number of time steps
nout = 50;         % number of time steps plotted
dt   = 0.25*dx*dx; % time step
nc   = 3;          % number of components
ns   = 4;          % number of solids
% initialisation
C      = zeros(size(x,2),nc);
S      = zeros(size(x,2),ns);
Ceq(2) = ( -(K(1)+1)+sqrt( (K(1)+1)^2 - 4* (2*K(2)) *(-1) ) ...
           )/(2*(2*K(2))); % abc formula for equilibrium 2nd component
Ceq(1) = K(1)*Ceq(2);      % calculate equilibrium of first component
Ceq(3) = K(2)*Ceq(2)^2;    % calculate equilibrium of third component
Ci(2)  = ( -(Ki(1)+1)+sqrt( (Ki(1)+1)^2 - 4* (2*Ki(2)) *(-1) ) ...
           )/(2*(2*Ki(2))); % calculate incoming fluid compositions
Ci(1)  = Ki(1)*Ci(2);
Ci(3)  = Ki(2)*Ci(2)^2;
for ic = 1:nc
  C(:,ic) = ones(size(x,2),1)*Ceq(ic);
  C(1,ic) = Ci(ic);
end
for is = 1:ns
  S(:,is) = ones(size(x,2),1)*solids(is);
  S(1,is) = 0;
```

```
end
% processing
for it = 1:nt
  % Transport
  for ic = 1:nc
    C(2:end-1,ic) = C(2:end-1,ic) + D*diff(C(:,ic),2)/dx^2*dt;
    C(2:end-1,ic) = C(2:end-1,ic) - q*(diff(C(1:end-1,ic))/dx)*dt;
  end
  for ix = 2:size(x,2)
    % Invariant titration
    if S(ix,1)>0 && S(ix,2)>0 && S(ix,3)>0
      dC      = C(ix,:)-Ceq;
      dCm     = [-dC(1); -dC(2)]*phi*Cl;
      mat     = [ 2   0;
                  -2  -2];
      f       = mat\dCm;
      dS(1)   = -f(1);
      dS(2)   = 3*f(1)+2*f(2);
      dS(3)   = -f(2);
      dS(4)   = -6*f(1)-4*f(2);
      S(ix,:) = S(ix,:) + dS;
      C(ix,:) = Ceq;
    end
    % Univariant-line: Muscovite out
    if S(ix,1)==0 && S(ix,2)>0 && S(ix,3)>0
      a       = K(2);
      b       = 2*K(2)*C(ix,2)+0.5;
      c       = K(2)*C(ix,2)^2-C(ix,3);
      dC(1)   = 0;
      dC(2)   = (-b+sqrt(b^2-4*a*c))/(2*a);
      dCm     = dC*Cl*phi;
      S(ix,2) = S(ix,2) - dCm(2);
      S(ix,3) = S(ix,3) + 0.5*dCm(2);
      S(ix,4) = S(ix,2) + 2*dCm(2);
      C(ix,1) = C(ix,1) + dC(1);
      C(ix,2) = C(ix,2) + dC(2);
      C(ix,3) = (1- C(ix,1) - C(ix,2))/2;
    end
    % Univariant-line: Anorthite out
    if S(ix,1)>0 && S(ix,2)>0 && S(ix,3)==0
      dC(2)   = (C(ix,1)-K(1)*C(ix,2))/(1+K(1));
      dC(1)   = -dC(2);
      dCm(1)  = dC(1)*Cl*phi;
      dCm(2)  = dC(2)*Cl*phi;
      S(ix,1) = S(ix,1) + 0.5*dCm(2);
      S(ix,2) = S(ix,2) - (3/2)*dCm(2);
      S(ix,4) = S(ix,4) + 3*dCm(2);
      C(ix,1) = C(ix,1) + dC(1);
      C(ix,2) = C(ix,2) + dC(2);
      C(ix,3) = (1- C(ix,1) - C(ix,2))/2;
    end
    % Univariant-line: Sanidine out
    if S(ix,1)>0 && S(ix,2)==0 && S(ix,3)>0
      C1      = C(ix,1);
      C2      = C(ix,2);
      C3      = C(ix,3);
```

```
      a       = K(3)*C1^4+16*K(3)*C1^3*C2+24*K(3)*C1^2*C2^2-27/4*C3;
      b       = 2*K(3)*C1^4*C2+8*K(3)*C1^3*C2^2+9/2*C3^2;
      c       = K(3)*C1^4*C2^2-C3^3;
      dC(2)   = (-b+sqrt(b^2-4*a*c))/(2*a);
      dC(1)   = 2*dC(2);
      dCm(1)  = dC(1)*Cl*phi;
      dCm(2)  = dC(2)*Cl*phi;
      S(ix,1) = S(ix,1) - dCm(2);
      S(ix,3) = S(ix,3) + (3/2)*dCm(2);
      C(ix,1) = C(ix,1) + dC(1);
      C(ix,2) = C(ix,2) + dC(2);
      C(ix,3) = (1- C(ix,1) - C(ix,2))/2;
    end
  end
  C0    = find(C<0);
  C(C0) = 0;
  S0    = find(S<0);
  S(S0) = 0;
  % postprocessing
  Smod = S./repmat(molcm3',nx,1);
  AL   = 3*S(:,1)+S(:,2)+2*S(:,3);
  X    = C(:,3)./C(:,2).^2;
  Y    = C(:,1)./C(:,2);
  if mod(it,nout)==1
    subplot(131),plot(x,C),title(num2str(it))
    subplot(132),plot(x,Smod,x,AL)
    legend('mu','san','an','qtz','Al')
    subplot(133),loglog(X,Y,'.-'),axis([0.1 10 0.01 1]),grid
    drawnow
  end
end
```

C.2.3 Multicomponent metasomatism (fo-py-di-en)

```
clear,clf
% Metasomatism Svartberget:
% The Forsterite-Diopside-Pyrope + Enstatite system
% physics
L      = 1;   % length of the domain
D      = 1;   % diffusivity
q      = 100; % fluid flux
phi    = 0.1; % porosity
%        [fo      di    py    en];
modes  = [0.2    0.3   0.15   0.3];
rho    = [3.27   3.278 3.78   3.2];
%        [Ca     Al    Mg     Si     O     ];
MW     = [40.078 26.98 24.305 28.085 15.999];
stoich = [0 0 2 1  4;
    1 0 1 2  6;
    0 2 3 3 12;
    0 0 2 2  6];
molw   = stoich*MW';
molcm3 = rho'./molw;
solids = molcm3.*modes';
% chemistry
```

```
Ceq  = [0.3 0.2 0.1];
tot  = 5e-3; % equivalent to the chlorinity in san-mus-an case
K1   = 1/(Ceq(2)^2*Ceq(1)^4);
K2   = 1/(Ceq(3)^2*Ceq(1)^4);
K3   = (K1^2)/(K2);
K    = [K1 K2 (K1^2)/(K2)];  % equilibrium constants
Ci   = [0.5 0.1 0.1];         % incoming fluid composition
% numerics
nx   = 100;         % number of grid points
dx   = L/(nx-1);    % step in x direction
x    = 0:dx:L;      % x-array
nt   = 8000;        % number of time steps
nout = 100;         % number of time steps plotted
dt   = 0.25*dx*dx; % time step
nc   = 3;           % number of components
ns   = 4;           % number of solids
% initialisation
C      = zeros(size(x,2),nc);
S      = zeros(size(x,2),ns);
for ic = 1:nc
    C(:,ic) = ones(size(x,2),1)*Ceq(ic);
    C(1,ic) = Ci(ic);
end
for is = 1:ns
    S(:,is) = ones(size(x,2),1)*solids(is);
    S(1,is) = 0;
end
% processing
for it = 1:nt
    % Transport
    for ic = 1:nc
        C(2:end-1,ic) = C(2:end-1,ic) + D*diff(C(:,ic),2)/dx^2*dt;
        C(2:end-1,ic) = C(2:end-1,ic) - q*(diff(C(1:end-1,ic))/dx)*dt;
    end
    for ix = 2:size(x,2)
        % Invariant titration
        if S(ix,1)>0 && S(ix,2)>0 && S(ix,3)>0
            dC    = C(ix,:)-Ceq;
            dCm   = [-dC(1); -dC(2)]*phi*tot;
            mat   = [-4  -4;
                      -2   0];
            f     = mat\dCm;
            dS(1)   = -2*f(1)-4*f(2);
            dS(2)   =  2*f(1)+2*f(2);
            dS(3)   =  2*f(2);
            dS(4)   =  f(1)+f(2);
            S(ix,:) = S(ix,:) + dS;
            C(ix,:) = Ceq;
        end
        % Univariant-line: Forsterite out
        if S(ix,1)==0 && S(ix,2)>0 && S(ix,3)>0
            C1 = C(ix,1);
            C2 = C(ix,2);
            C3 = C(ix,3);
            a = 16*K3*C2^3*C1^3-1/4+6*K3*C2^4*C1^2+6*K3*C2^2*C1^4;
            b = C3+4*K3*C2^4*C1^3+4*K3*C2^3*C1^4;
```

```
78              c = K3*C2^4*C1^4-C3^2;
79              dC(1) = (-b+sqrt(b^2-4*a*c))/(2*a);
80              dC(2) =    dC(1);
81              dCm = dC*phi*tot;
82              S(ix,2) = S(ix,2) - dCm(1);
83              S(ix,3) = S(ix,3) + 1/2*dCm(1);
84              S(ix,4) = S(ix,4) - 1/4*dCm(1);
85              C(ix,1) = C(ix,1) + dC(1);
86              C(ix,2) = C(ix,2) + dC(2);
87              C(ix,3) = (1- C(ix,1) - C(ix,2));
88          end
89          % Univariant-line: Pyrope out
90          if S(ix,1)>0 && S(ix,2)>0 && S(ix,3)==0
91              C1 = C(ix,1);
92              C2 = C(ix,2);
93              C3 = C(ix,3);
94              a = 6*C2^2*C1^2+4*C2*C1^3+(1/4)*C1^4;
95              b = 4*C2^2*C1^3+C2*C1^4;
96              c = C2^2*C1^4-1/K1;
97              dC(1)   = (-b+sqrt(b^2-4*a*c))/(2*a);
98              dC(2)   = 1/2*dC(1);
99              dCm(1)  = dC(1)*tot*phi;
100             dCm(2)  = dC(2)*tot*phi;
101             S(ix,1) = S(ix,1) + 0.5*dCm(1);
102             S(ix,2) = S(ix,2) - 0.5*dCm(1);
103             S(ix,4) = S(ix,4) - 0.25*dCm(1);
104             C(ix,1) = C(ix,1) + dC(1);
105             C(ix,2) = C(ix,2) + dC(2);
106             C(ix,3) = (1- C(ix,1) - C(ix,2));
107         end
108         % Univariant-line: Diopside out
109         if S(ix,1)>0 && S(ix,2)==0 && S(ix,3)>0
110             C1 = C(ix,1);
111             C2 = C(ix,2);
112             C3 = C(ix,3);
113             a  = 6*C3^2*C1^2+4*C3*C1^3+(1/4)*C1^4;
114             b  = 4*C3^2*C1^3+C3*C1^4;
115             c  = C3^2*C1^4-1/K2;
116             dC(1)   = (-b+sqrt(b^2-4*a*c))/(2*a);
117             dC(2)   = 0;
118             dCm(1)  = dC(1)*tot*phi;
119             S(ix,1) = S(ix,1) + dCm(1);
120             S(ix,3) = S(ix,3) - 0.5*dCm(1);
121             S(ix,4) = S(ix,4) - 0.25*dCm(2);
122             C(ix,1) = C(ix,1) + dC(1);
123             C(ix,2) = C(ix,2) + dC(2);
124             C(ix,3) = (1- C(ix,1) - C(ix,2));
125         end
126     end
127     C0 = find(C<0);
128     C(C0) = 0;
129     S0 = find(S<0);
130     S(S0) = 0;
131     % postprocessing
132     Smod = S./repmat(molcm3',nx,1);
133     X    = 1./(C(:,2).^2.*C(:,1).^4);
```

```
    Y    = 1./(C(:,3).^2.*C(:,1).^4);
    x1   = [K1 K1];
    y1   = [100 K2];
    x2   = [100 K1];
    y2   = [K2 K2];
    x3   = [K1 1e4];
    y3   = [K1^2/K3 1e4^2/K3];
    if mod(it,nout)==1
        subplot(121),plot(x,C,'LineWidth',2) ...
            title(num2str(it)) ...
            xlabel('x'),ylabel('Fluid Concentration')
        legend('SiO_2','CaO','Al_2O_3')
        subplot(122),plot(x,Smod,'LineWidth',2) ...
            xlabel('x'),ylabel('Mineral modes')
        legend('fo','di','py','en')
        drawnow
    end
end
```

C.2.4 FEM

Main code

```
clear,clf
%physics
Lx     = 1; % length of the domain in x-direction
Ly     = 1; % length of the domain in x-direction
alpha  = 1; % dimensionless alpha = alpha*dT = 1e-5*200
ΔT = 1; % temperature increase
asp    = 1; % aspect ratio of the peridotite enclave

%              container; melting gneiss; peridotite
E_arr       = [1e1,       1e0,            1e1  ]; % Young's modulus
if_melt_arr = [  0,       1,              0    ]; % melting switch:
                                                    % 1 = melting
                                                    % 0 = not melting
% STRESS UNIT = ALPHA*DELTA_T*E
%numerics
[n2g,xg,yg,nel,phase,bnd,nnod] = meshgenerator2(Lx,Ly,asp);
nip = 1;
npe = 3;
W   = 0.5;
ndf = 2;
E   = 1;
nu  = 1/3;
%initialisation
A = sparse(nnod*ndf,nnod*ndf);
b = zeros(nnod*ndf,1);
%preprocessing
for ip = 1:nip
    dNdS(1,1,ip) = -1;
    dNdS(1,2,ip) =  1;
    dNdS(1,3,ip) =  0;
    dNdS(2,1,ip) = -1;
    dNdS(2,2,ip) =  0;
```

```
    dNdS(2,3,ip) =  1;
end
n2g              =  n2g';
l2g              =  zeros(npe*ndf,nel);
l2gc             = [2*n2g(:,:)-1 2*n2g(:,:)];
l2g(1:ndf:end,:) = l2gc(1:end,1:nel);
l2g(2:ndf:end,:) = l2gc(1:end,nel+1:end);
%processing
for iel = 1:nel
    A_sm = zeros(npe*ndf,npe*ndf);
    b_sm = zeros(npe*ndf,1);

    E            = E_arr(phase(iel) + 1);
    therm_strain = [alpha; alpha; 0]*ΔT*if_melt_arr(phase(iel)+1);
    D = [E*(1-nu)/(1+nu)/(1-2*nu) E/(1+nu)/(1-2*nu)*nu     0         ;
         E/(1+nu)/(1-2*nu)*nu     E*(1-nu)/(1+nu)/(1-2*nu) 0         ;
         0                        0            E/(1+nu)/2];

    for k = 1:nip
        phys_co   = [xg(n2g(:,iel)) yg(n2g(:,iel))];
        Jac       = dNdS(:,:,k)*phys_co;
        dN        = inv(Jac)*dNdS(:,:,k);
        B    = [dN(1,1), 0      , dN(1,2), 0      , dN(1,3), 0       ;
                0      , dN(2,1), 0      , dN(2,2), 0      , dN(2,3) ;
                dN(2,1), dN(1,1), dN(2,2), dN(1,2), dN(2,3), dN(1,3)];
        A_sm      = A_sm  + B'*D*B*det(Jac)*W(k);
        b_sm(:,1) = b_sm(:,1) + B'*D*therm_strain*det(Jac)*W(k);
    end
    for i = 1:npe*ndf
        for j = 1:npe*ndf
            A(l2g(i,iel),l2g(j,iel)) = A(l2g(i,iel),l2g(j,iel)) ...
                                     + A_sm(i,j);
        end
        b(l2g(i,iel),1) = b(l2g(i,iel),1) + b_sm(i,1);
    end
end
% Boundary conditions
bndi  = find(bnd==1);
xbndi = bndi*ndf-1;
ybndi = bndi*ndf;
A(xbndi,:) = 0;
for i = 1:size(xbndi,1)
    A(xbndi(i),xbndi(i)) = 1;
    b(xbndi(i),1) = 0;%-xg(bndi(i));
end
A(ybndi,:) = 0;
for i = 1:size(ybndi,1)
    A(ybndi(i),ybndi(i)) = 1;
    b(ybndi(i),1) = 0;
end
sol = A\b;
solx = sol(1:ndf:end);
soly = sol(2:ndf:end);
% Stress calculation
for iel = 1:nel
    E            = E_arr(phase(iel) + 1);
```

```
    therm_strain = [alpha; alpha; 0]*ΔT*if_melt_arr(phase(iel)+1);
    D = [E*(1−nu)/(1+nu)/(1−2*nu) E/(1+nu)/(1−2*nu)*nu     0         ;
         E/(1+nu)/(1−2*nu)*nu     E*(1−nu)/(1+nu)/(1−2*nu) 0         ;
         0                        0            E/(1+nu)/2];
    for k = 1:nip
        phys_co   = [xg(n2g(:,iel)) yg(n2g(:,iel))];
        Jac       = dNdS(:,:,k)*phys_co;
        dN        = inv(Jac)*dNdS(:,:,k);
        B     = [dN(1,1), 0      , dN(1,2),0      , dN(1,3), 0       ;
                 0      , dN(2,1), 0      ,dN(2,2), 0      , dN(2,3) ;
                 dN(2,1), dN(1,1), dN(2,2),dN(1,2), dN(2,3), dN(1,3)];
    end
    U          = zeros(2*npe,1);
    U(1:2:end) = solx(n2g(:,iel));
    U(2:2:end) = soly(n2g(:,iel));
    stress(:,iel)   = D*(B*U−therm_strain);
end
Ps = −(stress(1,:)'+stress(2,:)')/2;  % calculate the solid pressure
n2g=n2g';
patch(xg(n2g)', yg(n2g)',repmat(Ps',3,1))
axis equal,axis tight,shading interp
title('\Delta P /(E \alpha \Delta T )','FontSize',24)
set(gcf, 'Renderer', 'zbuffer'),colorbar
axis([−0.08 0.08 −0.08 0.08]),axis off
```

Meshgenerator function

```
function [n2g,xg,yg,nel,phase,bnd,nnod] = meshgenerator2(Lx,Ly,asp)
% geom1
geom2
% geom3
nnod = size(nodes,2); % number of nodes
nseg = size(segs,2); % number of segments
nhol = size(holes,2); % number of holes
nreg = size(regs,2);  % number of regions
%create input file
fid = fopen('mesh.poly','w');
%nodes
fprintf(fid,'%d %d %d %d\n',nnod,2,0, 0);
for i = 1:nnod
    fprintf(fid,'%d %f %f\n',i,nodes(1,i),nodes(2,i));
end
%segments
fprintf(fid,'%d %d\n',nseg,1);
for i = 1:nseg
    fprintf(fid,'%d %d %d %d\n',i,segs(1,i),segs(2,i),seg_m(1,i));
end
%holes
fprintf(fid,'%d\n',nhol);
for i = 1:nhol
    fprintf(fid,'%d %f %f\n',i,holes(1,i),holes(2,i));
end
%regions
fprintf(fid,'%d\n',nreg);
for i = 1:nreg
```

```
    fprintf(fid,'%d %f %f %d\n',i,regs(1,i),regs(2,i),regs(3,i));
end
fclose(fid);
%call program
!triangle -pIq25a0.00005A mesh.poly
%read output
%nodes
nnod  = dlmread('mesh.node','',[0 0 0 0]);
xg    = dlmread('mesh.node','',[1 1 nnod 1]);
yg    = dlmread('mesh.node','',[1 2 nnod 2]);
bnd   = dlmread('mesh.node','',[1 3 nnod 3]);
%elements
nel   = dlmread('mesh.ele','',[0 0 0 0]);
n2g   = dlmread('mesh.ele','',[1 1 nel 3]);
phase = dlmread('mesh.ele','',[1 4 nel 4]);
```

Geometry set up function

```
% geometry script for circles in circles for input in meshgenerator
% Object 1
radius   = 0.2;
npts1    = 360;
dphi     = 2*pi/npts1;
phi      = 0:dphi:2*pi-dphi;
x_circ1   = radius*cos(phi);
y_circ1   = radius*sin(phi);
sqr_nod1 = [x_circ1; y_circ1];
sqr_seg1 = [1:npts1;2:npts1 1];
sqr_hol1 = [];
sqr_reg1 = [0; 0.15; 0];
% Object 2
radius   = 0.05;
npts2    = 360;
dphi     = 2*pi/npts2;
phi      = 0:dphi:2*pi-dphi;
x_circ2   = radius*cos(phi);
y_circ2   = radius*sin(phi);
sqr_nod2 = [x_circ2; y_circ2];
sqr_seg2 = [1:npts2;2:npts2 1];
sqr_hol2 = [];
sqr_reg2 = [0; 0.05; 1];
% Object 3
radius   = 0.01;
npts3    = 40;
dphi     = 2*pi/npts3;
phi      = 0:dphi:2*pi-dphi;
x_circ3   = radius*cos(phi);
y_circ3   = asp*radius*sin(phi);
sqr_nod3 = [x_circ3; y_circ3];
sqr_seg3 = [1:npts3;2:npts3 1];
sqr_hol3 = [];
sqr_reg3 = [0; 0; 2];

sqr_seg2 = sqr_seg2+max(sqr_seg1(:));

```

```
nodes = [sqr_nod1 sqr_nod2 sqr_nod3];
segs  = [sqr_seg1 sqr_seg2 sqr_seg3+max(sqr_seg2(:))];
seg_m = [1*ones(1,npts1) 100*ones(1,npts2) 100*ones(1,npts3)];
holes = [sqr_hol1 sqr_hol2 sqr_hol3];
regs  = [sqr_reg1 sqr_reg2 sqr_reg3];
```

Substitute parameters

```
clear,clf
% Script for substituting real values for melting overpressure model
rho_new = 2290;  % melt density
rho_ref = 2650;  % solid density
Vnew    = 1/rho_new; % melt volume
Vref    = 1/rho_ref; % solid volume
Tnew    = 800; % liquidus temperature
Tref    = 600; % solidus temperature
a       = (1/Vnew)*(Vnew-Vref)/(Tnew-Tref); % thermal expansion coeff.
b       = 1e-11; % typical compressibility for rocks
visc    = 1e22;  % rock viscosity
dT      = 100; % temperature increase
years   = 1e4; % time interval
dt      = years*3600*24*365.25; % time in seconds
Ptilde  = 1.8; % dimensionless pressure calculated with FEM
dPe     = Ptilde*(a/b)*dT;  % pressure increase (elastic)
dPv     = Ptilde*visc*a*dT/dt; % pressure increase (viscous)
dPe     = dPe/1e9 % pressure increase in purely elastic case in GPa
dPv     = dPv/1e9 % pressure increase in purely viscous case in GPa
```

C.2.5 Mass balance

```
clear,clf
% Read and analyse XRF data (fresh start)
[data,txt]= ...
    xlsread('D:\Work\Excel\XRF_tables\XRFdata_sorted_matlab.xls');
%%%%%%%%%%%%%%%%%%%%%%%% DATA part %%%%%%%%%%%%%%%%%%%%%%%%%%%%%%%%%%%%%%%
% restructure data and strings
group      = data(:,1);
data       = data(:,2:end);
ele        = txt(1,3:end);
sample     = txt(2:end,1);
aver       = zeros(max(group),size(data,2));
% set non-measured values to 0 to calculate averages
dNaN       = find(isnan(data));
data(dNaN) = 0;
% for each separate group
for i = 1:max(group)
    ind  = find(group==i);
    % calculate averages for groups
    for j = 1:size(ele,2)
        aver(i,j) = mean(data(ind,j));
    end
end
% put back NaN for non-measured values to avoid plotting
d0          = find(data==0);
```

```
data(d0)     = NaN;
aver0        = find(aver==0);
aver(aver0) = NaN;
%%%%%%%%%%%%%%%%%%%%%%%%%%%%%%%%%%%%%%%%%%%%%%%%%%%%%%%%%%%%%%%%%%%%%%%%%%%%%%%
% Mass balance
%%%%%%%%%%%%%%%%%%%%%%%%%%%%%%%%%%%%%%%%%%%%%%%%%%%%%%%%%%%%%%%%%%%%%%%%%%%%%%%
% Parameters
maj      = 1:10;  % choose major elements to plot
trc      = 11:28; % choose trace elements to plot
grp(1,:) = [1 1 13]; % index unaltered rocks
grp(2,:) = [3 5 7];  % index altered rocks
rho_A    = [3.34 3.34 3.0]; % densities of unaltered rocks
rho_B    = [3.32 3.32 3.4]; % densities of altered rocks
fv       = 1;                  % Gresens volume factor
phi      = [0.082 0.76 0.158]; % Volume fraction of altered rocks
                               %(unaltered rock=100%)
% Initialise
gresens  = zeros(size(grp,2),size(data,2));
% Gresens formula
for ig = 1:size(grp,2)
    A             = aver(grp(1,ig),:); % Unaltered rock
    B             = aver(grp(2,ig),:); % Altered rock
    gresens(ig,:) = phi(ig)*(fv*(rho_B(ig)/rho_A(ig)).*B-A);
end
% plotting
x_m         = 1:size(maj,2);
x_t         = 1:size(trc,2);
figure(1)
subplot(321),bar(gresens(:,maj)','BarWidth',1)...
    legend('groupB','groupC','grtite')
set(gca,'XTick',x_m),set(gca,'XTickLabel',ele(maj))...
    axis([0 11 0.25 5]),title('Gresens-majors')

subplot(323),bar(gresens(:,maj)','BarWidth',1)
set(gca,'XTick',x_m),set(gca,'XTickLabel',ele(maj))...
    axis([0 11 -0.25 0.25])

subplot(325),bar(gresens(:,maj)','BarWidth',1)
set(gca,'XTick',x_m),set(gca,'XTickLabel',ele(maj))...
    axis([0 11 -5 -0.25])

subplot(322),bar(gresens(:,trc)','BarWidth',1)...
    legend('groupB','groupC','grtite')
set(gca,'XTick',x_t),set(gca,'XTickLabel',ele(trc))...
    title('Gresens-traces'),axis([0 19 5 50])

subplot(324),bar(gresens(:,trc)','BarWidth',1)
set(gca,'XTick',x_t),set(gca,'XTickLabel',ele(trc))...
    axis([0 19 -5 5])

subplot(326),bar(gresens(:,trc)','BarWidth',1)
set(gca,'XTick',x_t),set(gca,'XTickLabel',ele(trc))...
    axis([0 19 -410 -5])
```

C.2.6 Thermodynamics

Fo-Fa system

```
clear,clf
% get TD properties
% physics
Phases  = {'fo','foL','fa','faL'};
R       = 8.3144;
T_ref   = 298;
Tliq    = 1500;
Tsol    = 1100;
X       = 0.4;
eps     = 1e-5;
Xs      = eps:0.01-eps:1-eps;
Xm      = eps:0.01-eps:1-eps;
fo_m    = (24.305*2+28.086+4*15.999)/1000;
fa_m    = (55.847*2+28.086+4*15.999)/1000;
% numerics
dT      = 50;
dP      = 5e8; % 1 kbar
P_arr   = 1e5:dP:1e10;
T_arr   = T_ref:dT:2400;
P       = repmat(P_arr,size(T_arr,2),1);
T       = repmat(T_arr',1,size(P_arr,2));
nphi    = (Tliq-Tsol)/dT;
dphi    = 1/(nphi-1);
% Initialisation
g_id  = zeros(size(T_arr,2),size(P_arr,2),size(Xs,2));
phi   = zeros(size(T_arr,2),size(P_arr,2),size(Xs,2)+size(Xm,2));
vol   = zeros(size(T_arr,2),size(P_arr,2)-1,size(Xs,2)+size(Xm,2));
%get Gibbs energy
g       = gibbscalc(T_ref,T_arr,P_arr,Phases);
g_fo    = squeeze(g(:,:,1));
g_mfo   = squeeze(g(:,:,2));
g_fa    = squeeze(g(:,:,3));
g_mfa   = squeeze(g(:,:,4));
% ideal mixing
for i = 1:size(Xs,2)
    g_id(:,:,i) = (1-Xs(i))*g_fo  + Xs(i)*g_fa ...
        + R*T*((1-Xs(i))*log(1-Xs(i))+ Xs(i)*log(Xs(i)));
end
im = 0;
for i = size(Xm,2)+1:size(Xs,2)+size(Xm,2)
    im          = im +1;
    g_id(:,:,i) = (1-Xm(im))*g_mfo + Xm(im)*g_mfa + ...
        R*T*((1-Xm(im))*log(1-Xm(im))+ Xm(im)*log(Xm(im)));
end
% Calculate volumes (the volume for every phase at all
% temperatures and all pressures (minus 1 due to diff))
for k = 1:size(Xs,2)+size(Xm,2)
    vol(:,:,k) = diff(g_id(:,:,k) ,1,2)./diff(P,1,2);
end
% Gibbs minimisation to find the correct phase proportions
A   = [];
```

```
b   = [];
Aeq = [Xs Xm; ones(1,size(Xs,2)+size(Xs,2))];
beq = [X; 1];
LB  = zeros(1,size(Xs,2) + size(Xm,2));
UB  = ones (1,size(Xs,2) + size(Xm,2));
for iT = 1:size(T_arr,2)
    for iP = 1:size(P_arr,2)
        phi(iT,iP,:) = ...
            linprog(squeeze(g_id(iT,iP,:))',A,b,Aeq,beq,LB,UB);
        if iP < size(P_arr,2)
            vol_tot(iT,iP) = ...
                squeeze(vol(iT,iP,:))'*squeeze(phi(iT,iP,:));
        end
    end
end
% Construct phase matrix (melt, solid and solid+melt)
phi_m = sum(phi(:,:,size(Xs,2)+1:end),3);
for iT = 1:size(T_arr,2)
    for iP = 1:size(P_arr,2)
        if phi_m(iT,iP) > 0.9
            phase(iT,iP) = 2;
        elseif phi_m(iT,iP) < 0.1
            phase(iT,iP) = 0;
        else
            phase(iT,iP) = 1;
        end
    end
end
subplot(1,2,1),contourf(T_arr-273,P_arr(1:end-1)/1e9,vol_tot',20)...
colorbar,axis([1200 2100 1e-3 9]),axis square,
xlabel('T(\circC)'),ylabel('P(GPa)'),title('volume')
subplot(1,2,2),contourf(T_arr-273,P_arr/1e9,phi_m',10),colorbar
axis([1200 2100 1e-3 9]),axis square,
xlabel('T(\circC)'),ylabel('P(GPa)'),title('\phi_{melt}')
```

Gibbs energy calculator

```
function g = gibbscalc(T_ref,T_arr,P_arr,Phases)
%read data from Excel
[data,text] = xlsread('HP98conv2');
%find rows containing desired phases
Num = zeros(length(Phases),1);
for i = 1:length(Phases)
    Str(:,i) = strcmpi(text(2:end,1),Phases(i));
    Num(i)   = find(Str(:,i));
    Phs(i,:) = data(Num(i),:);
end
%indices of the parameters
H       = find(strcmpi(text(1,2:end),'H'));
S       = find(strcmpi(text(1,2:end),'S'));
V       = find(strcmpi(text(1,2:end),'V'));
a       = find(strcmpi(text(1,2:end),'a'));
b       = find(strcmpi(text(1,2:end),'b'));
c       = find(strcmpi(text(1,2:end),'c'));
d       = find(strcmpi(text(1,2:end),'d'));
```

```
a_0      = find(strcmpi(text(1,2:end),'a_0'));
K        = find(strcmpi(text(1,2:end),'K'));
Tc       = find(strcmpi(text(1,2:end),'Tc'));
Smax     = find(strcmpi(text(1,2:end),'Smax'));
Vmax     = find(strcmpi(text(1,2:end),'Vmax'));
%initialisation
C_p      = zeros(length(T_arr),length(Phs(:,1)));
G        = zeros(length(T_arr),length(P_arr),length(Phs(:,1)));
G_exc    = zeros(length(T_arr),length(P_arr),length(Phs(:,1)));
for k = 1:length(Phs(:,1));
    S_i(1,k) = Phs(k,S);
    V_i(1,k) = Phs(k,V);
    k_t(1,k) = Phs(k,K);
    G_i(1,k) = Phs(k,H)-298*Phs(k,S);
    %calculation
    for i = 2:length(T_arr);
        C_p(i,k)  = Phs(k,a) + Phs(k,b)*T_arr(i) + ...
                    Phs(k,c)*T_arr(i)^-2 + Phs(k,d)*T_arr(i)^(-1/2);
        S_i(i,k)  = S_i(i-1,k) + ...
                   (C_p(i,k)*(T_arr(i)-T_arr(i-1))/T_arr(i));
        G_i(i,k)  = G_i(i-1,k) - S_i(i,k)*(T_arr(i)-T_arr(i-1));
        V_i(i,k)  = V_i(1,k)*( 1 + Phs(k,a_0)*(T_arr(i)-T_ref) ...
                  - 20*Phs(k,a_0)* (sqrt(T_arr(i))-sqrt(T_ref)));
        k_t(i,k)  = k_t(1,k)*(1-1.5e-4*(T_arr(i)-T_ref));
        G(i,1,k)  = G_i(i,k);
    end
    for j = 1:length(P_arr);
        for i = 1:length(T_arr);
            T_c  = Phs(k,Tc)+ ...
                  (Phs(k,Vmax)/Phs(k,Smax))*(P_arr(j)-P_arr(1));
            if (~isnan(Phs(k,Tc)))
                kappa        = k_t(1,k)*(1-1.5e-4*(T_arr(i)-T_ref));
                Q_298        = (1-298/Phs(k,Tc))^(1/4);
                Q            = (1-(T_arr(i)/T_c))^(1/4);
                h_298        = Phs(k,Smax)*Phs(k,Tc)...
                             *(Q_298^2-(1/3)*Q_298^6);
                s_298        = Phs(k,Smax)*Q_298^2;
                v_t          = Phs(k,Vmax)*Q_298^2*(1+Phs(k,a_0)...
                             *(T_arr(i)-T_ref)-20*Phs(k,a_0)...
                             *(sqrt(T_arr(i))-sqrt(T_ref)));
                intvdP       = (1/3)*v_t*kappa*...
                              ((1+(4*P_arr(j))/kappa)^(3/4)-1);
                G_land       = Phs(k,Smax)*((T_arr(i)-T_c)*Q^2 ...
                             + (1/3)*T_c*Q^6);
                G_exc(i,j,k) = 1*h_298-1*T_arr(i)*s_298+1*intvdP;
                if T_arr(i) <=T_c
                    G_exc(i,j,k)  = G_exc(i,j,k) + G_land;
                end
            end
            G(i,j,k) = G_i(i,k) + ...
                       V_i(i,k)*k_t(i,k)/3*...
                      ((1+4*(P_arr(j)-P_arr(1))/k_t(i,k))^(3/4)-1)...
                      + G_exc(i,j,k);
        end
    end
end
```

```
75 g = G;
```

References

Ague, J. J. (1994). Mass-Transfer during Barrovian Metamorphism of Pelites, South-Central Connecticut .1. Evidence for Changes in Composition and Volume. *American Journal of Science*, 294(8):989–1057.

Ai, Y. (1994). A revision of the garnet-clinopyroxene Fe^{2+}-Mg exchange geothermometer. *Contributions to Mineralogy and Petrology*, 115(4):467–473.

Andersen, T., Mair, K., Austrheim, H., Podladchikov, Y. Y., and Vrijmoed, J. C. (2008). Stress release in exhumed intermediate and deep earthquakes determined from ultramafic pseudotachylyte. *Geology*, 36(12):995–998.

Andersen, T. B. (1998). Extensional tectonics in the Caledonides of southern Norway, an overview. *Tectonophysics*, 285(3-4):333–351.

Austrheim, H. (1987). Eclogitization of Lower Crustal Granulites by Fluid Migration through Shear Zones. *Earth and Planetary Science Letters*, 81(2-3):221–232.

Austrheim, H., Corfu, F., Bryhni, I., and Andersen, T. B. (2003). The Proterozoic Hustad igneous complex: a low strain enclave with a key to the history of the Western Gneiss Region of Norway. *Precambrian Research*, 120(1-2):149–175.

Austrheim, H., Erambert, M., and Engvik, A. K. (1997). Processing of crust in the root of the Caledonian continental collision zone: The role of eclogitization. *Tectonophysics*, 273(1-2):129–153.

Avigad, D., Chopin, C., and Le Bayon, R. (2003). Thrusting and extension in the southern dora-maira ultra-high-pressure massif (Western alps): View from below the coesite-bearing unit. *Journal of Geology*, 111(1):57–70.

Barron, L. (2005). A linear model and topology for the host-inclusion mineral system involving diamond. *The Canadian Mineralogist*, 43:203–224.

Bass, J. D. (1995). Elasticity of Minerals, Glasses, and Melts. *Mineral physics and Crystallography*, AGU Reference Shelf 2:45–63.

Bea, F., Pereira, M. D., and Stroh, A. (1994). Mineral Leucosome Trace-Element Partitioning in a Peraluminous Migmatite (a Laser Ablation-Icp-Ms Study). *Chemical Geology*, 117(1-4):291–312.

Beard, B. L., Medaris, L. G., Johnson, C. M., Brueckner, H. K., and Misar, Z. (1992). Petrogenesis of Variscan High-Temperature Group-a Eclogites from the Moldanubian Zone of the Bohemian Massif, Czechoslovakia. *Contributions to Mineralogy and Petrology*, 111(4):468–483.

Becker, H. (1996). Geochemistry of garnet peridotite massifs from lower Austria and the composition of deep lithosphere beneath a Palaeozoic convergent plate margin. *Chemical Geology*, 134(1-3):49–65.

Blundy, J., Cashman, K., and Humphreys, M. (2006). Magma heating by decompression-driven crystallization beneath andesite volcanoes. *Nature*, 443(7107):76–80.

Bodinier, J. L., Garrido, C. J., Chanefo, I., Bruguier, O., and Gervilla, F. (2008). Origin of pyroxenite-peridotite veined mantle by refertilization reactions: Evidence from the Ronda peridotite (Southern Spain). *Journal of Petrology*, 49(5):999–1025.

Bodinier, J. L. and Godard, M. (2003). Orogenic, ophiolitic, and abyssal peridotites. In Carlson, R. W., editor, *Geochemistry of the Mantle and Core*, volume 2 of *Treatise on Geochemistry*, pages 103–170. Elsevier, Amsterdam.

Brey, G. and Köhler, T. (1990). Geothermobarometry in Four-phase Lherzolites II. New Thermobarometers, and Practical Assessment of Existing Thermobarometers. *Journal of Petrology*, 31(6):1353–1378.

Brueckner, H. K., Carswell, D. A., and Griffin, W. L. (2002). Paleozoic diamonds within a Precambrian peridotite lens in UHP gneisses of the Norwegian Caledonides. *Earth and Planetary Science Letters*, 203(3-4):805–816.

Brueckner, H. K. and Medaris, L. G. (2000). A general model for the intrusion and evolution of 'mantle' garnet peridotites in high-pressure and ultra-high-pressure metamorphic terranes. *Journal of Metamorphic Geology*, 18(2):123–133.

Brueckner, H. K. and Van Roermund, H. L. M. (2004). Dunk tectonics: A multiple subduction/eduction model for the evolution of the scandinavian caledonides.

Bryhni, I. (1989). Status of the supracrustal rocks in the Western Gneiss Region, S. Norway. In Gayer, R., editor, *The Caledonide Geology of Scandinavia*, pages 221–228. Graham & Trotman.

Bryhni, I., Austrheim, H., and Solli, A. (1989). Hustad berggrunnskart 1220 1.

Bryhni, I. and Sturt, B. A. (1985). Caledonides of southwestern Norway. In Gee, D. G. and Sturt, B. A., editors, *The Caledonide Orogen; Scandinavia and related areas*, volume 1, pages 89–107. John Wiley & Sons, Chichester, United Kingdom.

Bundy, F. P. (1980). The P, T phase and reaction diagram for elemental carbon. *Journal of Geophysical Research*, 85:6930–6936.

Carlson, W. D. (2002). Scales of disequilibrium and rates of equilibration during metamorphism. *American Mineralogist*, 87(2-3):185–204.

Carlson, W. D. (2006). Rates of Fe, Mg, Mn, and Ca diffusion in garnet. *American Mineralogist*, 91(1):1–11.

Carswell, D. A. (1990). *Eclogite facies rocks*. Chapman and Hall, New York.

Carswell, D. A., Brueckner, H. K., Cuthbert, S. J., Mehta, K., and O'Brien, P. J. (2003a). The timing of stabilisation and the exhumation rate for ultra-high pressure rocks in the Western Gneiss Region of Norway. *Journal of Metamorphic Geology*, 21(6):601–612.

Carswell, D. A. and Compagnoni, R. (2003). Introduction with review of the definition, distribution and geotectonic significance of ultrahigh pressure metamorphism. In Carswell, D. A. and Compagnoni, R., editors, *Ultrahigh Pressure Metamorphism*, volume 5 of *EMU Notes in Mineralogy*, pages 3–9. Eötvös University Press, Budapest.

Carswell, D. A. and Cuthbert, S. J. (2003). Ultrahigh pressure metamorphism in the Western Gneiss region of Norway. In Carswell, D. A. and Compagnoni, R., editors, *Ultrahigh Pressure Metamorphism*, volume 5 of *EMU notes in Mineralogy*, pages 51–73. Eötvös University Press, Budapest.

Carswell, D. A. and Harley, S. L. (1990). Mineral barometry and thermometry. In Carswell, D., editor, *Eclogite facies rocks*, pages 83–110. Blackie, Glasgow.

Carswell, D. A. and Harvey, M. A. (1982). The Intrusive History and Tectono-Metamorphic Evolution of the Basal Gneiss Complex in the Moldefjord Region, W Norway. *Journal of the Geological Society*, 139(May):368–368.

Carswell, D. A., Harvey, M. A., and Alsamman, A. (1983). The petrogenesis of contrasting Fe-Ti and Mg-Cr garnet peridotite types in the high-grade gneiss complex of Western Norway. *Bulletin De Minéralogie*, 106(6):727–750.

Carswell, D. A., Krogh, E. J., and Griffin, W. L. (1985). Norwegian orthopyroxene eclogites: calculated equilibrium conditions and petrogenetic implications. In Gee, D. G. and Sturt, B. A., editors, *The Caledonide Orogen; Scandinavia and related areas*, volume 2, pages 823–841. John Wiley & Sons, Chichester, United Kingdom.

Carswell, D. A., Tucker, R. D., O'Brien, P. J., and Krogh, T. E. (2003b). Coesite micro-inclusions and the U/Pb age of zircons from the Hareidland eclogite in the Western Gneiss Region of Norway. *Lithos*, 67(3-4):181–190.

Carswell, D. A. and Van Roermund, H. L. M. (2005). On multi-phase mineral inclusions associated with microdiamond formation in mantle-derived peridotite lens at Bardane on Fjørtoft, west Norway. *European Journal of Mineralogy*, 17(1):31–42.

Carswell, D. A., van Roermund, H. L. M., and Wiggers de Vries, D. F. (2006). Scandian Ultrahigh-Pressure Metamorphism of Proterozoic Basement Rocks on Fjørtoft and Otrøy, Western Gneiss Region, Norway. *International Geology Review*, 48(11):957–977.

Chakraborty, S. and Ganguly, J. (1992). Cation Diffusion in Aluminosilicate Garnets - Experimental-Determination in Spessartine-Almandine Diffusion Couples, Evaluation of Effective Binary Diffusion-Coefficients, and Applications. *Contributions to Mineralogy and Petrology*, 111(1):74–86.

Chemenda, A. I., Mattauer, M., Malavieille, J., and Bokun, A. N. (1995). A Mechanism for Syn-Collisional Rock Exhumation and Associated Normal Faulting - Results from Physical Modeling. *Earth and Planetary Science Letters*, 132(1-4):225–232.

Chernoff, C. B. and Carlson, W. D. (1997). Disequilibrium for Ca during growth of pelitic garnet. *Journal of Metamorphic Geology*, 15(4):421–438.

Chernoff, C. B. and Carlson, W. D. (1999). Trace element zoning as a record of chemical disequilibrium during garnet growth. *Geology*, 27(6):555–558.

Chopin, C. (1984). Coesite and pure pyrope in high-grade blueschists of the Western Alps - a first record and some consequences. *Contributions to Mineralogy and Petrology*, 86(2):107–118.

Chopin, C. (2003). Ultrahigh-pressure metamorphism: tracing continental crust into the mantle. *Earth and Planetary Science Letters*, 212(1-2):1–14.

Clemens, J. D. and Droop, G. T. R. (1998). Fluids, P-T paths and the fates of anatectic melts in the Earth's crust. *Lithos*, 44(1-2):21–36.

Coleman, R. G. and Wang, X. (1995). Overview of the geology and tectonics of UHPM. In Coleman, R. and Wang, X., editors, *Ultra-High Pressure Metamorphism (UHPM)*, pages 1–32. Cambridge University Press, Cambridge.

Connolly, J. A. D. (2005). Computation of phase equilibria by linear programming: A tool for geodynamic modeling and its application to subduction zone decarbonation. *Earth and Planetary Science Letters*, 236(1-2):524–541.

Corfu, F. (2004). U-Pb age, setting and tectonic significance of the anorthosite-mangerite-charnockite-granite suite, Lofoten-Vesterålen, Norway. *Journal of Petrology*, 45(9):1799–1819.

Cuthbert, S. J. and Carswell, D. A. (2003). The HP-UHP transition in the Nordfjord-Stadlandet region, Western Gneiss Complex, Norway. *NGU-report*, 2003.055:39–40.

Cuthbert, S. J., Carswell, D. A., Krogh-Ravna, E. J., and Wain, A. (2000). Eclogites and eclogites in the Western Gneiss Region, Norwegian Caledonides. *Lithos*, 52(1-4):165–195.

Dabrowski, M., Podladchikov, Y. Y., and Hartz, E. H. (2008). Migmatization induced overpressure, East Greenland case study. *Geophysical Research Abstracts*, 10:EGU2008–A–11303.

de Capitani, C. and Brown, T. H. (1987). The computation of chemical-equilibrium in complex-systems containing non-ideal solutions. *Geochimica Et Cosmochimica Acta*, 51(10):2639–2652.

Dobrzhinetskaya, L. F., Eide, E. A., Larsen, R. B., Sturt, B. A., Tronnes, R. G., Smith, D. C., Taylor, W. R., and Posukhova, T. V. (1995). Microdiamond in high-grade metamorphic rocks of the Western Gneiss Region, Norway. *Geology*, 23(7):597–600.

Dodson, M. H. (1973). Closure Temperature in Cooling Geochronological and Petrological Systems. *Contributions to Mineralogy and Petrology*, 40(3):259–274.

Droop, G. T. R. (1987). A General Equation for Estimating Fe^{3+} Concentrations in Ferromagnesian Silicates and Oxides from Microprobe Analyses, Using Stoichiometric Criteria. *Mineralogical Magazine*, 51(361):431–435.

Ellis, D. J. and Green, D. H. (1979). Experimental-Study of the Effect of Ca Upon Garnet-Clinopyroxene Fe-Mg Exchange Equilibria. *Contributions to Mineralogy and Petrology*, 71(1):13–22.

Ernst, W. G. (1973). Interpretative Synthesis of Metamorphism in Alps. *Geological Society of America Bulletin*, 84(6):2053–2078.

Ernst, W. G. and Liou, J. G. (2008). High- and ultrahigh-pressure metamorphism: Past results and future prospects. *American Mineralogist*, 93(11-12):1771–1786.

Fabriès, J., Bodinier, J. L., Dupuy, C., Lorand, J. P., and Benkerrou, C. (1989). Evidence for Modal Metasomatism in the Orogenic Spinel Lherzolite Body from Caussou (Northeastern Pyrenees, France). *Journal of Petrology*, 30(1):199–228.

Faure, G. (1986). *Principles of isotope geology*. John Wiley and Sons, New York, second edition edition.

Fletcher, R. and Hofmann, A. (1974). Simple models of diffusion and combined infiltration-diffusion metasomatism. In Hofmann, A., Giletti, B., Yoder, Jr., H., and Yund, R., editors, *Geochemical transport and kinetics*, volume 634, pages 243–259. Carnegie Institution of Washington Publication.

Fletcher, R. and Vidale, R. (1976). Analysis of infiltration metasomatism in a multicomponent chemical system. *EOS, Transactions American Geophysical Union*, 57(12):1015.

Ford, M., Duchene, S., Gasquet, D., and Vanderhaeghe, O. (2006). Two-phase orogenic convergence in the external and internal SW Alps. *Journal of the Geological Society*, 163:815–826.

Ganguly, J. and Tirone, M. (1999). Diffusion closure temperature and age of a mineral with arbitrary extent of diffusion: theoretical formulation and applications. *Earth and Planetary Science Letters*, 170(1-2):131–140.

Ganguly, J., Tirone, M., and Hervig, R. L. (1998). Diffusion Kinetics of Samarium and Neodymium in Garnet, and a Method for Determining Cooling Rates of Rocks. *Science*, 281(5378):805–807.

Gerya, T. V., Perchuk, L. L., and Burg, J. P. (2008). Transient hot channels: Perpetrating and regurgitating ultrahigh-pressure, high-temperature crust-mantle associations in collision belts. *Lithos*, 103(1-2):236–256.

Gerya, T. V., Stöckhert, B., and Perchuk, A. L. (2002). Exhumation of high-pressure metamorphic rocks in a subduction channel: A numerical simulation. *Tectonics*, 21(6):1056.

Gillet, P., Ingrin, J., and Chopin, C. (1984). Coesite in Subducted Continental-Crust - P-T History Deduced from an Elastic Model. *Earth and Planetary Science Letters*, 70(2):426–436.

Gilotti, J. A. and Mcclelland, W. C. (2007). Characteristics of, and a tectonic model for, Ultrahigh-Pressure metamorphism in the overriding plate of the Caledonian orogen. *International Geology Review*, 49(9):777–797.

Godard, G., Smith, D. C., and Thouvenin, C. (2003). Microdiamond within zircon in thin section in the Straumen coesite-kyanite-eclogite pod, Norway. *NGU-report*, 2003.055:54.

Green, H. W. (2005). Psychology of a changing paradigm: 40+ years of high-pressure metamorphism. *International Geology Review*, 47(5):439–456.

Gresens, R. L. (1967). Composition-volume relationships of metasomatism. *Chemical Geology*, 2:47–65.

Griffin, W. L. (1987). On the Eclogites of Norway - 65 Years Later. *Mineralogical Magazine*, 51(361):333–343.

Griffin, W. L., Austrheim, H., Brastad, K., Bryhni, I., Krill, A. G., Krogh, E. J., Mørk, M. B. E., Qvale, H., and Torudbakken, B. (1985). High-pressure metamorphism in the Scandinavian Caledonides. In Gee, D. G. and Sturt, B. A., editors, *The Caledonide Orogen; Scandinavia and related areas*, volume 2, pages 783–801. John Wiley & Sons, Chichester, United Kingdom.

Griffin, W. L. and Brueckner, H. K. (1985). Ree, Rb-Sr and Sm-Nd Studies of Norwegian Eclogites. *Chemical Geology*, 52(2):249–271.

Guiraud, M. and Powell, R. (2006). P-V-T relationships and mineral equilibria in inclusions in minerals. *Earth and Planetary Science Letters*, 244(3-4):683–694.

Guy, B. (1993). Mathematical Revision of Korzhinskii Theory of Infiltration Metasomatic Zoning. *European Journal of Mineralogy*, 5(2):317–339.

Hacker, B., Root, D., Walsh, E., Young, D., and Mattinson, J. (2001). Recent progress on the Norwegian HP-UHP eclogites. *Abstract to UHPM Workshop at Waseda University, Japan*, 4B06:174.

Hacker, B. R. (2007). Ascent of the ultrahigh-pressure Western Gneiss Region, Norway. In Cloos, M., Carlson, W. D., Gilbert, M. C., Liou, J. G., and Sorensen, S. S., editors, *Convergent Margin Terranes and Associated Regions: A Tribute to W. G. Ernst*, volume 419 of *Geological Society of America Special Paper*, pages 1–14. Geological Society of America, USA.

Harley, S. L. (1984a). An Experimental-Study of the Partitioning of Fe and Mg between Garnet and Ortho-Pyroxene. *Contributions to Mineralogy and Petrology*, 86(4):359–373.

Harley, S. L. (1984b). The Solubility of Alumina in Orthopyroxene Coexisting with Garnet in FeO-MgO-Al_2O_3-SiO_2 and CaO-FeO-MgO-Al_2O_3-SiO_2. *Journal of Petrology*, 25(3):665–696.

Harley, S. L. and Green, D. H. (1982). Garnet Ortho-Pyroxene Barometry for Granulites and Peridotites. *Nature*, 300(5894):697–701.

Hartz, E. H., Podladchikov, Y. Y., and Dabrowski, M. (2007). Tectonic and reaction overpressures: Theoretical models and natural examples. *Geophysical Research Abstracts*, 9:EGU2007–A–10430.

Harvey, M. A. (1983). A geochemical and Rb-Sr study of the Proterozoic augen orthogneisses on the Molde peninsula, west Norway. *Lithos*, 16(4):325–338.

Hemingway, B. S., Bohlen, S. R., Hankins, W. B., Westrum, E. F., and Kuskov, O. L. (1998). Heat capacity and thermodynamic properties for coesite and jadeite, reexamination of the quartz-coesite equilibrium boundary. *American Mineralogist*, 83(5-6):409–418.

Hermann, J. (2003). Experimental evidence for diamond-facies metamorphism in the Dora-Maira massif. *Lithos*, 70(3-4):163–182.

Hermann, J. and Spandler, C. J. (2008). Sediment melts at sub-arc depths: An experimental study. *Journal of Petrology*, 49(4):717–740.

Holland, T. J. B. and Powell, R. (1998). An internally consistent thermodynamic data set for phases of petrological interest. *Journal of Metamorphic Geology*, 16(3):309–343.

Hwang, S. L., Shen, P. Y., Yui, T. F., and Chu, H. T. (2003). Metal-sulfur-COH-silicate fluid mediated diamond nucleation in Kokchetav ultrahigh-pressure gneiss. *European Journal of Mineralogy*, 15(3):503–511.

Jamtveit, B. (1987a). Magmatic and Metamorphic Controls on Chemical Variations within the Eiksunddal Eclogite Complex, Sunnmore, Western Norway. *Lithos*, 20(5):369–389.

Jamtveit, B. (1987b). Metamorphic evolution of the Eiksunddal eclogite complex. Western Norway, and some tectonic implications. *Contributions to Mineralogy and Petrology*, 95(1):82–99.

Jaoul, O. and Bejina, F. (2005). Empirical determination of diffusion coefficients and geospeedometry. *Geochimica Et Cosmochimica Acta*, 69(4):1027–1040.

Jaoul, O. and Sautter, V. (1999). A new approach to geospeedometry based on the 'compensation law'. *Physics of the Earth and Planetary Interiors*, 110(1-2):95–114.

Jin, Z. M., Zhang, J., Green, H. W., and Jin, S. (2001). Eclogite rheology: Implications for subducted lithosphere. *Geology*, 29(8):667–670.

John, T., Medvedev, S., Rüpke, L. H., Andersen, T., Podladchikov, Y. Y., and Austrheim, H. (2009). Self-localizing thermal runaway as a mechanism for intermediate deep focus earthquakes. *Nature Geoscience*, in press.

Kanamori, H. (1979). Physics of the earth's interior, Proceedings of the International School of Physics Enrico Fermi, Course LXXVIII. *Varenna on Lake Como, Villa Monastero*, 23rd July-4th August:531–555.

Kanamori, H. (1994). Mechanics of Earthquakes. *Annual Review of Earth and Planetary Sciences*, 22:207–237.

Kelemen, P. B. and Hirth, G. (2007). A periodic shear-heating mechanism for intermediate-depth earthquakes in the mantle. *Nature*, 446(7137):787–790.

Klemme, S. (2004). The influence of Cr on the garnet-spinel transition in the Earth's mantle: experiments in the system MgO-Cr_2O_3-SiO_2 and thermodynamic modelling. *Lithos*, 77(1-4):639–646.

Konrad-Schmolke, M., Handy, M. R., Babist, J., and O'Brien, P. J. (2005). Thermodynamic modelling of diffusion-controlled garnet growth. *Contributions to Mineralogy and Petrology*, 149(2):181–195.

Konrad-Schmolke, M., O'Brien, P. J., de Capitani, C., and Carswell, D. A. (2008a). Garnet growth at high- and ultra-high pressure conditions and the effect of element fractionation on mineral modes and composition. *Lithos*, 103(3-4):309–332.

Konrad-Schmolke, M., Zack, T., O'Brien, P. J., and Jacob, D. E. (2008b). Combined thermodynamic and rare earth element modelling of garnet growth during subduction: Examples from ultrahigh-pressure eclogite of the Western Gneiss Region, Norway. *Earth and Planetary Science Letters*, 272(1-2):488–498.

Korzhinskii, D. S. (1970). *Theory of metasomatic zoning*. Clarendon Press, Oxford.

Krabbendam, M. and Dewey, J. F. (1998). Exhumation of UHP rocks by transtension in the Western Gneiss Region, Scandinavian Caledonides. *Geological Society Special Publications*, 135:159–181.

Krabbendam, M., Wain, A., and Andersen, T. B. (2000). Pre-Caledonian granulite and gabbro enclaves in the Western Gneiss Region, Norway: indications of incomplete transition at high pressure. *Geological Magazine*, 137(3):235–255.

Kretz, R. (1983). Symbols for Rock-Forming Minerals. *American Mineralogist*, 68(1-2):277–279.

Krill, A. G. (1980). Tectonics of the Oppdal area, central Norway. *Geologiska Föreningens i Stockholm Förhandlingar*, 102(4):523–530.

Krill, A. G. (1985). Relationships between the Western Gneiss Region and the Trondheim region; stockwerk-tectonics reconsidered. In Gee, D. G. and Sturt, B. A., editors, *The Caledonide Orogen; Scandinavia and related areas*, volume 1, pages 475–483. John Wiley & Sons, Chichester, United Kingdom.

Krogh, E. and Carswell, D. (1995). HP and UHP Eclogites and Garnet Peridotites in the Scandinavian Caledonides. In Coleman, R. and Wang, X., editors, *Ultrahigh Pressure Metamorphism*, Cambridge Topics in Petrology, pages 244–298. Cambridge University Press.

Krogh, E. J. (1977). Evidence of Precambrian continent-continent collision in Western Norway. *Nature*, 267(5606):17–19.

Krogh, E. J. (1988). The garnet-clinopyroxene Fe-Mg geothermometer - a reinterpretation of existing experimental data. *Contributions to Mineralogy and Petrology*, 99(1):44–48.

Krogh, T., Kwok, Y., Robinson, P., and Terry, M. (2004). U-Pb age constraints on the subduction-extension interval in the Averøya-Nordøyane area, Western Gneiss Region, Norway. *Geochimica Et Cosmochimica Acta*, 68(11):A611–a611.

Krogh, T., Robinson, P., and Terry, M. (2003). Precise U-Pb zircon ages define 18 and 19 m.y. Subduction to uplift intervals in the Averøya-Nordøyane area, Western Gneiss Region. *NGU-report*, 2003-055:71–72.

Krogh, T. E. (1973). Low-Contamination Method for Hydrothermal Decomposition of Zircon and Extraction of U and Pb for Isotopic Age Determinations. *Geochimica Et Cosmochimica Acta*, 37(3):485–494.

Kylander-Clark, A. R. C., Hacker, B. R., and Mattinson, J. M. (2008). Slow exhumation of UHP terranes: Titanite and rutile ages of the Western Gneiss Region, Norway. *Earth and Planetary Science Letters*, 272(3-4):531–540.

Labrousse, L., Jolivet, L., Andersen, T., Agard, P., Maluski, H., and Schärer, U. (2004). Pressure-temperature-time-deformation history of the exhumation of ultra-high-pressure rocks in the Western Gneiss Region, Norway. *Geol. Soc. Am., Special Paper*, 380:155–183.

Lappin, M. A. and Smith, D. (1981). Carbonate, silicate and fluid relationships in eclogites, Selje District and environs, SW Norway. *Trans. Roy. Soc. Edinburgh*, 72:171–193.

Lappin, M. A. and Smith, D. C. (1978). Mantle-Equilibrated Ortho-Pyroxene Eclogite Pods from Basal Gneisses in Selje-District, Western Norway. *Journal of Petrology*, 19(3):530–584.

Lasaga, A. C. (1983). Geospeedometry: An Extension of Geothermometry. In Saxena, S. K., editor, *Kinetics and Equilibrium in Mineral Reactions*, volume 3 of *Advances in Physical Geochemistry*. Springer-Verlag, New York.

Lasaga, A. C. and Jiang, J. X. (1995). Thermal History of Rocks - P-T-T Paths from Geospeedometry, Petrological Data, and Inverse-Theory Techniques. *American Journal of Science*, 295(6):697–741.

Leake, B. E., Woolley, A. R., Arps, C. E. S., Birch, W. D., Gilbert, M. C., Grice, J. D., Hawthorne, F. C., Kato, A., Kisch, H. J., Krivovichev, V. G., Linthout, K., Laird, J., Mandarino, J. A., Maresch, W. V., Nickel, E. H., Rock, N. M. S., Schumacher, J. C., Smith, D. C., Stephenson, N. C. N., Ungaretti, L., Whittaker, E. J. W., and Guo, Y. Z. (1997). Nomenclature of amphiboles: Report of the subcommittee on amphiboles of the International Mineralogical Association, Commission on New Minerals and Mineral Names. *Canadian Mineralogist*, 35:219–246.

Lee, H. Y. and Ganguly, J. (1988). Equilibrium Compositions of Coexisting Garnet and Orthopyroxene - Experimental Determinations in the System FeO-MgO-Al_2O_3-SiO_2, and Applications. *Journal of Petrology*, 29(1):93–113.

Ludwig, K. (1999). ISOPLOT/EX version 2.03. A geochronological toolkit for MICROSOFT excel. *Berkeley Geochron. Center. Spec. Publ.*, 1:43.

Lund, M. G. and Austrheim, H. (2003). High-pressure metamorphism and deep-crustal seismicity: evidence from contemporaneous formation of pseudotachylytes and eclogite facies coronas. *Tectonophysics*, 372(1-2):59–83.

Macgregor, I. D. (1974). The System MgO-Al_2O_3-SiO_2 : Solubility of Al_2O_3 in Enstatite for Spinel and Garnet Peridotite Compositions. *American Mineralogist*, 59(1-2):110–119.

Mancktelow, N. S. (1993). Tectonic Overpressure in Competent Mafic Layers and the Development of Isolated Eclogites. *Journal of Metamorphic Geology*, 11(6):801–812.

Medaris, L. G., Beard, B. L., Johnson, C. M., Valley, J. W., Spicuzza, M. J., Jelinek, E., and Misar, Z. (1995). Garnet Pyroxenite and Eclogite in the Bohemian Massif - Geochemical Evidence for Variscan Recycling of Subducted Lithosphere. *Geologische Rundschau*, 84(3):489–505.

Michard, A., Avigad, D., Goffe, B., and Chopin, C. (2004). The high-pressure metamorphic front of the south Western Alps (Ubaye-Maira transect, France, Italy). *Schweizerische Mineralogische Und Petrographische Mitteilungen*, 84(3):215–235.

Mørk, M. B. E. (1985a). A Gabbro to Eclogite Transition on Flemsøy, Sunnmore, Western Norway. *Chemical Geology*, 50:283–310.

Mørk, M. B. E. (1985b). Incomplete High P-T Metamorphic Transitions within the Kvamsøy Pyroxenite Complex, West Norway - a Case-Study of Disequilibrium. *Journal of Metamorphic Geology*, 3(3):245–264.

Mørk, M. B. E. and Mearns, E. W. (1986). Sm-Nd isotopic systematics of a gabbro-eclogite transition. *Lithos*, 19(3-4):255–267.

Mosenfelder, J. L. and Bohlen, S. R. (1997). Kinetics of the coesite to quartz transformation. *Earth and Planetary Science Letters*, 153(1-2):133–147.

Mosenfelder, J. L., Schertl, H. P., Smyth, J. R., and Liou, J. G. (2005). Factors in the preservation of coesite: The importance of fluid infiltration. *American Mineralogist*, 90(5-6):779–789.

Mposkos, E. D. and Kostopoulos, D. K. (2001). Diamond, former coesite and supersilicic garnet in metasedimentary rocks from the Greek Rhodope: a new ultrahigh-pressure metamorphic province established. *Earth and Planetary Science Letters*, 192(4):497–506.

Nasdala, L. and Massonne, H. J. (2000). Microdiamonds from the Saxonian Erzgebirge, Germany: in situ micro-Raman characterisation. *European Journal of Mineralogy*, 12(2):495–498.

Nauman, E. B. and He, D. Q. (2001). Nonlinear diffusion and phase separation. *Chemical Engineering Science*, 56(6):1999–2018.

Nichols, G. T., Wyllie, P. J., and Stern, C. R. (1994). Subduction Zone-Melting of Pelagic Sediments Constrained by Melting Experiments. *Nature*, 371(6500):785–788.

Nickel, K. G. and Green, D. H. (1985). Empirical Geothermobarometry for Garnet Peridotites and Implications for the Nature of the Lithosphere, Kimberlites and Diamonds. *Earth and Planetary Science Letters*, 73(1):158–170.

O'Brien, P. J. (2008). Challenges in high-pressure granulite metamorphism in the era of pseudosections: reaction textures, compositional zoning and tectonic interpretation with examples from the Bohemian Massif. *Journal of Metamorphic Geology*, 26(2):235–251.

O'Brien, P. J. and Ziemann, M. A. (2008). Preservation of coesite in exhumed eclogite: insights from Raman mapping. *European Journal of Mineralogy*, 20:827–834.

O'Neill, H. S. C. (1980). Correction. *Contributions to Mineralogy and Petrology*, 72(3):337–337.

O'Neill, H. S. C. (1981). The Transition between Spinel Lherzolite and Garnet Lherzolite, and Its Use as a Geobarometer. *Contributions to Mineralogy and Petrology*, 77(2):185–194.

O'Neill, H. S. C. and Wood, B. J. (1979). Experimental-Study of Fe-Mg Partitioning between Garnet and Olivine and Its Calibration as a Geothermometer. *Contributions to Mineralogy and Petrology*, 70(1):59–70.

Perrillat, J. P., Daniel, I., Lardeaux, J. M., and Cardon, H. (2003). Kinetics of the Coesite-Quartz Transition: Application to the Exhumation of Ultrahigh-Pressure Rocks. *Journal of Petrology*, 44(4):773–788.

Petrini, K. and Podladchikov, Y. (2000). Lithospheric pressure-depth relationship in compressive regions of thickened crust. *Journal of Metamorphic Geology*, 18(1):67–77.

Platt, J. P. (1986). Dynamics of Orogenic Wedges and the Uplift of High-Pressure Metamorphic Rocks. *Geological Society of America Bulletin*, 97(9):1037–1053.

Powell, R. (1985). Regression Diagnostics and Robust Regression in Geothermometer Geobarometer Calibration - the Garnet Clinopyroxene Geothermometer Revisited. *Journal of Metamorphic Geology*, 3(3):231–243.

Powell, R. and Holland, T. J. B. (1988). An Internally Consistent Dataset with Uncertainties and Correlations .3. Applications to Geobarometry, Worked Examples and a Computer-Program. *Journal of Metamorphic Geology*, 6(2):173–204.

Powell, R. and Holland, T. J. B. (2008). On thermobarometry. *Journal of Metamorphic Geology*, 26(2):155–179.

Råheim, A. and Green, D. H. (1974). Experimental Determination of the Temperature and Pressure Dependence of the Fe-Mg Partition Coefficient for Coexisting Garnet and Clinopyroxene. *Contributions to Mineralogy and Petrology*, 48:179–203.

Rampone, E. and Morten, L. (2001). Records of crustal metasomatism in the garnet peridotites of the Ulten Zone (Upper Austroalpine, Eastern Alps). *Journal of Petrology*, 42(1):207–219.

Ravna, E. K. (2000). The garnet-clinopyroxene Fe_2-Mg geothermometer: an updated calibration. *Journal of Metamorphic Geology*, 18(2):211–219.

Ravna-Krogh, E. and Paquin, J. (2003). Thermobarometric methodologies applicable to eclogites and garnet ultrabasites. In Carswell, D. A. and Compagnoni, R., editors, *Ultrahigh Pressure Metamorphism*, volume 5 of *EMU Notes in Mineralogy*, pages 229–259. Eötvös University Press, Budapest.

Renshaw, C. E. and Schulson, E. M. (2007). Limits on rock strength under high confinement. *Earth and Planetary Science Letters*, 258(1-2):307–314.

Reverdatto, V. V., Selyatitskiy, A. Y., and Carswell, D. A. (2008). Geochemical distinctions between "crustal" and mantle-derived peridotites/pyroxenites in high-/ultrahigh pressure metamorphic complexes. *Russian Geology and Geophysics*, 49(2):73–90.

Roberts, D. (2003). The Scandinavian Caledonides: event chronology, palaeogeographic settings and likely, modern analogues. *Tectonophysics*, 365(1-4):283–299.

Robinson, P. (1995). Extension of Trollheimen tectono-stratigraphic sequence in deep synclines near Molde and Brattvåg, Western Gneiss Region, Southern Norway. *Norsk Geologisk Tidsskrift*, 75(4):181–197.

Root, D. B., Hacker, B. R., Gans, P. B., Ducea, M. N., Eide, E. A., and Mosenfelder, J. L. (2005). Discrete ultrahigh-pressure domains in the Western Gneiss Region, Norway: implications for formation and exhumation. *Journal of Metamorphic Geology*, 23(1):45–61.

Sambridge, M. and Lambert, D. D. (1997). Propagating errors in decay equations: Examples from the Re-Os isotopic system. *Geochimica Et Cosmochimica Acta*, 61(14):3019–3024.

Scambelluri, M., Pettke, T., and van Roermund, H. L. M. (2008). Majoritic garnets monitor deep subduction fluid flow and mantle dynamics. *Geology*, 36(1):59–62.

Schärer, U. (1984). The effect of initial ^{230}Th disequilibrium on young U-Pb ages: the Makalu Case, Himalaya. *Earth and Planetary Science Letters*, 67(2):191–204.

Schmid, D. W., Abart, R., Podladchikov, Y. Y., and Milke, R. (2009). Matrix rheology effects on reaction rim growth II: coupled diffusion and creep model. *Journal of Metamorphic Geology*, 27:83–91.

Schmidt, H. (1963). *Petrology and structure of the Eiksundal Eclogite Complex, Hareidlandet, Sunnmore, Norway*. Ph.d. thesis, Harvard University U.S.A.

Scholz, C. H. (2004). *The mechanics of earthquakes and faulting (2nd edition)*. Cambridge University Press, Cambridge, UK.

Sekine, T. and Wyllie, P. J. (1982). Phase-Relationships in the System $KAlSiO_4$-Mg_2SiO_4-SiO_2-H_2O as a Model for Hybridization between Hydrous Siliceous Melts and Peridotite. *Contributions to Mineralogy and Petrology*, 79(4):368–374.

Seranne, M. (1992). Late Paleozoic Kinematics of the Mre-Trondelag Fault Zone and Adjacent Areas, Central Norway. *Norsk Geologisk Tidsskrift*, 72(2):141–158.

Shewchuk, J. R. (2005). Triangle 1.6. In *http://www.cs.cmu.edu/ quake/triangle.html*. Internet.

Simakov, S. K., Dubinchuk, V. T., Novikov, M. P., and Drozdova, I. A. (2008). Formation of diamond and diamond-type phases from the carbon-bearing fluid at P-T parameters corresponding to processes in the Earth's crust. *Doklady Earth Sciences*, 421(1):835–837.

Smith, D. (1995). Chlorite-Rich Ultramafic Reaction Zones in Colorado Plateau Xenoliths - Recorders of Sub-Moho Hydration. *Contributions to Mineralogy and Petrology*, 121(2):185–200.

Smith, D. (2008). Raman confirmation of haematite leads to a new (U)HPM indicator paragenesis : haematite + carbon. *Book of Abstracts: GeoRaman '08: 8th International Conference on Raman Spectroscopy Applied to the Earth Sciences - Sensu Latu*.

Smith, D. and Barron, B. R. (1991). Pyroxene-garnet equilibration during cooling in the mantle. *American Mineralogist*, 76(11-12):1950–1963.

Smith, D. C. (1984). Coesite in clinopyroxene in the Caledonides and its implications for geodynamics. *Nature*, 310(5979):641–644.

Smith, D. C. (1985). Coesite in the Straumen eclogite pod, Norway. *Terra Cognita*, 5:226–227.

Smith, D. C. (1988). A review of the peculiar mineralogy of the "Norwegian coesite-eclogite province", with crystal-chemical, petrological, geochemical and geodynamical notes and an extensive bibliography. In Smith, D. C., editor, *Eclogites and Eclogite-Facies Rocks*, volume 12 of *Developments in Petrology*, pages 1–206. Elsevier, Amsterdam.

Smith, D. C., Godard, G., Dobrzhinetskaya, L., Green, H., and Belleil, M. (2004). A preliminary comparative Raman mapping study of contrasting zircon/diamond/-graphite relations at Kokchetav, Kazakhstan. In Fredericks, P. M., Frost, R., and Rintoul, L., editors, *Proceedings, XIXth International Conference on Raman Spectroscopy*, pages 562–563. Csiro publishing, Queensland, Australia.

Smith, D. C. and Lappin, M. A. (1989). Coesite in the Straumen kyanite-eclogite pod, Norway. *Terra Nova*, 1(1):47–56.

Sobolev, N. V. and Shatsky, V. S. (1990). Diamond Inclusions in Garnets from Metamorphic Rocks - a New Environment for Diamond Formation. *Nature*, 343(6260):742–746.

Spear, F. S. and Menard, T. (1989). Program GIBBS: A generalized Gibbs method algorithm. *American Mineralogist*, 74(7-8):942–943.

Spear, F. S. and Selverstone, J. (1983). Quantitative P-T Paths from Zoned Minerals - Theory and Tectonic Applications. *Contributions to Mineralogy and Petrology*, 83(3-4):348–357.

Spengler, D. (2006). *Origin and evolution of deep upper mantle rocks from Western Norway* . Doctoral, Utrecht University.

Stacey, J. S. and Kramers, J. D. (1975). Approximation of Terrestrial Lead Isotope Evolution by a 2-Stage Model. *Earth and Planetary Science Letters*, 26(2):207–221.

Stalder, P., Ulmer, P., Thompson, A. B., and Gunther, D. (2000). Experimental approach to constrain second critical end points in fluid/silicate systems: Near-solidus fluids and melts in the system albite-H_2O. *American Mineralogist*, 85(1):68–77.

Stöckhert, B., Duyster, J., Trepmann, C., and Massonne, H. J. (2001). Microdiamond daughter crystals precipitated from supercritical COH plus silicate fluids included in garnet, Erzgebirge, Germany. *Geology*, 29(5):391–394.

Sun, S. S. and McDonough, W. F. (1989). Chemical and isotopic systematics of oceanic basalts: implications for mantle composition and processes. *Geological Society Special Publication*, 42:313–345.

Suzuki, A. and Ohtani, E. (2003). Density of peridotite melts at high pressure. *Physics and Chemistry of Minerals*, 30(8):449–456.

Terry, M. P. and Robinson, P. (2003). Evolution of amphibolite-facies structural features and boundary conditions for deformation during exhumation of high- and ultrahigh-pressure rocks, Nordoyane, Western Gneiss Region, Norway. *Tectonics*, 22(4):1036, 10.1029/2001TC001349.

Terry, M. P. and Robinson, P. (2004). Geometry of eclogite-facies structural features: Implications for production and exhumation of ultrahigh-pressure and high-pressure rocks, Western Gneiss Region, Norway. *Tectonics*, 23(2):TC2001, 10.1029/2002TC001401.

Terry, M. P., Robinson, P., and Ravna, E. J. K. (2000a). Kyanite eclogite thermobarometry and evidence for thrusting of UHP over HP metamorphic rocks, Nordøyane, Western Gneiss Region, Norway. *American Mineralogist*, 85(11-12):1637–1650.

Terry, M. P., Robinson, P., Ravna, E. J. K., Hamilton, M. A., and Jercinovic, M. J. (2000b). Monazite geochronology of UHP and HP metamorphism, deformation, and exhumation, Nordøyane, Western Gneiss Region, Norway. *American Mineralogist*, 85(11-12):1651–1664.

Thompson, Jr., J. B. (1959). Local Equilibrium in Metasomatic Processes. In Abelson, P. H., editor, *Researches in Geochemistry*, volume 1, pages 427–457. John Wiley and Sons, Inc., New York.

Thöni, M. (2002). Sm-Nd isotope systematics in garnet from different lithologies (Eastern Alps): age results, and an evaluation of potential problems for garnet Sm-Nd chronometry. *Chemical Geology*, 185(3-4):255–281.

Torsvik, T. H., Smethurst, M. A., Meert, J. G., VanderVoo, R., McKerrow, W. S., Brasier, M. D., Sturt, B. A., and Walderhaug, H. J. (1996). Continental breakup and collision in the Neoproterozoic and Palaeozoic - A tale of Baltica and Laurentia. *Earth-Science Reviews*, 40(3-4):229–258.

Trepmann, C. and Stöckhert, B. (2001). Mechanical twinning of jadeite - an indication of synseismic loading beneath the brittle-plastic transition. *International Journal of Earth Sciences*, 90(1):4–13.

Trepmann, C. A. and Stöckhert, B. (2003). Quartz microstructures developed during non-steady state plastic flow at rapidly decaying stress and strain rate. *Journal of Structural Geology*, 25(12):2035–2051.

Tucker, R. D., Krogh, T. E., and Råheim, A. (1990). Proterozoic Evolution and Age-Province Boundaries in the Central Part of the Western Gneiss Region, Norway; Results of U-Pb Dating of Accessory Minerals from Trondheimsfjord to Geiranger. In Gower, C. F., Rivers, T., and Ryan, B., editors, *Special Paper - Geological Association of Canada*, volume 38 of *Mid-Proterozoic Laurentia-Baltica* , pages 149–173. Geological Association of Canada, Toronto.

Tucker, R. D., Robinson, P., Solli, A., Gee, D. G., Thorsnes, T., Krogh, T. E., Nordgulen, Ø., and Bickford, M. E. (2004). Thrusting and extension in the

scandian hinterland, Norway: New U-Pb ages and tectonostratigraphic evidence. *American Journal of Science*, 304(6):477–532.

Turcotte, D. L. and Schubert, G. (2002). *Geodynamics (Second Edition)*. Cambridge University Press, Cambridge.

Tveten, E., Lutro, O., and Thornes, T. (1998). *ÅLESUND, Geological map*. Norges geologiske undersøkelse.

Van der Molen, I. and Van Roermund, H. L. M. (1986). The Pressure Path of Solid Inclusions in Minerals - the Retention of Coesite Inclusions during Uplift. *Lithos*, 19(3-4):317–324.

Van Orman, J. A., Grove, T. L., Shimizu, N., and Layne, G. D. (2002). Rare earth element diffusion in a natural pyrope single crystal at 2.8 GPa. *Contributions to Mineralogy and Petrology*, 142(4):416–424.

Van Roermund, H. L. M., Carswell, D. A., Drury, M. R., and Heijboer, T. C. (2002). Microdiamonds in a megacrystic garnet websterite pod from Bardane on the island of Fjørtoft, western Norway: Evidence for diamond formation in mantle rocks during deep continental subduction. *Geology*, 30(11):959–962.

Van Roermund, H. L. M. and Drury, M. R. (1998). Ultra-high pressure (P > 6 GPa) garnet peridotites in Western Norway: exhumation of mantle rocks from > 185 km depth. *Terra Nova*, 10(6):295–301.

Van Roermund, H. L. M., Spengler, D., and Wiggers de Vries, D. (2005). Evidence for ultra-high pressure (UHP) metamorphism within Proterozoic basement rocks on Otrøy, Western Gneiss Region, Norway. *Mitteilungen der Österreichischen Mineralogischen Gesellschaft*, 150:159.

Van Straaten, B., Wiggers de Vries, D., Van Roermund, H., and Drury, M. (2003). A structural, metamorphic and geochronological study of eclogites and country rock gneisses from Otrøy (Moldefjord), WGR, Norway. *Norges Geologiske Undersøkelse, Trondheim*, Report 2003.055:155–156.

Vrijmoed, J., Smith, D. C., and Van Roermund, H. (2008). Raman Confirmation of Microdiamond in the Svartberget Fe-Ti type garnet peridotite, Western Gneiss Region, Western Norway. *Terra Nova*, 40:295–301.

Vrijmoed, J., Smith, D. C., and Van Roermund, H. (in prep.). A new in-situ microdiamond locality in the Scandinavian Caledonides: Svartberget. *Terra Nova*.

Vrijmoed, J. C. (2008). Stop 10.1. Diamond-bearing Svartberget olivine-websterite. In Robinson, P., Roberts, D., and D., G., editors, *A tectonostratigraphic transect across the central Scandinavian Caledonides, Part II Preliminary*, volume 2008.064, pages 2–5. Norges geologiske undersøkelse, Trondheim.

Vrijmoed, J. C. (2009). Pressure variations during ultra-high pressure metamorphism from single grain up to outcrop scale? *in preparation*.

Vrijmoed, J. C., Austrheim, H., John, T., R., H., Davies, G. R., and Corfu, F. (2009). Metasomatism of the ultra-high pressure Svartberget Fe-Ti type garnet-peridotite, Western Gneiss Region, Norway. *in preparation*.

Vrijmoed, J. C., Van Roermund, H. L. M., and Davies, G. R. (2006). Evidence for diamond-grade ultra-high pressure metamorphism and fluid interaction in the Svartberget Fe-Ti garnet peridotite-websterite body, Western Gneiss Region, Norway. *Mineralogy and Petrology*, 88(1-2):381–405.

Wain, A. (1997). New evidence for coesite in eclogite and gneisses: Defining an ultrahigh-pressure province in the Western Gneiss region of Norway. *Geology*, 25(10):927–930.

Wain, A., Waters, D., Jephcoat, A., and Olijynk, H. (2000). The high-pressure to ultrahigh-pressure eclogite transition in the Western Gneiss Region, Norway. *European Journal of Mineralogy*, 12(3):667–687.

Wain, A. L., Waters, D. J., and Austrheim, H. (2001). Metastability of granulites and processes of eclogitisation in the UHP region of western Norway. *Journal of Metamorphic Geology*, 19(5):607–623.

Walsh, E. O. and Hacker, B. R. (2004). The fate of subducted continental margins: Two-stage exhumation of the high-pressure to ultrahigh-pressure Western Gneiss Region, Norway. *Journal of Metamorphic Geology*, 22(7):671–687.

Walsh, E. O., Hacker, B. R., Gans, P. B., Grove, M., and Gehrels, G. (2007). Protolith ages and exhumation histories of (ultra)high-pressure rocks across the Western Gneiss Region, Norway. *Geological Society of America Bulletin*, 119(3-4):289–301.

Wells, P. R. A. (1977). Pyroxene Thermometry in Simple and Complex Systems. *Contributions to Mineralogy and Petrology*, 62(2):129–139.

Wheeler, J. (1987). The significance of grain-scale stresses in the kinetics of metamorphism. *Contributions to Mineralogy and Petrology*, 97(3):397–404.

Wheeler, J. (1991). Structural Evolution of a Subducted Continental Sliver - the Northern Dora Maira Massif, Italian Alps. *Journal of the Geological Society*, 148:1101–1113.

Wood, B. J. (1974). Solubility of Alumina in Orthopyroxene Coexisting with Garnet. *Contributions to Mineralogy and Petrology*, 46(1):1–15.

Ye, K., Liou, J. B., Cong, B., and Maruyama, S. (2001). Overpressures induced by coesite-quartz transition in zircon. *American Mineralogist*, 86:1151–1155.

Zhang, Y. (1998). Mechanical and phase equilibria in inclusion-host systems. *Earth and Planetary Science Letters*, 157:209–222.